DOCTOR OF PHILOSOPHY

Molecular wires and molecular rectification from ionically coupled structures

Urasinska-Wojcik, Barbara

Award date:
2008

Awarding institution:
Bangor University

Molecular Wires and Molecular Rectification from Ionically Coupled Structures

A thesis submitted to the
University of Wales
in candidature for the

Degree of
Doctor of Philosophy

by

Barbara Urasinska-Wojcik

Supervisor: Professor Geoffrey J. Ashwell

School of Chemistry
Prifysgol – Bangor University

2008

Acknowledgements

I would like to thank Professor Geoffrey J. Ashwell for giving me the opportunity to study for the PhD in his group. I am grateful to many people who have been very helpful to me during my time at Cranfield as well as Bangor University. I would like to thank in particular Dr Anne Whittam, Dr Wayne Tyrrell and Dr Benjamin Robinson for advice and all their kindnesses. Thanks to all my colleagues, the English and the Polish, for the nice time throughout the last 3 years.

I especially want to thank my parents and my brothers for their support, help and showing me the way. Finally and the most importantly thanks to my husband Jacek, for care, love and his support.

Abstract

It is important to design molecular junctions with molecules as active electrical components, which may be applicable in future electronic devices. This thesis reports the electrical properties of molecular diodes, as well as molecular wires. The work is concentrated, to a large extent, on observations of molecular rectification from monolayer and bilayer assemblies based on sterically hindered A^{+}–π–D dyes, and protonated molecular wires of different lengths, which are then ionically coupled with anionic strong donors. The second part presents the studies of the electric properties of various single-molecule wires. The growth of the molecular assembly process was observed with the quartz crystal microbalance technique (QCM).

Scanning tunnelling microscopy (STM) was used to analyse the electron transport through the molecule. I-V characteristics of these new types of organic rectifying junctions were obtained, with the high current being observed in the negative quadrant of the I-V plots. These devices exhibited rectification ratios of 20-500 at ±1 V, and even in excess of 3000 at ± 1 V for a particular type of A^{+}–π–D|D^{-} compound. This significant enhancement of the rectification behaviour was achieved by using ionically coupled structures; it may provide a solution to the ultimate challenge of electronic device miniaturisation.

Organic rectifying junctions which incorporated protonated forms of arylene-ethynylene molecular wires were seen to exhibit rectification with current ratios of 15-80 at ± 1 V, whereas, self-assembled monolayers (SAMs) of the neutral forms of these wires, on gold substrates, exhibited symmetrical I-V curves when contacted by gold and PtIr tips. The 7 nm and the 10 nm wires presented in this thesis are the longest to date to be used for single-molecule electrical studies.

The spontaneous formation of stable molecular wires between the tip and the sample was monitored using I(t) and I(s) methods, for the measurements of single-molecule current. Electrical contact between the molecule and the gold probe was achieved by the use of thiol groups present at each end of the molecules. Histograms of the measured current jumps at a constant sample bias of –0.3 V were prepared to assess the single-molecule current.

Contents

1. Introduction

1.1 Molecular electronics

Molecular electronics is a young field that requires knowledge from both physical chemistry and material science. One of the key concepts of modern electronics was highlighted in Richard Feynman's lecture to the American Physical Society in 1956 [1] in which he proposed that electronic components could be miniaturised.

Molecular electronics was conceptually defined by Aviram and Ratner [2], as a "study of molecular properties that may lead to signal processing" [3]. However, creating molecular electronics as functional, manufacturable devices will require revolutions in circuit architecture, fabrication and design philosophy, in addition to gaining a fundamental understanding of conduction and electronic interactions in single molecules [4].

One of the key interests is the design of molecules that possess functional electronic behaviour such that they may be utilised as replacements (or to use in conjunction with) inorganic materials; for example, in computer technology. Currently, computers are based on silicon oxide gate semiconductor transistors. However, silicon device technology is approaching the fundamental physical limitations of operation. The need to produce progressively smaller structures has so far been satisfied by lithography (and related techniques) for the construction of electronic components and microelectromechanical systems. During the past few decades, the semiconductor industry has followed the so-called "Moore's law" [5]. By the downsizing of components, the transistor density on integrated circuits has been almost doubled every year, and so provided a continuous increase in the speed and performance of devices (see Figure 1). It is necessary to emphasise that it is not a law at all, in either the scientific or legal senses. It is instead a testament to the power and efficacy of engineering to make continual incremental improvements to a well-established technology [6]. Despite these achievements, the actual trend in electronics described by Gordon Moore [5] (see Figure 1) can only be continued for a finite time. This

observation did not consider the restrictions dictated by the laws of physics. It follows that the reduction of silicon oxide components cannot be pushed much further and that new device operating principles, along with materials, must evolve [7],[8].

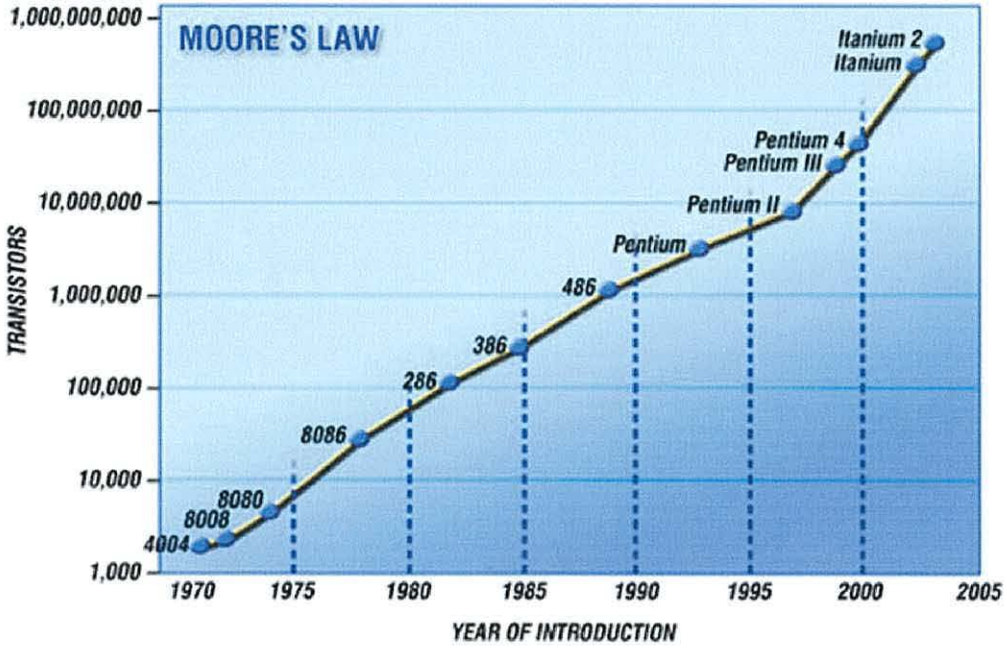

Figure 1 Graphic representation of Moore's law [9].

Chemistry, by its nature, operates at the nanometer scale by controlling the placement of individual atoms and functional groups on molecules. Nowadays, molecular electronics is a technology that utilises small groups of molecules, carbon nanotubes or nanoscale metallic or semiconductor wires to perform electronic functions [10],[11],[12],[13]. Current research on molecular electronics focuses upon electro-active components such as diodes [14],[15],[16],[17], switches [18],[19], and wires [20],[21] for electronic applications in molecular devices like liquid crystals, light emitting diodes (LED), transistors, laser, and sensors [22],[23],[24]. The distinction between these applications, and molecular scale electronics is not just one of size, but lies in the design concept of the molecules that constitute the active elements [21],[25],[26]. It is a very promising route, but one with many obstacles to overcome if future electronic devices are to become a reality.

1.2 Motivation and objectivities

Many molecules have been proposed for use in molecular electronics. For those proposed, there are several mechanisms for controlling the molecules, including: electric fields, electromechanical and photochromic actuation, and electrochemistry. Consequently, this thesis is focused on compounds that are controlled by an electric field, in particular on the possible ways of preparing organic devices for rectification and electrical conductivity applications.

The major objective of this thesis was the verification of electron transport mechanisms within molecular junctions using the Aviram and Ratner model [2]. The model is based on the use of electron-donating, spacer, and electron-accepting functionalities. Self-assembled monolayers (SAMs) containing donor-(π-bridge)-acceptor chromophores deposited on gold-coated substrates were investigated with the quartz crystal microbalance (QCM) technique. Their electrical properties were monitored by a scanning tunnelling microscope (STM). The same techniques also allowed investigation of the electronic properties of various single-molecular wires. Manipulation of the molecular structures, packing, and different assembly methods all had a direct influence on the electrical asymmetry.

2. Molecular self-assembly

Self-assembly is a well-known mechanism in nature, from simple molecules to much more complex biological systems, it contributes to making patterns and order in systems [27]. The term self-assembly is now widely used and in a general sense may be defined as "the spontaneous formation of complex hierarchical structures from pre-designed building blocks, typically involving multiple energy scales and multiple degrees of freedom" [28],[29]. It is a parallel fabrication process which can generate three-dimensional structures with sub-nanometer precision at the molecular level [27]. The first reported example of this formation was published by Bigelow, Pickett and Zisman in 1946 [30]. The discovery of SAMs has essentially transformed surface chemistry and has also opened a new area of research for physically oriented groups. Self-assembly has been employed to make molecular electronic devices, memories, and photonic bandgap materials in research labs. It is also expected that SAMs will be a cost effective and efficient method for manufacturing nano-scale devices. The study of defects in this system will play a prominent role in transferring self-assembly from research laboratories to device manufacturing [27].

Specifically, SAMs are ordered molecular assemblies that are formed spontaneously by the adsorption (either by chemisorption, or less ordered physisorption) of a surfactant with a specific affinity of its headgroup to a substrate. The self-assembly process is distinguished from normal adsorption by the strength of this interaction. Another feature is that the molecules adsorb in an ordered fashion (assembly) usually as a result of van der Waals interactions between alkyl chains [31]. SAMs are usually prepared from solution, although some systems can be prepared from the gas phase, and the best examples are organic molecular beam deposition (OMBD), or organic molecular beam epitaxy (OMBE). Both of these techniques allow the use of ultrahigh vacuum (UHV); they have the advantage of providing both layer thickness control and a clean environment and substrate [32]. Although the gas phase offers much more stable SAMs, it utilises expensive equipment. Therefore growth from solution is a more popular and cost effective way for SAM formation.

2.1 Formation and characteristics of covalent SAMs

The procedure for the preparation of a SAM from solution generally follows that illustrated in Figure 2. A schematic diagram of an ideal SAM of alkanethiolates on a gold surface is highlighted.

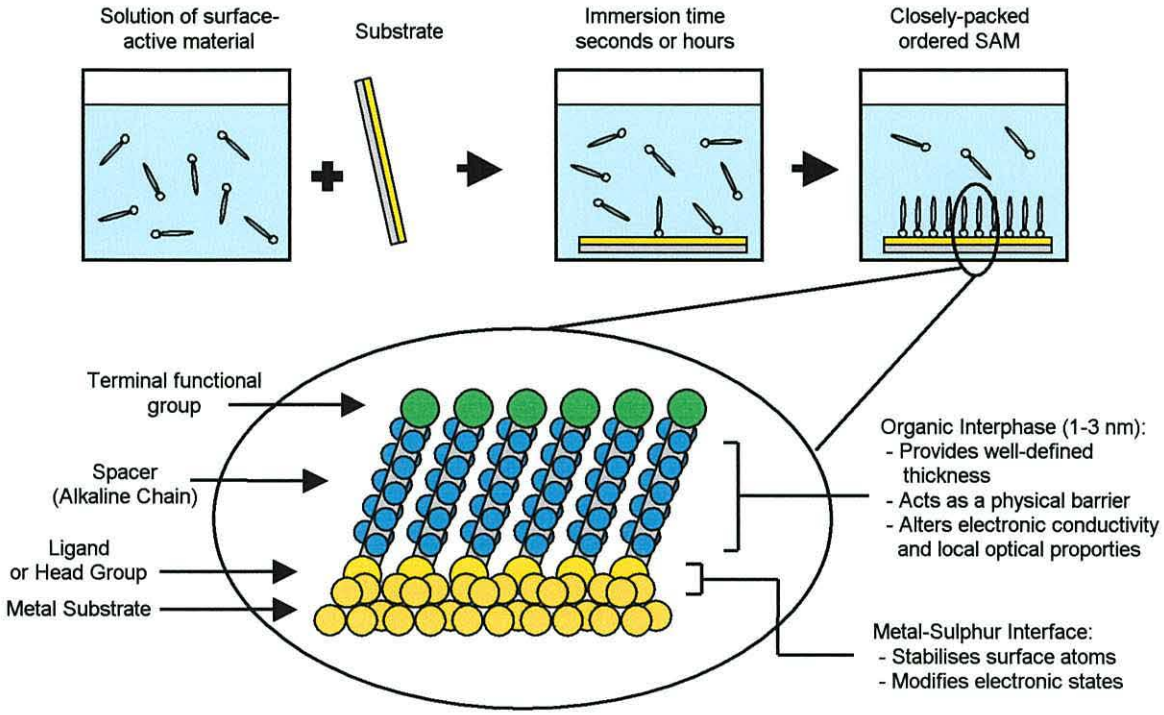

Figure 2 Formation of SAM by immersion of a substrate into a solution of surface-active material. The anatomy and characteristics of the SAM are highlighted.

Twenty four years after the pioneering work of Nuzzo and Allara, into thiols on gold [33], the area is still growing and becoming more diverse. The number of published articles on self-assembly (SA) is constantly increasing, and several different varieties of SAMs have been investigated, including alkanethiols on Au (see Figure 3), Ag, and Cu, and alkyltrichlorosilanes on SiO_2 [34], Al_2O_3, and mica [35]. There have also been a number of reports that have examined the assembly of SAMs on the surface of liquid mercury [36],[37],[38],[39].

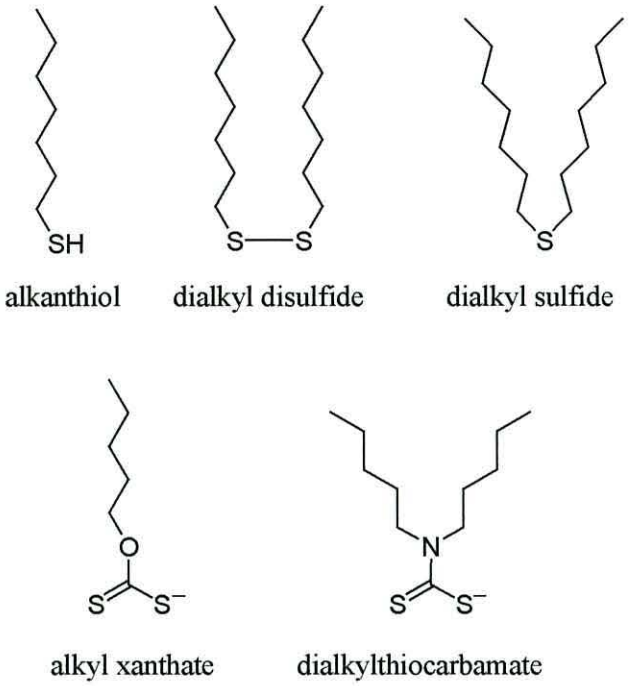

Figure 3 Surface-active organosulphur compounds that form monolayers on gold [35].

Gold is a good substrate for studying SAMs because it is easy to obtain, both as a thin film and as a colloid. Also, it is straightforward to prepare thin films of gold, e.g. by physical vapour deposition. Although expensive, and not essential to most studies of SAMs, single crystals are available commercially. Gold is a reasonably inert metal: it does not oxidise at temperatures below its melting point, it does not react with atmospheric O_2 or most chemicals [40]. Thin gold films are common substrates, used for a number of existing spectroscopies and analytical techniques, including surface plasmon resonance (SPR), and QCM. These characteristics of gold make it a good choice as a substrate for studying SAMs.

Gold binds thiols with a high affinity. The formation of a thiolate bond requires the chemical activation of the S–H bond of the thiol, or the S–S bond of the disulfide. The adsorption, more exactly chemisorption, of simple alkanethiols onto gold surfaces in solution leads to the loss of one hydrogen from its thiol group (–SH). At this point the molecule gains a negative charge ($-S^-$), which forms a bond with a metal ion (Au_3^+). If the thiol hydrogen is not lost in the form of H_2, the presence of oxygen in the reaction medium may also lead to the formation of water. The combination of hydrogen atoms at

the metal surface, to yield H_2 molecules, is an important exothermic step in the overall chemisorption energy.

Thiols and disulfides, bound to gold surfaces, are the subject of intensive studies. Initially it was assumed that the S atoms occupied the 3-fold hollow sides of the Au (111) surface [41],[42]. This assumption is now being challenged; a wide range of experimental and theoretical studies concluded that the sulphur was directly bound to only one metal atom [42],[43],[44]. This very strong chemical bonding corresponds to an energy of ~ 40 kcal mol^{-1} [35]. There are a number of different reports on chain tilt in SAMs on gold, these report a systematic dependence of the tilt structure (i.e. the tilt angle and the tilt direction) of the alkanethiols as a function of the chain length (C10-C30). On Au(111) ordered surface structures, a full coverage monolayer is a ($\sqrt{3} \times \sqrt{3}$)R30° lattice [45],[46],[47]. This supports the evidence that alkyl chains in SAMs of thiolates on Au(111) are usually tilted ~26-32° from the surface normal [35],[48],[49],[50].

SAMs naturally exhibit a high degree of structural order after assembly [51]. Most SAMs are formed at a reactive interface, i.e. the adsorbate and the substrate are both transformed to some degree by the reaction that leads to the formation of the SAM. Their structures are usually perceived to contain few defects. This is due to the structures being substantially more complex than the simple, but highly ordered, arrangements that are commonly assumed. External factors, such as: cleanliness of the substrate, methods used for substrate preparation and the purity of the sample solution, can all affect defects in SAMs. The substrates on which SAMs are formed have many structural defects, e.g. polycrystalline gold can possess grain structures characterised by dense arrangements of integration boundaries, occlusions and other structural irregularities [40]. Moreover, careful control of experimental methods can minimise complications in the final structure formation. STM investigations revealed that there were many defects in SAM such as missing-rows and pits [52],[53],[54]. These findings were later confirmed with the defects being attributed to an etching process of the gold by the adsorption of the SH group to the Au(111) surface [54]. The missing-row defects were attributed to the orientational and translational domain boundary, pits were

revealed to be the vacancy island of the gold atoms [55]. It is important to reduce the density of defects and this is possible (e.g. by thermal annealing of SAMs at 70-100 °C). However, during annealing, precise control of the temperature is required in order to avoid desorption of the molecules, this is true for all practical applications of SAMs [52]. There are also different kinds of SAM defects, which are not related to the characteristics of the substrate or the purity of the adsorbates. These are the defects that are intrinsic to the dynamic nature of the SAM itself, and the chain dynamics of alkanethiolate SAMs on gold are the perfect example.

2.2 Electrostatic self-assembly

A new method for creating ultra thin films, based on the electrostatic attraction between opposite charges, was first proposed by Iler in 1966 [56], and was first observed practically in the early 1990s by Decher's group [57],[58]. This technique is also known as "self-assembly" adsorption [59], "layer by layer" method, or (the most popular) electrostatic self-assembly (ESA). It relies on the alternating adsorption of anions and cations, which leads to the formation of multilayer assemblies [60],[61]. These multilayer structures are fabricated as outlined schematically in Figure 4.

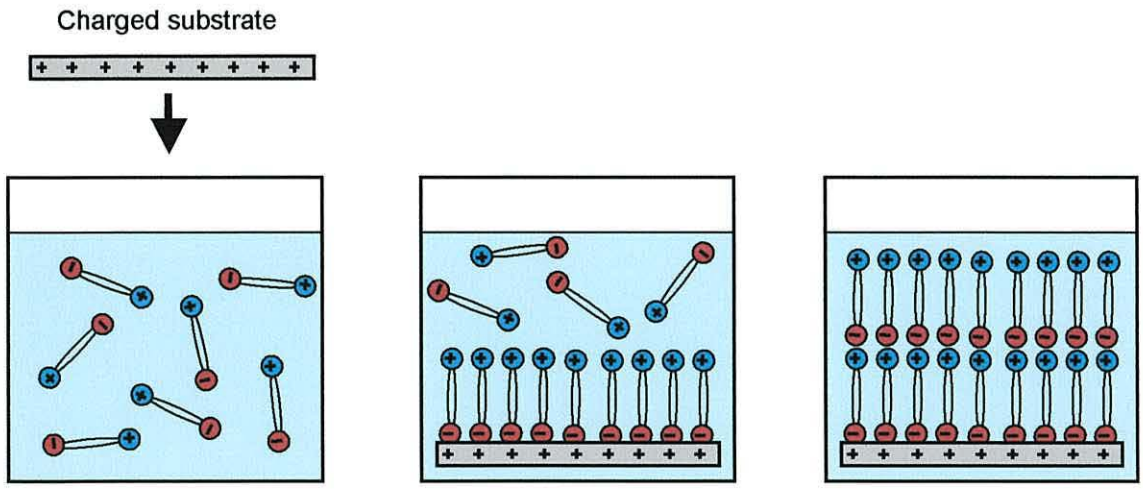

Figure 4 Simplified molecular picture of the first two adsorption steps, depicting film deposition starting with a positively charged substrate.

A positively charged solid substrate (but also an inert surface, such as graphite) can be immersed into a polyanionic and then a polycationic aqueous solution; electrostatic interaction between them occurs to create a monolayer. Deposition of the second layer is usually a longer process, because the polycationic moieties penetrate spaces between those previously deposited.

There are two important factors involved in the ESA technique that can affect the order of the films produced. The first of which is the immersion time, which depends on the material used and its concentration. There is no restriction, with respect to substrate size and topography, because the process involves adsorption from solution. The most extensively studied materials for ESA are polyelectrolytes (see Figure 5), charged nanoobjects, such as molecular aggregates (small organic molecules, polymers, natural proteins), inorganic clusters and colloids; so this method of deposition may have a variety of applications.

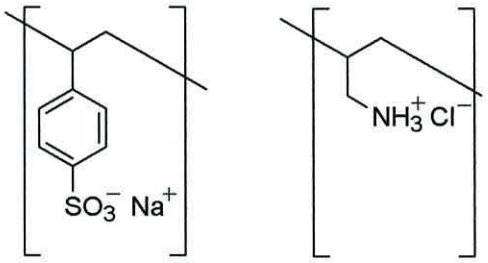

Figure 5 Structures of two polyions, the sodium salt of poly(styrene sulfonate) (left), and poly(allylamine hydrochloride) (right).

The adsorbate-adsorbate interactions are usually comparable in strength to the adsorbate–substrate interactions, all of which are dominated by van der Waals forces [62]. Interactions between most charged species are highly specific and go beyond the simple Coulomb law, e.g. very different behaviour of AgCl and $AgNO_3$ was observed compared to KCl and KNO_3 even though the hydratation energies of Ag^+ and K^+ are virtually the same [61].

The major advantages of ESA from solution are that many different materials can be incorporated into individual multilayer films and that the film architectures are

completely determined by the deposition sequence. Also, features such as simplicity, versatility and speed, characterise this technique.

3. Monolayer characterisation methods

Monolayer characterisation methods allow the exploration of organic surfaces at different scales in various ambient conditions. Making use of them has allowed us to approach the nanoworld in various ways, which go far beyond pure optical imaging of a surface. Being able to manipulate single molecules at room temperature [63] has opened new avenues towards the study of conformational and nanomechanical properties of individual molecules [64]. Probing the electronic properties of single molecules by means of scanning tunnelling spectroscopy (STS), using an STM tip to study the electroluminescence of a conjugated thin film [65], and detection of micromass changes (and physical properties) of thin layers using QCM [66],[67], are just a few examples. Other experimental techniques including X-ray photoelectron spectroscopy (XPS) [68], SPR [69], and X-ray diffraction (XRD) [70] have also been used to characterise organic thin films (e.g. their thickness and purity). These techniques possess high sensitivity and are able to identify chemical elements down to 0.1 % in concentration. XPS is probably the most utilised for recognition of chemical surfaces of monolayers, and it relies on the electron spectra emitted from core atomic levels under irradiation of X-rays.

The QCM and SPR techniques can be used to monitor adsorption of the organic materials onto metallic surfaces from the solution phase, both have similar resolution and follow deposition in real time [71],[72]. In this Chapter the QCM technique and current-voltage (I-V) characteristics from STM are described.

3.1 Quartz crystal microbalance (QCM)

The mechanism of the QCM technique relies upon the piezoelectric effect in quartz crystals. The theoretical foundation of piezoelectricity was first pioneered by Raleigh in 1885, but the first investigation was performed by the Curie brothers in 1880 [73],[74].

QCM is a simple, cost effective technique, which is used to detect the mass changes and physical properties of thin layers deposited on crystal surfaces [66],[73]. A single QCM is a thin quartz disc with metal electrodes attached to both sides (see Figure 6), the

quartz crystal is an anisotropic piezoelectric material. Typically, for QCM applications, quartz crystals a few tenths of a mm in thickness are cut in the AT form, at an angle of approximately 35° with respect to the X-axis [66],[73],[75],[76]. This geometry provides stable oscillations, which contribute to the extremely sensitive nature of piezoelectric devices towards mass changes.

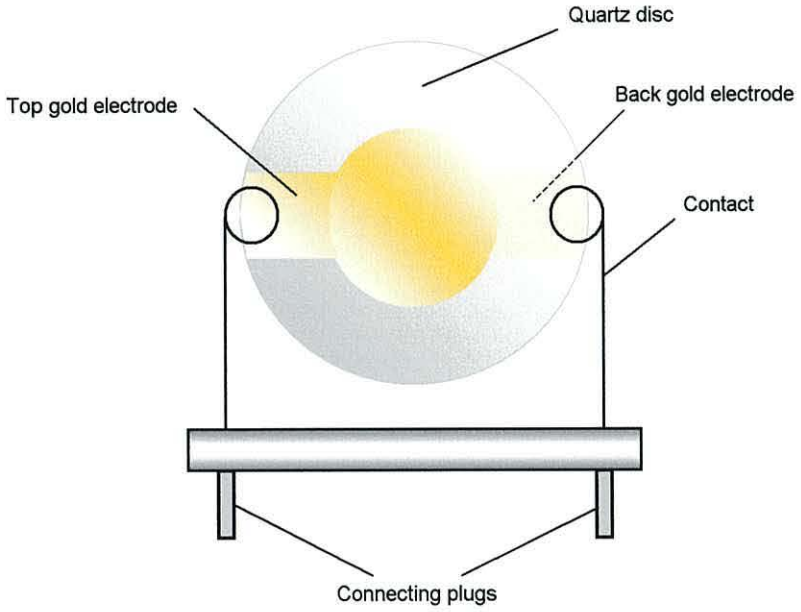

Figure 6 Schematic of a QCM with deposited electrodes.

A resonant oscillation is achieved when the crystal is included in an oscillation circuit, in which the electric and the mechanical oscillations are near to the fundamental frequency of the crystal. The fundamental frequency depends on the thickness of the wafer, its chemical structure, its shape and its mass. In 1959, Sauerbrey [77] provided a description and experimental verification of the mass/frequency relationship of rigid deposited layers on the quartz crystal electrodes. The results from this work are embodied in the Sauerbrey equation, which relate the mass change per unit area at the crystal electrode surface to the observed change in oscillation frequency of the crystal:

$$\Delta F = \frac{-2F_0^2}{A\sqrt{\rho_q \cdot \mu_q}}\Delta m \qquad (1)$$

Where ΔF is the calculated frequency shift; F_0 the unperturbed resonant frequency (obtained without mass adsorption); Δm the mass change; A the piezoelectrically active area of the excitation electrodes (0.196 cm^2 in many applications); ρ_q the density of quartz (2.65 g/cm^3) and μ_q the shear modulus of quartz ($2.95 \cdot 10^{11}$ dyn/cm^2).

According to equation *(1)* the resonant frequency decreases proportionally to the mass of the layer adsorbed on the electrodes.

There has been increasing interest in use of the QCM technique for aqueous-based biological applications [66],[74],[78]. Moreover, due to its inherent ability to monitor processes in real-time, it has found a wide range of applications in the areas of environmental, food and clinical analysis [74].

3.2 Current - Voltage (I-V) characterisation using scanning tunnelling microscopy (STM)

Gerd Binnig and Heinrich Rohrer, from the IBM Research Laboratory in Zurich, received the Nobel Prize in Physics for the invention of the STM [79]. This development lead to the understanding of surface topography, composition, structure and mechanical properties [31]. STM allowed, for the first time, the production of real–space images of electrically conductive surfaces with resolution on the sub-nanometer scale [80],[81].

STM is a part of STS, and is related to scanning probe microscopies (SPMs). A significant advantage of SPMs is that they can operate in different media; such as air, liquid and gas streams, therefore allowing investigations in environments that are more easily accessible and less expensive than UHV [81],[80]. The main principles of STM operation and also SPM are the same. The tip or probe (usually PtIr or Au), the end of which is formed by a single atom, is connected to a source of bias voltage (typically applied bias voltage $\leq$ 1.5 V with respect to the sample surface), which causes the tip to be positioned above the surface. When the tip is brought to within 2-5 Å (~ atomic diameters) of a conducting surface, electrons are forced to tunnel across the gap (it is

called the tunnelling current) from the sample through the gap into the tip (see Figure 7a), or vice versa (see Figure 7b), depending on the experimental setup. The interaction between the sharp tip and the conductive sample surface is observed as a change in current during scanning. The tunnelling current decays exponentially with the gap between the two conductors (see Chapter 4.1.). Therefore a small change in tip-sample distance results in a large change in the tunnelling current.

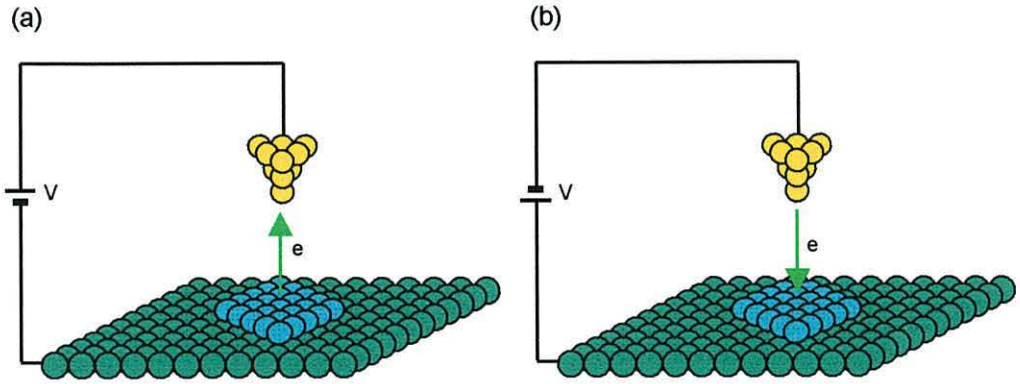

Figure 7 Schematic of the STM studies of molecular monolayers, showing the tunnelling barrier between the sample and STM tip. The diagram is not to scale.

While the tip is moved in the X and Y directions across the surface, using a piezoelectric crystal, a detection system records the tunnelling current at each scanning point (current is usually in the range of a few hundred pA to a few nA). This creates the current-voltage characteristics of the materials under study [82],[83], and atomic/molecular scale resolution images [84],[85],[86]. The quality of results is strongly limited by factors such as the bias voltage dependence and special tip states (generally the sharper the better) [87],[88],[89]. With the atomic resolution of STM, it is possible to determine the structure and conformation of adsorbed molecules on a metallic substrate [82],[88],[89]. It is important to consider how the presence of a molecule in the STM junction influences the electron transport. When the sample is biased negatively, electrons travel from the filled surface states to the tip through the highest occupied molecular orbital (HOMO) of the molecule. Whereas in the opposite case, of a positively charged sample, the lowest unoccupied molecular orbital (LUMO) of a molecule is involved. In both cases, the HOMO and LUMO are closer to the Fermi energy level of the substrate and tip respectively.

The main challenge in STM measurements is the positioning of the tip. The distance between the tip and the sample has to be precisely controlled without any interference, such as electrical or mechanical noises, or thermal effects, to prevent penetration of the tip into the sample. The control is maintained via a feedback loop, which is responsible for height adjustment of the tip, controlled by a piezoelectric element to keep the current constant. The feedback loop moves the tip away from the surface when the tunnelling current increases; if the tip is brought closer, the tunnelling current decreases. In the event of an atomically flat substrate, the tip is kept at a constant Z-distance position, so there is no need for control over the tunnelling current. The biggest limitation of STM is that it cannot image thick insulating layers, but according to estimates, the thickness of a non-conducting layer can be, at maximum around 2 nm at probing currents in the picoampere range [81].

An early demonstration of electrical characteristics, from relatively symmetric to highly asymmetric (or rectifying), obtained by STM, was made by Pomerantz *et al.* [90]. Copper phthalocyanine molecules were chemically attached to highly oriented pyrolytic graphite (HOPG). However, the observed asymmetry may have been due to formation of a Schottky barrier (described in more detail in Chapter 4.2.) from the chromium salt, formed by an acid-base reaction at the surface. Another example of STM being used to measure the I-V characteristics of SAMs used alkanethiolates. These have been used as model systems for measurements of electron transport through molecules. Alkanethiolates form excellent host matrices due to their ability to self-assemble, and dynamic formation allows the control of film quality. Moreover, they are chemically inert and have low electrical conductivity. Experiments performed by Weiss *et al.* [4] involved probing a SAM of decanethiol. The film was shown to give symmetrical I-V characteristics. As alkanethiolates are often used as an insulating host matrix, their electronic characteristics establish the background currents for many of the techniques used to characterise other molecules. More about STM techniques can be found in Chapter 4.3.1.

4. Molecular electronic junctions

The theme of molecular electronic junctions concerns electron transport through organic molecules and often involves metallic or semiconducting solids with which the molecules are in electrical contact. In order to transmit electrons through the molecule, molecular junctions incorporate one or more molecules in electrical contact, with usually two conductors [91]. Complete understanding of a molecular junction requires a view of the entire structure, as one electronic system, in order to consider perturbations of each component due to electronic interactions with others. Understanding how electrons traverse through the molecular junction is an important step towards the realisation of molecular electronics.

In particular, two main transport junctions have been considered, most commonly a SAM deposited on a metallic surface which is then measured, e.g. with a scanning probe tip, and a single molecule chemically bonded to metal electrodes through thiol linking groups [92]. Measurements in both of these systems record a current between the electrodes due to an applied voltage. A single molecule junction occurs when a single molecule can be observed to behave independently. The term "monolayer junction" is reserved for many molecules in a single oriented monolayer between the conducting contacts. A monolayer junction is intermediate between a single-molecule junction and a disordered (or crystalline) thin film device. In practice, a monolayer junction may be observed to exhibit molecular electronic properties such as rectification and conductance switching. The molecules in the junctions, on which this Chapter is focused, can be divided into the hard, rigid, linear structures characterised by molecular wires and the soft molecular organic materials such as 1,4-denzene dithiol or copper phthalocyanine.

4.1 Electron transport in molecules

Studying electron transport across nanometer scale metal-molecule-metal junctions is a key to the realisation of molecular-based electronics. The study of electronic devices based on molecular junctions requires characterisation of particular junctions with theoretical approaches to electron transport.

Electron transport mechanisms depend on molecular size, structure, temperature and the magnitude of the free energy difference between donor and acceptor. General electron transport, called tunnelling, is dictated by quantum mechanics and is based on the probability of an electron traversing a barrier of some thickness and height. The rate of tunnelling decreases exponentially with the thickness of the barrier, and is given in its simplest form, by the Simmons relation [93]:

$$J = B \cdot e^{-\beta d} \qquad (2)$$

Where J is current density, A/cm^2; B is a constant, and depends on the applied voltage, thickness, and height of the energy barrier; β is a constant, proportional to the square root of the barrier height, nm^{-1} or Å^{-1}; and d is barrier thickness.

Although observed tunnelling rates in molecular junctions depend exponentially on the junction thickness, the observed value of β assumes a different value. It is known from the Simmons relation that β values in molecular junctions are often near 1.0 Å^{-1} [36], whereas for weaker contacts this value is higher [83]. This characteristic is inversely proportional to the conductance. It can be used to classify the ability of molecular structures to provide a medium that facilitates tunnelling and to infer details of the electron transfer [94]. Conductance of SAMs in good contact with electrodes is generally dominated by superexchange [95]. Tunnelling that is assisted by superexchange usually occurs to ~25 Å. More complex phenomena, such as diffusive tunnelling or hopping, dominate over these distances [83]. Another factor that distinguishes these mechanisms is temperature. Hopping mechanism usually refers to thermally activated electron transfer based on a classical Arrhenius relation, whereas, tunnelling with or without superexchange should not depend on temperature (with some exceptions like conformational changes). Hopping involves electron motion over the energy barrier between relatively stable sites and is inversely proportional to the thickness barrier [83].

4.2 SAM based molecular junctions

The success of vapour deposition using a variety of metals on SAMs, for making a top electrode contact depends, in part, on reactions between the SAM and the metal. A Au/monolayer/Au junction incorporating the 2'-amino-4-ethynylphenyl-4'-ethynylphenyl-5'-nitro-1-benzenothiolate presented by Reed and Tour [96],[97],[98] is an example of electrode fabrication. The essential feature of the fabrication process was the use of a nanoscale device area. The starting substrate for the device fabrication was a double-sided polished silicon (100) wafer, on which 50 nm of Si_3N_4 was deposited by low-pressure chemical vapour deposition [98]. The authors estimated that the single circle hole of 30-50 nm diameter was made through the membrane by electron beam lithography, and contained ~1000 oriented structure [83]. The nanopore was filled with gold and then transferred into a solution to self-assemble the active component. The second Au electrode was evaporated on top of the molecular film, and then the device was diced into individual chips (see Figure 8a).

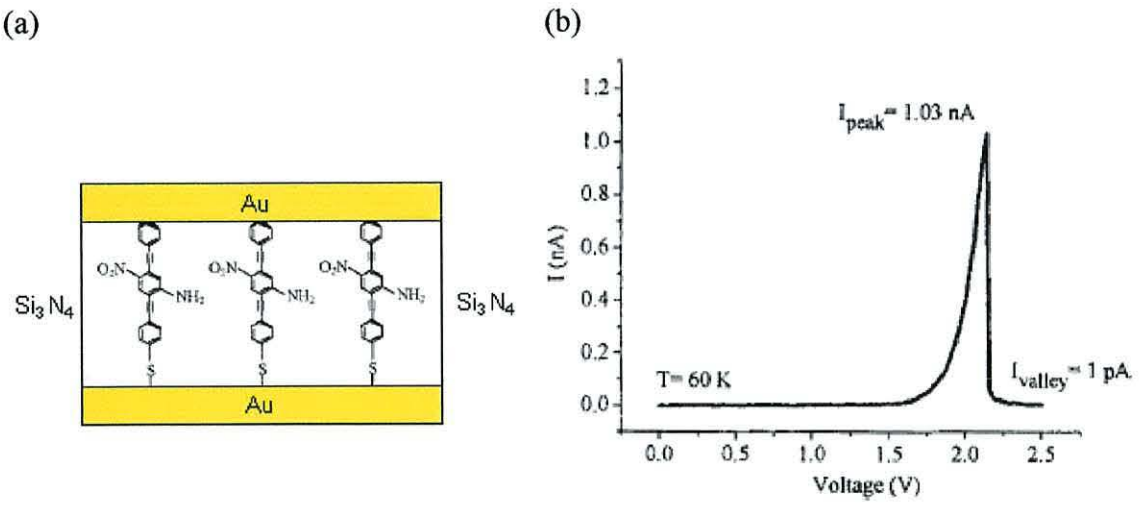

Figure 8 (a) Schematic illustration of the Au/SAM of 2'-amino-4-ethynylphenyl-4'-ethynylphenyl-5'-nitro-1-benzenothiolate/Au junction in the nanopore area. (b) I-V curve of the nanopore junction at 60 K. Taken from [83].

In this experiment the authors observed negative differential resistance (NDR) for the nanopore junction at 60 K (see Figure 8b). The I-V curves were fully stable and

reversible, and were a stimulus to consideration of practical applications of molecular electronic devices.

Many evaporated electrodes are oxidisable in air, for example, titanium [99],[100], aluminium [101] or lead [102], and this leads to Schottky barrier formation. The Schottky effect is attributed to the reduction of the potential barrier at interfaces of semiconductors with metals or others semiconductors, and it can induce very strong electrical asymmetries [83],[103]. A Schottky barrier usually arises from partial charge transfer from one phase to another at an interface, generating an electrostatic barrier. There are various examples of Schottky diodes, which can be observed during the measurement of electrical conductance for numerous different films. For example, alkoxynaphthalene thiol sandwiched at room temperature between Pt and an evaporated Ti film demonstrated strong current asymmetry with a rectification ratio of 5×10^5 at $\pm$ 2.3 V [100]. This is a perfect example of electrical asymmetry induced by metal oxide Schottky barrier. Another study showed a rectification ratio of more than six orders of magnitude for a Pd/n-Si diode at 700 °C [103]. The next class of compounds that are receiving attention, due to their interesting electrical characteristics, are metalophthalocyanines. Many metalophthalocyanines are known to exhibit p-type semiconducting electronic transport properties, when exposed to an oxygen-containing atmosphere [104]. It is supposed that oxygen partially "dopes" the material, creating highly delocalised holes as the charge carriers. Some metalophthalocyanines exhibiting such interesting doping have also demonstrated the Schottky effect [105]. Other experiments, which use acid-base reactions to attach molecules of copper phthalocyanine to the surface of HOPG, exhibited a rectifying Schottky barrier [90]. Consequently, metal evaporated junctions could be promising; however, the Schottky effect leads to highly unreliable results.

Another molecular junction, constructed between two mercury drops, or between Hg and solid metal (Au, Ag, Cu), was proposed by Majda [36] and Whitesides [94],[106]. The first reason for making these junctions was the advantage of using mercury as the electrode material. Mercury offers an atomically smooth, defect free, and highly reproducible surface for alkanethiol self-assembly. The use of Hg electrodes allows the

variation of the thickness of the assembled monolayer in a number of different ways [36]. The first involves the usual formation of ordered monolayers of thiols with varying lengths of alkyl chains, the second relies on the hanging mercury drop electrodes (HMDE) [37],[38]. Careful expansion of the mercury drop by means of the micrometric screw that controls the volume of drop, affects the monolayer thickness. Furthermore, the high surface tension of Hg should reduce the likelihood of metal penetration into the SAM, thereby reducing short circuit formation. Figure 9 presents both junction designs, in both cases formed whilst the Hg drop was immersed in a solution of active component.

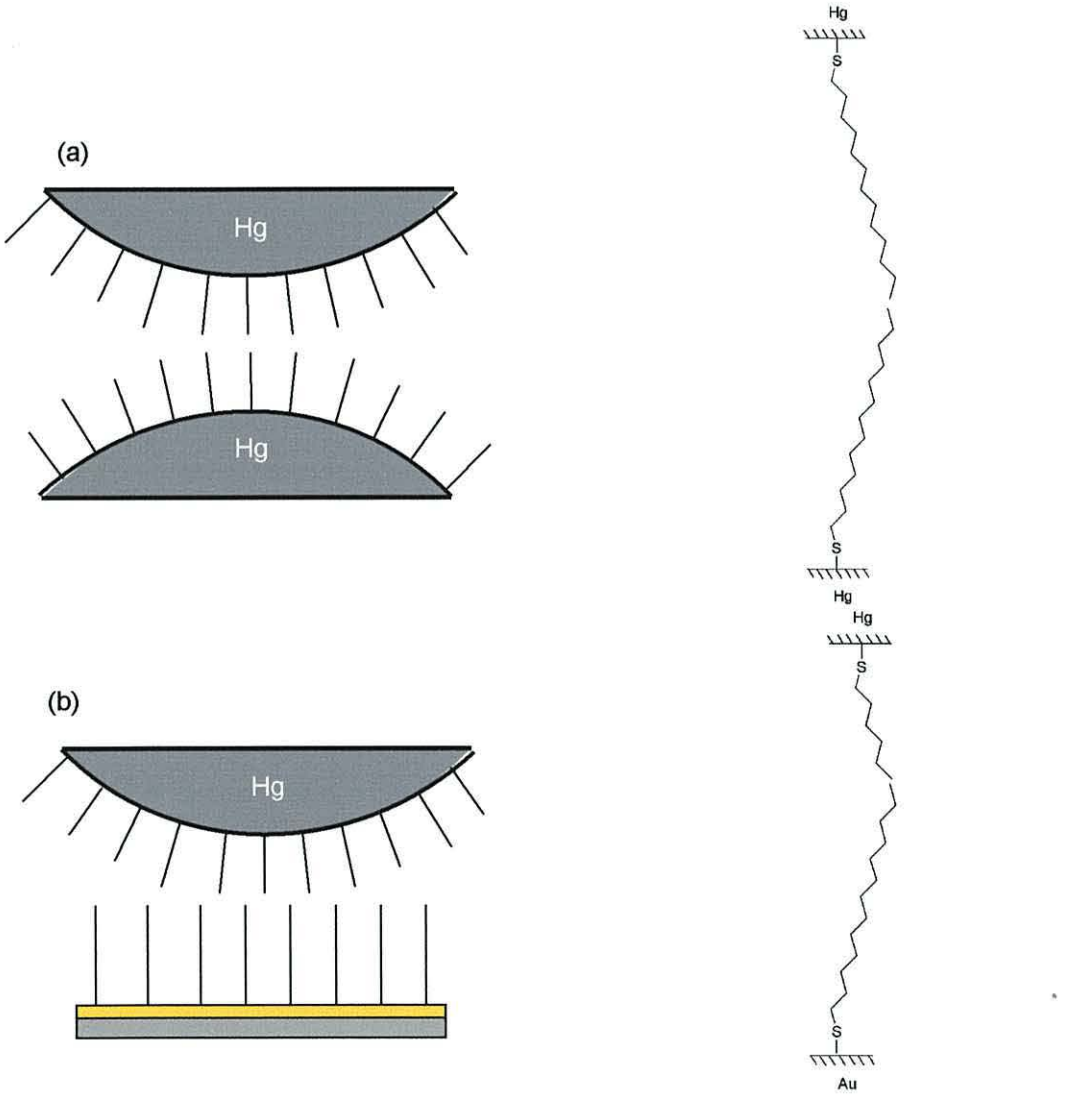

Figure 9 Schematic diagram of (a) Hg-SAM//SAM-Hg and (b) Hg/SAM//SAM/Au junctions. For (a) the two Hg drops are brought together in a solution of an alkanethiol. For (b) the Hg drop is lowered through the thiol solution onto the preformed SAM on the flat Au substrate.

The Hg/SAM interface is much larger in area compared to the nanopore, measuring ~1.0 mm in diameter and containing 10^{11}-10^{13} molecules [83]. Additionally, fabrication of this junction avoided lithography and the risk of monolayer damage by vapour deposited contacts. Despite this technique having the advantage of easy assembly, it does not have molecular resolution and is not amenable to incorporation in a practical microelectronic device. Recently, a review of this technique was published [107]. It provides similar data to those obtained via STM and is an appropriate method for supporting results.

The next fabrication method for molecular junctions incorporates two μm gold wires aligned perpendicular to each other. A SAM of the molecule of interest is deposited on one of the wires. The crossed-wire tunnel junction consists of the wire modified with a SAM, and a second wire, which can be brought into contact by fine-tuning of the deflection current obtained in the presence of a magnetic field. In this junction electron transfer occurs between closely positioned wires as a result of physical contact between the monolayer and the deflection wire [108],[109],[110] (see Figure 10).

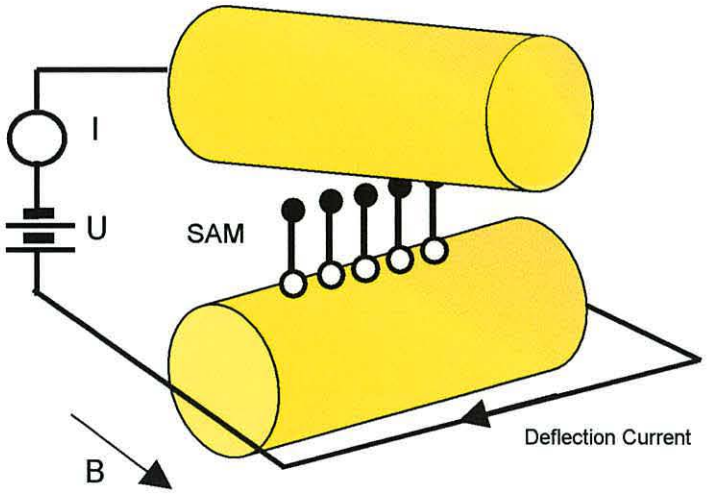

Figure 10 Schematic of the crossed-wire tunnel junction [106].

Charge transfer measurements across a monolayer of dithiol molecules was first presented by Kushmerick *et al.* [108],[109]. Comparison of conductance measurements from STM and crossed-wire junction techniques, for the same group of dithiol molecular wires, showed that the conductance rose linearly with the number of

molecules [94],[108]. Studies on highly conjugated molecular wires, such as oligo(phenylene ethylene) (OPE) and oligo (phenylene vinylene) (OPV), highlighted a particular contribution to molecular wire conductance [108],[109],[111]. Namely, it was shown that STM measurements on single molecules correlated with crossed-wire measurements of 10^3 molecules [108],[112]. The fabrication of a single molecule junction was performed by self-assembly of a single dithiol molecule onto a gold substrate, surrounded by C11 thiol molecules. The important factor was the possibility of the C11 molecules interacting with the nanoparticle, which would contribute to the overall measured tunnelling current [112]. The contact was formed via gold nanoparticles, to which dithiol molecules were covalently linked. This experiment indicated that intermolecular charge hopping did not strongly contribute to charge transport in a SAM [112].

4.3 Single molecule junction

The experimental techniques presented above, containing SAMs sandwiched between two metal electrodes, have been employed to determine the electrical conductivity of SAMs. Several methods to measure the conductivity of single molecules, chemically bonded between two metal electrodes, were proposed by Haiss *et al.*, Cui *et al.* and Xu *et al.* and are presented in this Chapter. Behaviour of single molecule junctions is not complicated by intermolecular interactions; it can be said that they represent the lower limit in dimensions for molecular electronics.

4.3.1 Scanning tunnelling microscopy (STM) techniques

A novel and simple method to measure single molecule conductivity, using the spontaneous formation of molecular wires between the STM tip and a metal substrate, was introduced by Xu, *et al.* [113], and Haiss *et al.* [114]. To use this type of method, molecules must possess thiol groups at both ends, which enable adsorption to the gold surface and to the STM tip, the molecules must also be highly stable in the redox states [114],[115]. It has been shown that dithiols adsorbed on to gold for short periods of time, hence may form a molecular bridge between the tip and substrate contacts [115],[116]

(see Figure 11a). These events can be monitored in the time domain; a characteristic current jump is presented in Figure 11b.

(a)

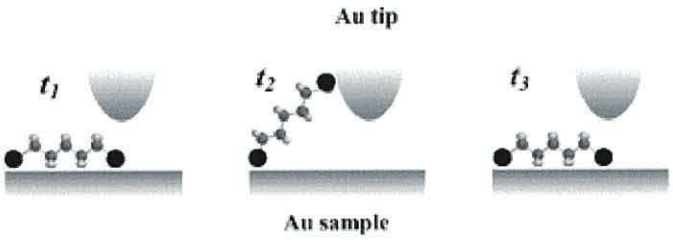

(b)

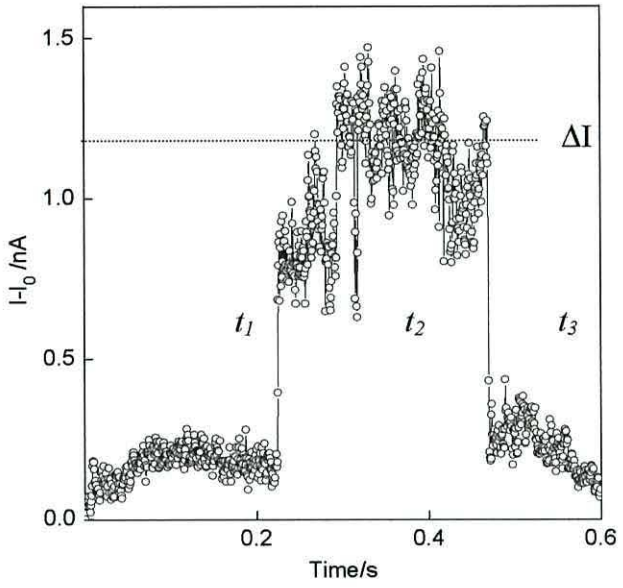

Figure 11 (a) Schematic diagram of an experiment showing the spontaneous formation of a single molecular wire between the tip and the substrate. At t_1 and t_3 the molecule is detached from the tip, and at t_2 the molecule is attached to both electrodes, giving rise to an increased current (ΔI). Copied from [114]. (b) Typical current jumps recorded on Au covered with a small surface concentration of molecular wire. Circles: original data; line: average of four data points.

The current-time measurements (I(t)) on surfaces, with high dithiol coverage, yielded large current fluctuations consistent with fast formation and breaking of molecular wires. Due to the high current noise no plateau formation (as shown in Figure 11b) could be observed, and hence they were unsuitable for measurements of single molecule conductivity.

The conductivity of the molecules in the gap can be calculated from the current jumps using the tunnelling current (I) as a function of time. When molecular bridges are formed, a sudden current jump is observed as ΔI ($\Delta I = I - I_0$, where I – current, I_0 – tunnelling current before the observation of the current jump). This method measured the difference in tunnelling current in the absence and presence of molecules in the tunnelling gap and hence, changes in conductance resulting from the incorporation of a molecule in the gap [114].

Observation of dithiol molecules, adsorbed on a metal substrate at low concentration, showed that the molecules spontaneously spanned the gap between the substrate and the STM tip. This was employed to investigate the current-distance dependence (I(s)) and hence measure the conductivity of a single molecule. This is the next simple and reproducible method, also introduced by Haiss *et al.* [115], to measure the conductivity of single molecules by comparison of I(s) curves in the presence and absence of molecules in the tunnelling gap [114],[115],[117]. The I(s) method of forming molecular wires between a gold STM tip and a substrate is illustrated in Figure 12.

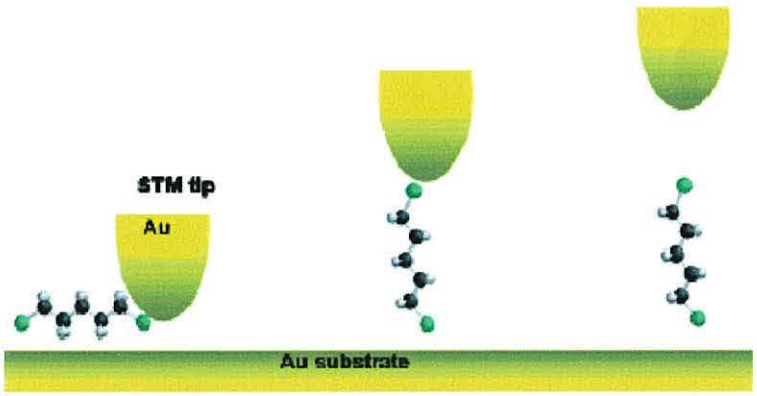

Figure 12 STM technique (called the I(s) method) of forming molecular wires between an Au tip and a substrate for single-molecule electrical property measurements. Taken from [117].

When the STM tip was brought close enough to the Au surface, which was experimentally achieved by increasing the tunnelling current setpoint (I_0), spontaneous formation of stable molecular wires between the tip and the sample was observed (see Figure 12). The tip was then lifted keeping a constant X-Y position, and the current-

distance I(s) relation was measured. Figure 13 presents typical current decay curves (I(s) scan) in the presence and absence of molecule(s) in the tunnelling gap.

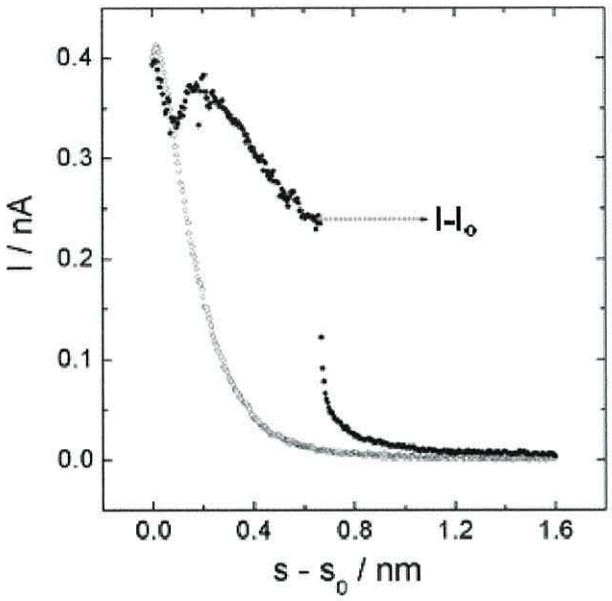

Figure 13 I(s) scan performed in the presence (solid circles) and the absence (open circles) of molecule(s) between tip and substrate. Taken from [114].

Two distinctive classes of I(s) scans were measured. The first of which was a fast exponential decay, typical of tunnelling between a tip and a substrate (open circles in Figure 13). The second was a less abrupt decay, followed by a characteristic current (I-I_0) (solid circles in Figure 13). At sufficiently large tip-sample separations the chemical contact of the molecular wire to the tip (or to the surface) was broken and the current dropped to zero.

The electrical conductivity of single alkanedithiol molecules was investigated over a range of temperature. Consideration was given to the temperature dependent conformer distribution and its influence on the tunnelling probability in a barrier tunnelling model [118]. This model also predicted an increase of the temperature dependence (in the range between 293 K and 353 K) of conductance with increasing chain length. Moreover, it has been found that the conductivity of single alkanethiol molecules is independent of the applied potential in the range from –1 to +1 V [114]. Similar experiments, relying on conductivity measurements for alkanedithiol molecules

chemically bonded between two metal electrodes, were investigated by two independent groups; Cui *et al.* [119] and Xu *et al.* [113]. The STM technique of single molecule electrical current measurement is also widely used in biological systems [120].

4.3.2 Break junctions

A conceptually simple configuration of a break junction would be one in which one molecule (or a few) is connected between metallic contacts. Such a metal-molecule(s)-metal configuration was first reported by Reed and Tour in 1997 [97],[98],[121]. The schematic process of the mechanically controllable break junction (MCB) is shown in Figure 14.

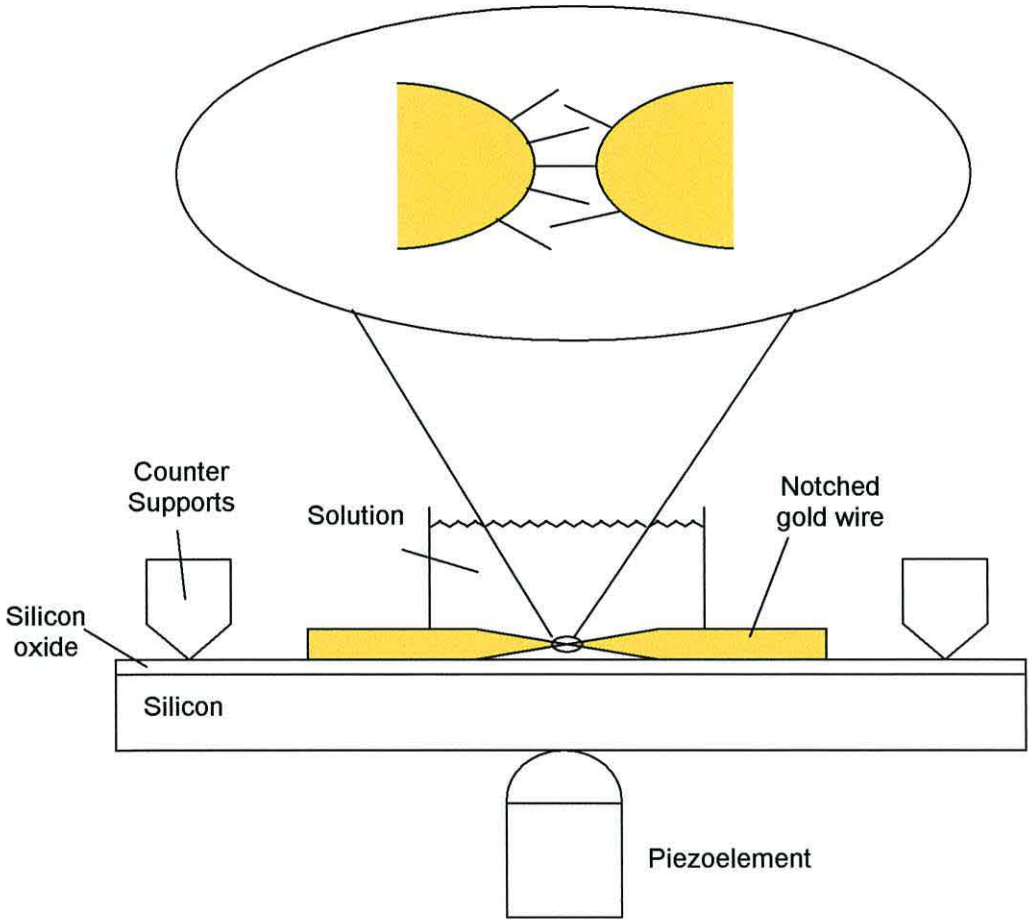

Figure 14 Schematic of the mechanically controllable break junction (MCB) showing split wire with deposited monolayer. Taken from [121].

In this approach, a notched wire is stuck onto a flexible substrate and is then fractured, and as shown in Figure 14, the wire breaks into two parts when a "bending beam" is stressed. The whole process takes place in a solution of dithiol molecules, slow elongation allows molecular layer assembly. After the adjustable gap between two Au contacts is established, the two half-wires are moved close together to establish the contact, which occurs via a single molecule (see Figure 14). For the molecules of benzene-1,4-dithiol used by Reed, I-V and conductance measurements of a singular observation implied that the configuration of two noninteracting self-assembled molecules in parallel was possible; the threshold resistance of a single molecule configuration was ~22 MΩ [121]. The reproducibility of a minimum conductance, at a consistent value, implies that the number of active molecules could be as few as one. The results from this system, as would be expected, yielded symmetrical I-V characteristics. This technique was also used by Reichert [122], who used the same conductance measurements through a self-assembled metal-molecule-metal junction. The I-V characteristics of a symmetrical molecule were found to be highly symmetrical, whereas an asymmetric contact could cause strong asymmetries in the I-V curves. This asymmetry also proved that the junction indeed contained only one molecule. The rather strong covalent bonding to the atomically disordered metallic electrode caused sample-to-sample fluctuations [123], which are undesirable for both controlled scientific investigation and engineering of electronic properties.

4.4 Summary

All the techniques presented in this Chapter can be applied to the investigation of molecules that are able to form a covalent bond to the surface. It is useful to consider a few of the many technical challenges posed by measurements of molecular junction behaviour. The realisation of useful microelectronic devices, like memories or processors, based on molecular junctions, requires not only a large number of molecular junctions but also a combination of empirical characterisation, of particular junctions, with sophisticated application of theoretical approaches, to electron transport.

The variety of methods available for contacting molecules; including contacting monolayers, together with mercury drop electrodes (Hg-based junctions), using dithiolated molecules with crossed wires, and metal/SAM/metal junctions, have all demonstrated that contact to a single molecule is difficult to achieve. Even though the STM techniques and MCB techniques are reliable methods to measure the conductivity of a single molecule and are stable for many voltage sweeps, they still cannot be integrated into device geometries. Nevertheless, using the techniques of STM or MCB opens new possibilities for establishing mechanisms of electron transport in both organic molecules and transition metal complexes, with clear applications in both fundamental single-molecule science and single molecule technology.

5. Molecular wires

One of the requirements for molecular electronics is the ability to create good electrical contacts in a device [124]; molecular wires are key components in this field. In their simplest form they can be viewed as a π-electron conjugated system that forms a one-dimensional electronic conductor to interconnect proposed molecular devices such as transistors, switches, and chemical sensors [12],[125],[126]. In an effort to understand the important characteristics of molecular wires, most research has been concentrated on linear, conjugated, oligomers; many synthetic methods have been presented in the literature [12],[127]. Transport of charge is possible due to the delocalisation of π-electrons over the entire molecule; some examples of molecular wires are shown in Figure 15.

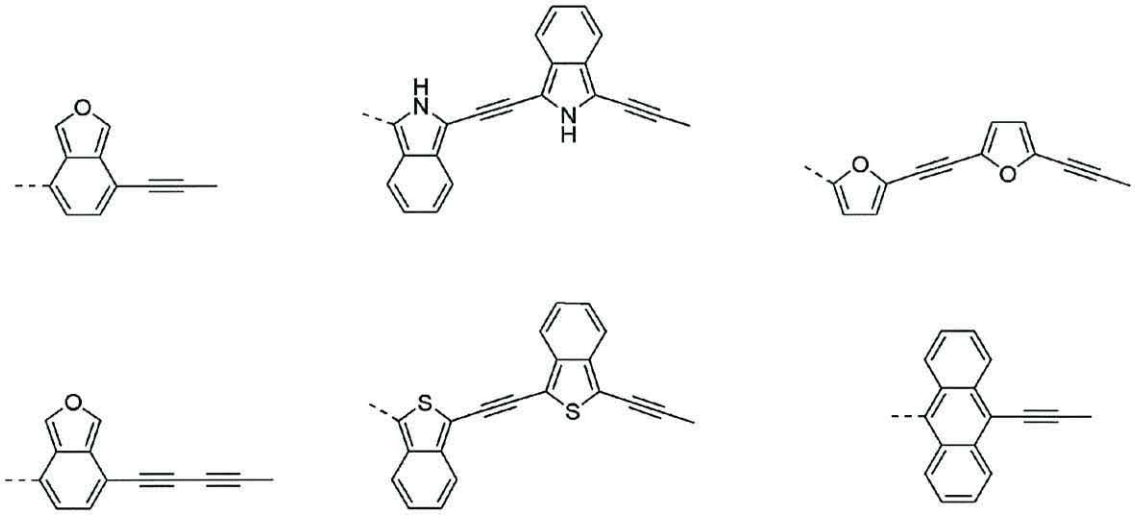

Figure 15 Examples of monomeric units of π-conjugated molecular wires [128].

Oxidation, reduction or introduction of a dopant into bulk structures can cause local deformation of the nuclear system and can create disturbances like polarons or charged solitons [129],[130]. Also, oxidation and reduction processes can make modifications to the structures resulting in salts with intra-chain charge carrier mobility, making it possible to create a junction. Good control of length, strength, periodicity and geometric parameters of molecular wires are useful in fabrication of nanodevices.

The conductivity of molecular wires is often associated with difficulties in connection of a single molecular wire to probes. Initially, Reed [99] developed a technique for determining the conductance of molecular wires using a nanopore arrangement, which was described in Chapter 4.2. Using this technique, I-V characteristics could be recorded on a series of molecular wire systems; and temperature-controlled variations demonstrated that the current could be modulated via temperature-induced variations in the molecular conformations. Collaboration between Weiss, Allara and Tour *et al.* [125] allowed investigations using mixed SAMs of molecular wires (4,4'-di(phenylene-ethynylene)benzenethiolate derivatives) and "nonconducting" (n-dodecanethiol) SAMs on Au(111) (see Figure 16).

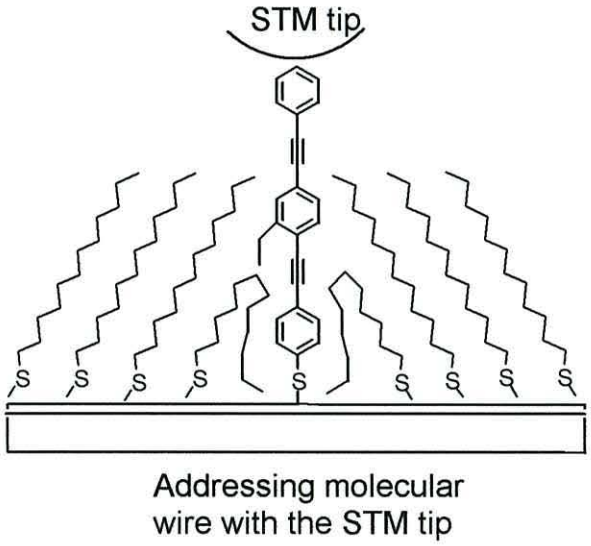

Figure 16 Single molecular wire inserted at grain boundaries within a SAM of dodecanothiolate on gold [125].

This technique permitted the isolation of single molecular wires from their neighbours; it also allowed the addressing of a vertically arranged system. Qualitative results of the conductance levels showed that the studied molecular wires, although topographically higher than the gold surface (as shown in Figure 16), were substantially more conducting compared to the insulating monolayer of n-dodecanethiol [125],[131]. This method, using mixed SAMs, could give more information on the conductivity of molecules, due to difficulties caused by the tunnelling barrier in obtaining an absolute value of conductivity for individual molecules.

Other methods allowed precise placement of molecular wire bundles at programmed positions [132]. This was achieved by applying controlled voltage pulses to an alkanethiolate SAM under a solution of molecular wires. The next challenge was to quantify the degree of current that could be passed through the single molecule. It was obtained by utilising an MCB method (described in Chapter 4.3.2.) for addressing single molecules. A 0.1 μA current was recorded through a single molecule of benzene-1,4-dithiol self-assembled on the two tips (see Figure 17) [121].

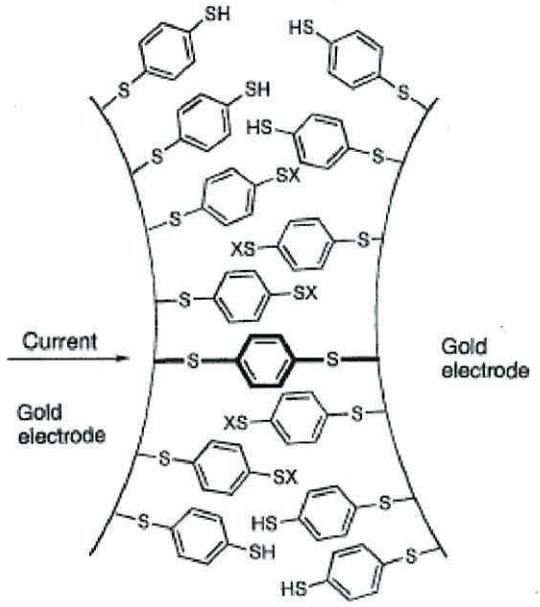

Figure 17 A schematic of a benzene-1,4-dithiolate SAM bridged between gold electrodes, formed in an MCB. End groups denoted as X can be either H or Au, with the Au potentially arising from a previous contact. Taken from [121].

Recently, the creation of individual molecular junctions was achieved by moving a gold STM tip into and out of contact with a gold substrate, whilst in a solution containing sample molecules. Proof of this was given by Xu and Tao [113] who investigated the conductance of a single molecule of 4,4'-bipyridine. During the initial stage of pulling the tip out of contact with the substrate, the conductance decreased with discrete steps. However, when the atomic chain was broken, by pulling the tip farther away, a new sequence of steps in a lower conductance regime appeared in the presence of 4,4'-bipyridine; this signalled the formation of a molecular junction. Similar measurements with the same molecular system were also performed using atomic force microscopy

(AFM) [133]. The measurements determined not only if and how the molecule was bonded to the probing electrode, but also took note of the electromechanical properties of the molecule, which depended on the molecule-electrode contacts. It also opened the door to the study of single-molecule electromechanical properties.

The importance of the molecular structure on conductance is significant as well. Mayor and Weber presented a characterisation of molecular rods, both consisted of a bis-9,10-phenylanthracene core with thiol anchor groups in the meta and para positions (see Figure 18) [123]. It was observed that when the binding SH group of a molecule was connected to a benzene ring in a para position (relative to the rest of the molecular structure), the resulting conductance was higher than in the case of the meta position. The lower current in the latter case also improved the stability of the junction [134].

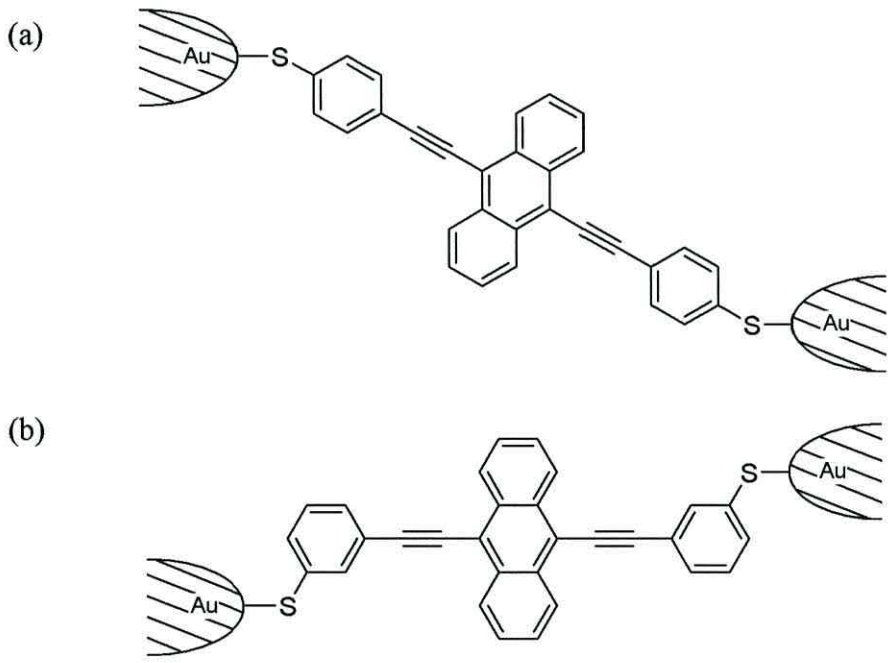

Figure 18 Effect of the molecular structure on conductance when the binding SH group of the molecule was connected to a benzene ring in (a) para, and (b) meta position relative to the rest of the molecular structure. Contacts between single molecules were made by MCB technique. Copied from [134].

The comparison between the molecules, presented in Figure 18 confirmed that the conductance did depend on the structure of the molecule, and could be altered on a molecular level by varying the position of the anchor group in the synthesis of the molecules [123].

Using the STM technique, the electrical properties of a single molecular wire can be controlled by the occupancy of energy levels within the molecules, including e.g. the viologen bridges [115]. It was found that charge trapping in molecular states leads to changes in electrical behaviour. Haiss *et al.* [115] used 6-[1'-(6-mercapto-hexyl)-[4,4']bipyridinium]-hexane-1-thiol iodide (see Figure 19) to measure single molecule conductivity. The thiol groups at both ends of the wire provided anchoring points to the gold surface and to the STM tip. The viologen group (redox group) has readily accessible energy levels, and is symmetrically placed between molecular tunnelling bridges at either end. In addition this molecule is highly stable in the redox state.

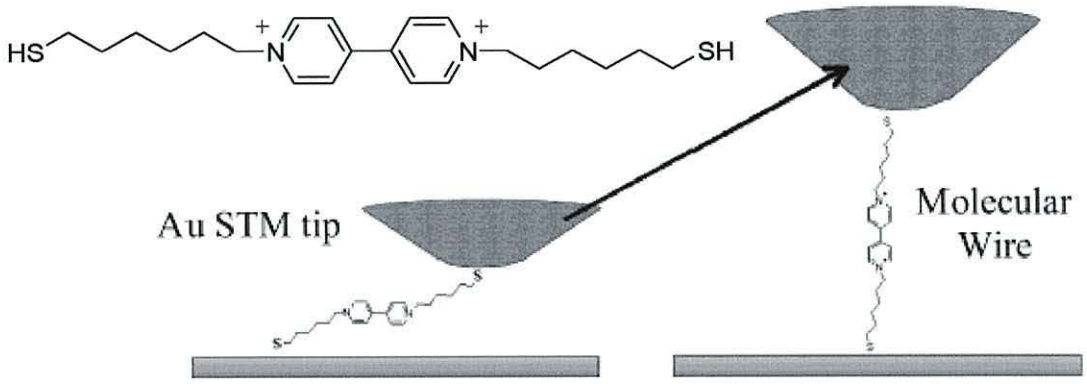

Figure 19 Schematic diagram of the experiment performed to study electrical properties of the molecule containing redox centre. Copied from [115].

Due to the presence of the molecular wire formed between the tip and the sample, current oscillations were observed. The lowest value of conductivity was 0.49 ± 0.08 nS at the tip-to-substrate potential difference of 0.2 V [115]. This might correspond to conduction through the single molecular wire. This value of conductivity can be compared with conductivity results of the analogues of the molecule presented above, chemically attached to nanoparticles incorporated in an hexanethiol monolayer on gold [135], which yielded a value of 0.56 ± 0.03 nS [116]. The similarity of the conductivity measured from both techniques indicates that this new method for the measurement of single molecule electrical properties is reliable. It can be applied in the electrochemical environment, enabling the redox state of molecules to be controlled during the measurements.

6. Molecular rectification

Molecular rectification of electrical current is a strongly asymmetric flow of electrons through a molecule because the conductivity from "the left side" of molecule to its "right" is very different from the conductivity going "right" to "left" [136],[137],[138],[139]. In rectification measurements, the rectification ratio (RR) is defined as:

$$RR(V) = \left| \frac{I(V_{n+})}{I(V_{n-})} \right| \qquad (3)$$

Where: $I\ (V_{n+})$ – values of current for positive bias values V_{n+}; and $I\ (V_{n-})$ – values of current for negative bias values V_{n-} corresponding to V_{n+}.

A rectification ratio for typical diodes based on a silicon system provides a value of two orders of magnitude [140]. Currently this value can be significantly extended to gain value in the range of 10^5-10^7 [103],[141],[142] for Schottky type diodes. Although molecular rectification of electrical current was first achieved a century ago, in vacuum diodes [143] and then in junctions of p-doped Ge accosted to n-doped Ge [144], a major experimental challenge has been to verify the theoretical basis provided by Aviram and Ratner for organic systems. This electronic process occurs in diodes and can be monitored by observation of I-V characteristics.

6.1 The Aviram - Ratner model

Aviram and Ratner suggested that for an organic molecule to show rectifier characteristics, it should have the properties of a p-n junction [2]. It was suggested that it would be possible to create relatively electron-poor (p-type) and electron-rich (n-type) molecular subunits by the use of substituent groups on aromatic systems. Substituents are classified as electron-withdrawing groups, if they result in a decrease of the π-electron density and thereby, raise the ionisation potential, hence can be a good electron acceptor (and vice-versa for electron donors). However, if the donor and acceptor subunits interact strongly with each other (i.e. through the molecule), the π-electron

density of the whole molecule will reach equilibrium and the rectification ability would be lost. Electron motion suggests that a rectifier could consist of donor and acceptor moieties insulated from each other. According to Aviram and Ratner, the necessary insulation could be provided by separating acceptor and donor parts with σ-electron bonds, which fulfill their function as a bridge connecting the two sides.

Aviram and Ratner presented an example of a rectifier molecule in their theoretical paper [2]. It was based on the acceptor tetracyanoquinodimethane (TCNQ) and the donor tetrathiofulvalene (TTF), separated by a σ-bridge to avoid coupling of donor and acceptor molecular orbitals (shown in Figure 20). However, this molecule has never been synthesised, but it is an ideal example for understanding rectifier behaviour.

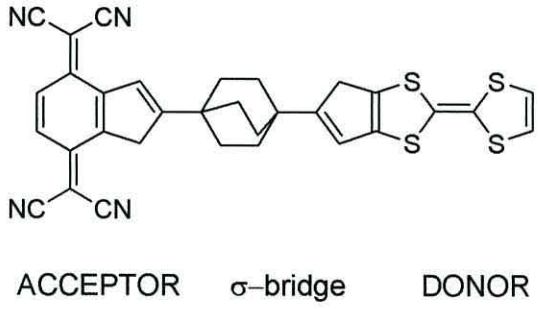

Figure 20 The Gedankenmolekűl (D-σ-A molecule) proposed by Aviram and Ratner as a molecular rectifier [2].

This simple example of a molecular rectifier would have the potential for tunnelling from the electrode at one end to the acceptor, and from the donor to the electrode on the other side. It is more difficult for electrons to flow in the opposite direction. This rectifying process, of an Aviram and Ratner molecular device, can be easily explained by examining the energy level diagrams presented in Figure 21.

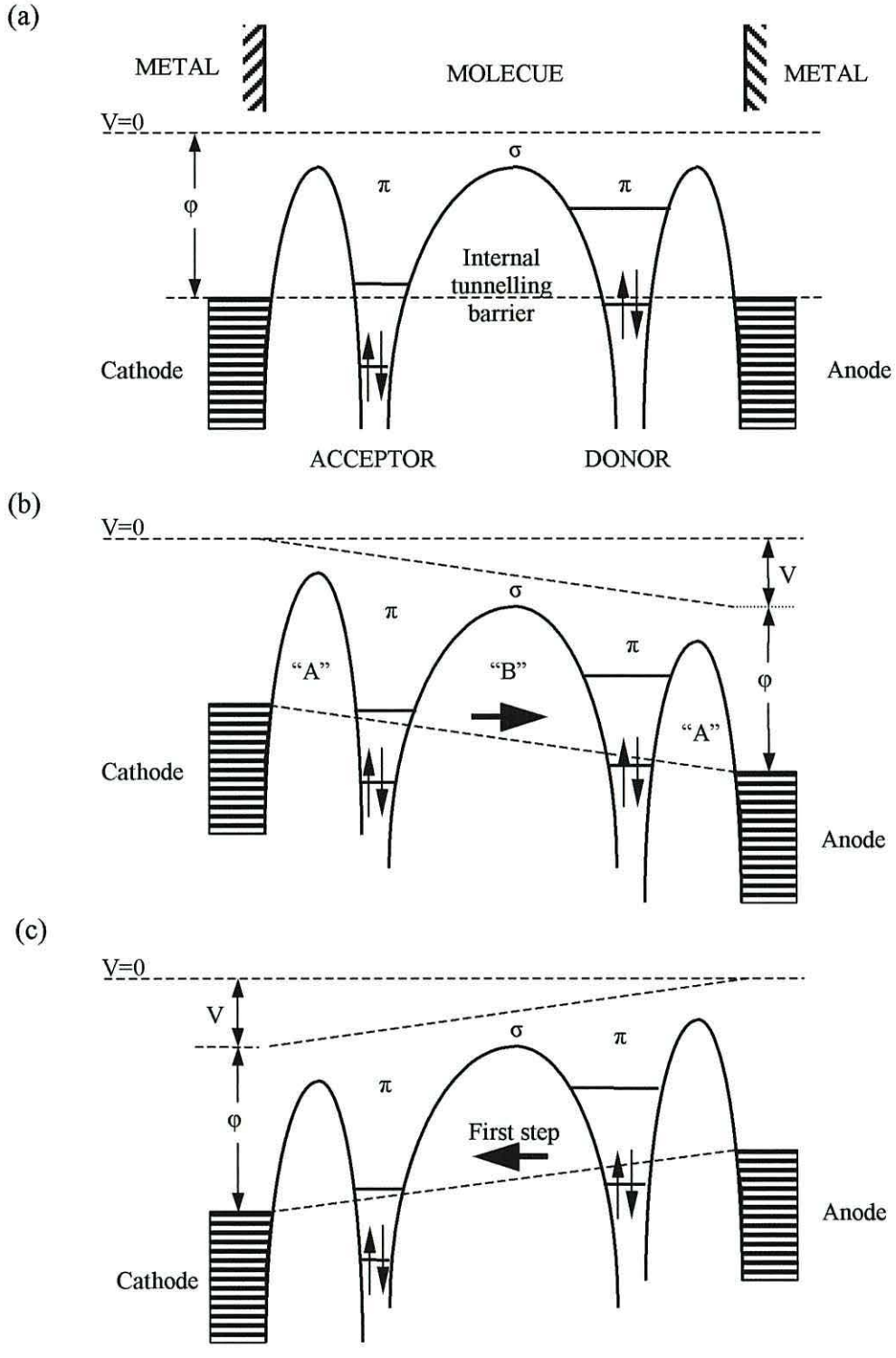

Figure 21 Energy diagrams of the Aviram and Ratner model. (a) D–σ–A molecule placed between electrodes with no applied voltage. (b) Forward bias causing realignment required to enable tunnelling within molecular junction. (c) Electron transfer under reverse bias from the HOMO of donor to the LUMO of the acceptor. V-potential applied to the electrode, φ-work function of the electrode. Figure adapted from [2].

For an ideal molecular rectifier, when the molecule is placed between two metal electrodes and no bias is applied (as shown in figure 21a), the acceptor subunit has poor electron density (in the range of 1-2.5 V) while the donor subunit has a high ionisation potential (in the range of 6-9 V). Therefore, the LUMO of the acceptor subunit is at a lower energy level than the LUMO of the donor subunit. Moreover, for proper rectifier behaviour, the LUMO of the acceptor should lie at or slightly above the Fermi level of the cathode; also the LUMO of the donor should be as high as possible above the Fermi level of the anode (see Figure 21a).

Conduction under forward bias is a two-stage process. The first process occurs when electrons flow from cathode to the LUMO of the acceptor and from the HOMO of the donor to the anode (labelled "A" in Figure 21b). During the second process, electrons tunnelling within the molecule from the excited state $A^{-}-\sigma-D^{+}$ to the ground state $A^{0}-\sigma-D^{0}$ (labelled "B" in Figure 21b). The possibility of electron transfer onto the acceptor under forward bias occurs when the cathode level overlaps the LUMO of the acceptor. Similarly, electron transfer from the donor to acceptor ensues when the HOMO of the donor overlaps the Fermi level of the anode (see Figure 21b). When the LUMO of the acceptor and HOMO of the donor are sufficiently close in energy, inelastic tunnelling of electrons may occur from the acceptor to donor. When polarity is reversed, as shown in Figure 21c, the LUMO of the donor would have to be lowered to the Fermi level of the donor. Thus the Fermi level of the cathode would have to be lowered below the HOMO of the acceptor in order to obtain tunnelling through these levels. The threshold voltage for this process would be relatively high.

Moreover, an additional conduction mechanism could take place between the donor and acceptor subunits. The first step of this mechanism involves internal tunnelling from the HOMO of the donor to the LUMO of the acceptor. This leads to creation of a hole on the right side, and an electron on the left side. Tunnelling would proceed from charged π-levels to and from the electrodes. This mechanism also involves a threshold voltage, and can only happen when the HOMO of the donor is energetically at or above the LUMO level of the acceptor (see Figure 21c).

Aviram and Ratner also calculated I-V characteristics, which are presented in Figure 22.

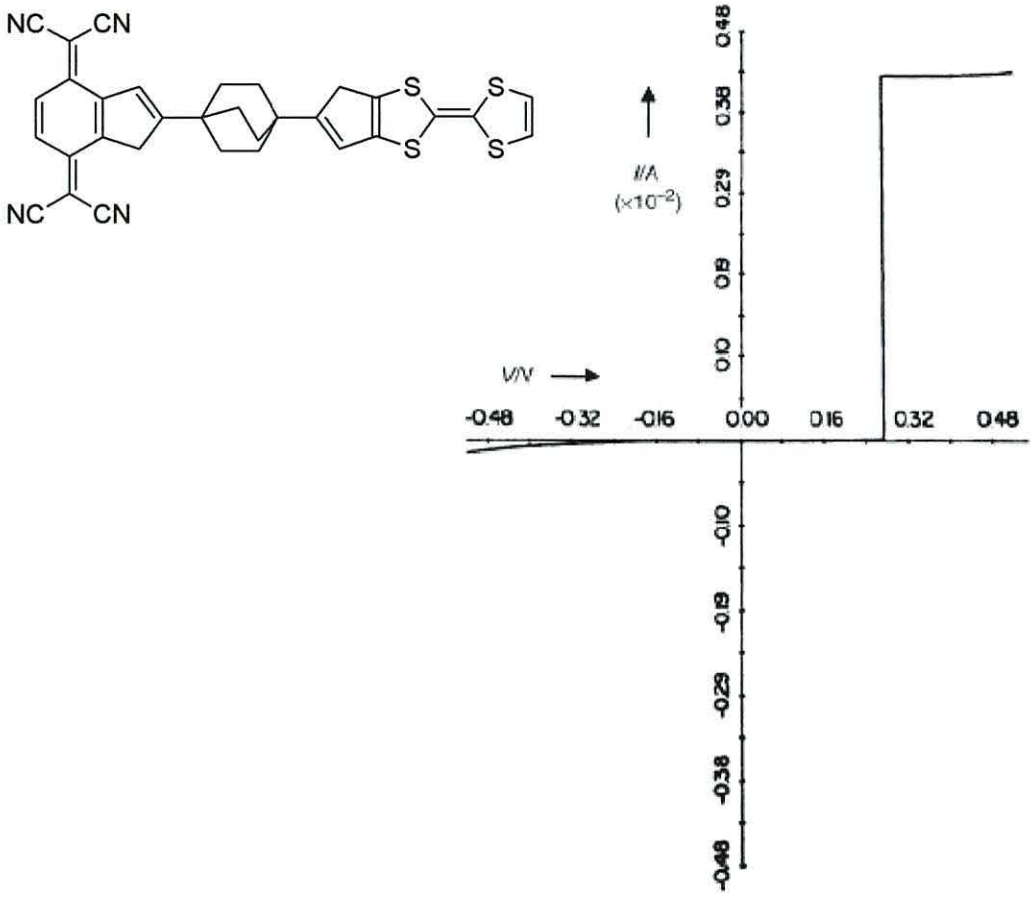

Figure 22 Molecular structure of an example D-σ-A molecular rectifier with the I-V characteristics proposed by Aviram and Ratner [2].

6.2 Other approaches of molecular rectification

Ellenbogen and Love [145] published a different mechanism of molecular rectification. These studies were similar to the operational principles of Aviram and Ratner's in the sense that an acceptor-bridge-donor molecule was used as a model, but the design of the presented molecule was different. They proposed a polyphenylene-based molecular wire as the conductive backbone to which donor and acceptor substituent groups were chemically bound (see Figure 23).

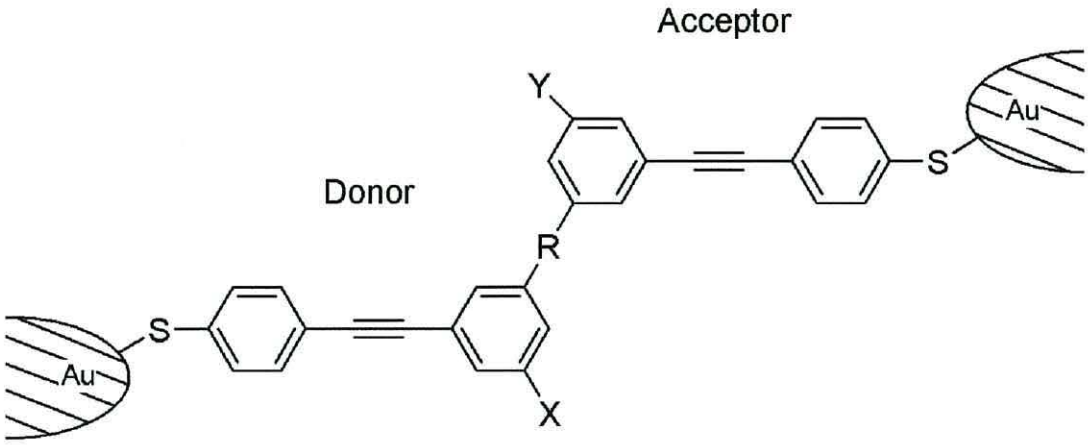

Figure 23 Proposed polyphenylene-based molecular diode [145].

The structure presented in Figure 23 has two intramolecular dopant groups: electron donating substituent group (X) and the electron withdrawing substituent group (Y). Groups such as $-NH_2$, $-OH$, $-CH_3$, $-CH_2CH_3$ are commonly used as electron donating substituents (X), whereas groups such as $-NO_2$, $-CN$, $-CHO$, $-COR'$ (where R' is an aliphatic chain), could be used as electron withdrawing substituents (Y). The most likely candidates for R were aliphatic groups such as sigma-bonded methylene or dimethylene groups.

The authors described, that at forward bias, which must be sufficient to raise the Fermi energy level at least as high as the energy of the LUMO π-orbital of the acceptor, electrons could tunnel from the right contact into the LUMO of the acceptor. Then once again to the left contact through the central insulating barrier, and the LUMO of the donor. To permit electrons to pass, the LUMO of the donor and acceptor must be close enough. In the reverse direction there was no resonance of the Fermi levels of the electrodes with the LUMOs of the molecule, thus they move away from each other. This should yield rectification.

Since Aviram and Ratner first theoretically demonstrated the possibility for an organic molecule to function as a molecular diode, a number of people have suggested using substituted benzene molecules (in the form of donor and acceptor molecular subunits), this was proposed by Majumder *et al.* [146] and Ellenbogen and Love [145]. The geometry was studied, as was the electronic structure of rectifying D-spacer-A

molecules. These molecules consisted of mono or disubstitued benzene with $-NH_2$ or $-NO_2$ functional groups, covalently linked by an insulating methylene or dimethylene bridge. The rectification behaviour in these molecules was analysed from the molecular orbital energy levels and the spatial orientations of the unoccupied molecular orbitals. The calculations showed that in such a molecular complex the LUMO was localised on the acceptor ring, whereas the HOMO was on the donor ring. The potential differences increased along with the tunnelling barrier length; for the monosubstitued complex the dimethylene bridge was found to be 2.05 eV. Also, the disubstitued rectifier complex had a value of potential difference of 2.76 eV.

In 2002 Kornilovitch *et al.* [147] published within their theoretical work, a general mechanism of molecular rectification in which a single electroactive unit was positioned asymmetrically with respect to the electrodes. However, the HOMO and the LUMO were positioned asymmetrically with respect to the Fermi level. As they reported, there were no special requirements to obtain this kind of rectifier. The only requirement was one conducting molecular level placed closer to one electrode than the other. This molecular rectifier, with an asymmetric tunnelling barrier, was divided into five structural parts (see Figure 24).

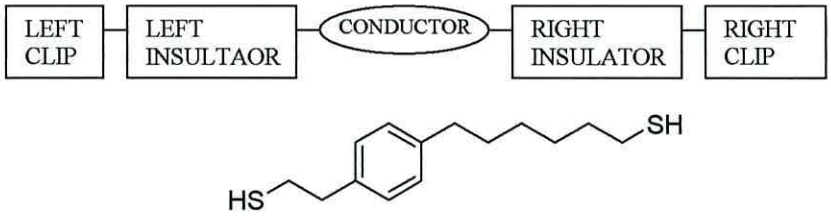

Figure 24 Schematic structure of an asymmetric tunnelling barrier molecular rectifier (top). An example of molecular rectifier (bottom), [147].

The molecule contained two saturated groups of different lengths, that insulated the central benzene ring, and also left and right clips (or end groups) that provided a contact between the electrodes and the molecule. The purpose of such a construction was to place the energy of the conjugated part (usually the LUMO) on the same level as the Fermi energies of the electrodes (see Figure 25a). Most of the applied voltage dropped on the longer insulating barrier as a result of the proportional dependence between the

insulator length and voltage drop, hence electrical rectification should be observed. The energy diagram of molecular rectification is shown in Figure 25b,c.

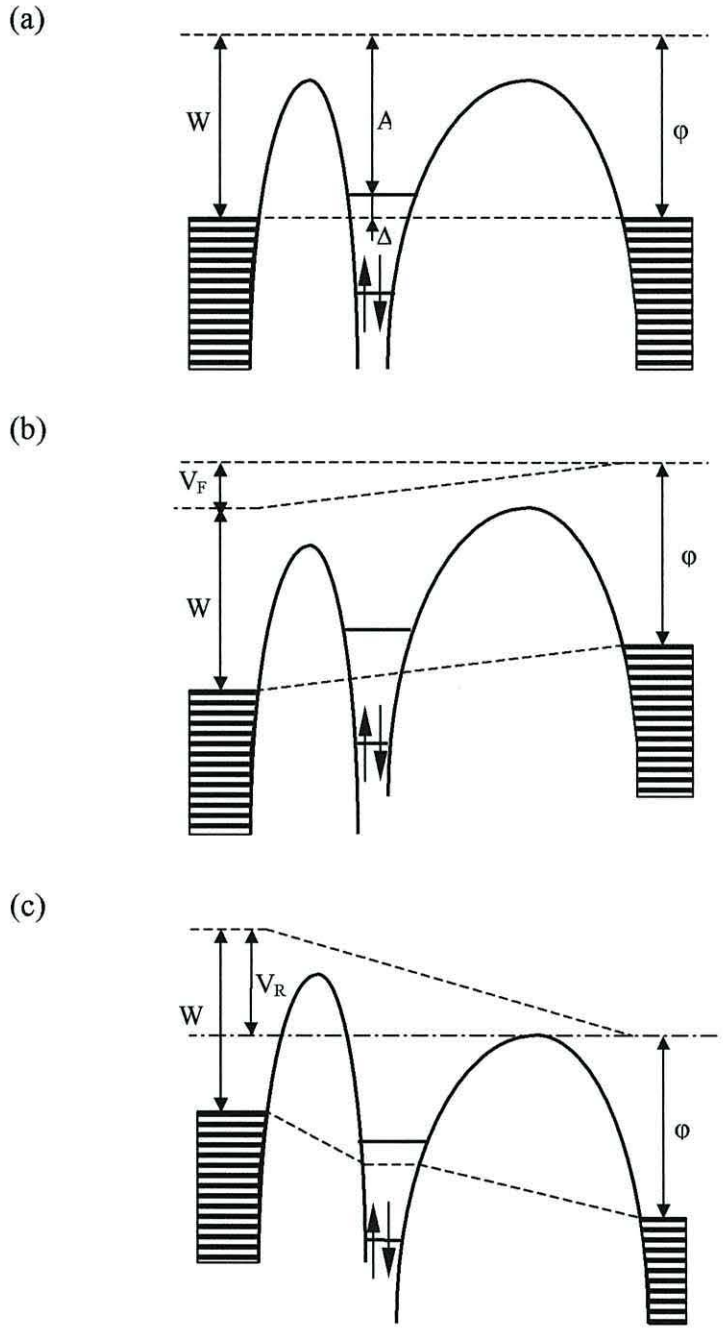

Figure 25 The energy diagram of molecular rectification according to the Kornilovitch theory: (a) asymmetric molecule placed between electrodes with no applied voltage, (b) under forward bias the current arises when Fermi level of anode aligns with LUMO, (c) under reverse bias the current arises when Fermi level of cathode aligns with LUMO. A- electron affinity, φ-work function of the electrode, V_F, V_R – forward and reverse voltages. Figure adapted from [147].

Under positive applied bias (see Figure 25b) the Fermi energy of the left electrode and the LUMO of the phenyl ring are lowered. The current rises when the Fermi level of the right electrode aligns with the conducting molecular level. Similarly, under reverse bias (see Figure 25c), both the Fermi level of the left electrode and the LUMO go up with the energy. The current rises when the Fermi level of the left electrode aligns with the conducting molecular level. The authors demonstrated that under forward and reverse bias the voltage behaved differently. Moreover, it was thought that for such a molecule, with simple conducting and insulating units, a rectification ratio in excess of one hundred would be expected.

Stokbro *et al.* [148] verified the Aviram and Ratner proposal but for a molecular wire. It was found that the electronic states were localised, either in the D or in the A part of the molecule. The exception occurred at particular biases where the voltage drop aligned two states, forming a resonant state delocalised over the entire molecule. The rectification was not observed for this investigation of a D-σ-A molecule. To obtain better diode characteristics the authors proposed other electroactive substituents to obtain a much smaller gap between the HOMO of the D part and the LUMO of the A part; resonant conditions could be obtained for a much smaller bias.

6.3 Experimental work

The first confirmed rectifier was a ground-state zwitterionic molecule, hexadecylquinolinium tricyanodimethanide ($C_{16}H_{33}$-Q3CNQ), depicted in Figure 26a, and was discovered by Ashwell, Sambles and co-workers [149],[150] in 1990. The active part of the molecule consists of an acceptor (excited state quinolinium moiety), and a donor (the excited state tricyanodimethanide: 3CNQ moiety) (see Figure 26a), connected by a twisted π-bridge (see Figure 26b). The novel D-π-A organic molecule showed asymmetric I-V characteristics when prepared as an LB monolayer situated between a magnesium pad on one side and platinum on the other.

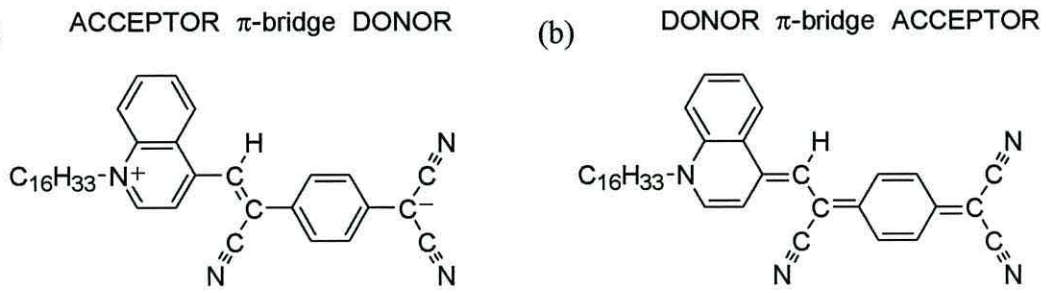

Figure 26 Molecular structure of (a) the ground state and (b) an excited state of $C_{16}H_{33}$-Q3CNQ [149],[150]. The electrons tunnel in the same direction as was predicted for the D-σ-A molecule.

The plausible mechanism for rectification of $C_{16}H_{33}$-Q3CNQ was attributed to the following mechanism:

step I $\quad Mg\,|\,A^{+}{-}\pi{-}D^{-}\,|\,Pt \rightarrow Mg\,|\,A^{0}{-}\pi{-}D^{0}\,|\,Pt$

step II $\quad Mg\,|\,A^{0}{-}\pi{-}D^{0}\,|\,Pt \rightarrow Mg\,|\,A^{+}{-}\pi{-}D^{-}\,|\,Pt$

This initial work seemed to show molecular rectification. However, magnesium is not the ideal material for an electrode because it oxidises easily. Further work [150] was concentrated in the prevention of molecular interactions with the electrodes. It was performed using ϖ-tricosenoic acid layers to insulate the metal from the rectifying molecule. The results were shown to support the initial studies and asymmetric I-V plots were obtained. The effect of bleaching modified the behaviour; junctions fabricated from a bleached film of $C_{16}H_{33}$-Q3CNQ exhibited different I-V characteristics [151]. The loss of the strong colour of the compound was accompanied by the absence of the strong I-V asymmetry that was observed in the unswitched form of the compound [152].

Further supporting work [136] related to the investigation of monolayers and multilayers of the zwitterions deposited between two aluminium electrodes. The aim was to eliminate the possibility that the asymmetry could arise from the different work functions of the electrodes. The result of this work was rectification with a current ratio of 26, but it is necessary to emphasise that an oxide layer covered the Al electrodes. Eleven years since the first confirmed rectifier was proposed, Metzger *et al.* [153], [154],[155] obtained improved rectification results for the same molecule. The organic

material was prepared as an LB monolayer, but in this case was situated between oxide-free Au electrodes, which eliminated any Schottky barrier effects.

6.3.1 Weak and strong molecular rectification from D-π-A molecules

Ashwell and Gandolfo [156] in 2001 presented a new rectifier, a cationic D-π-A dye. One year later, they reported [157] that by altering the length of the chain on the cationic dye (see Figure 27) the rectification could be reserved to the opposite quadrant of the I-V plot. This was as a consequence of anionic interactions, which polarised the dye and induced changes in its structure, switching the aromatic form to the quinonoid.

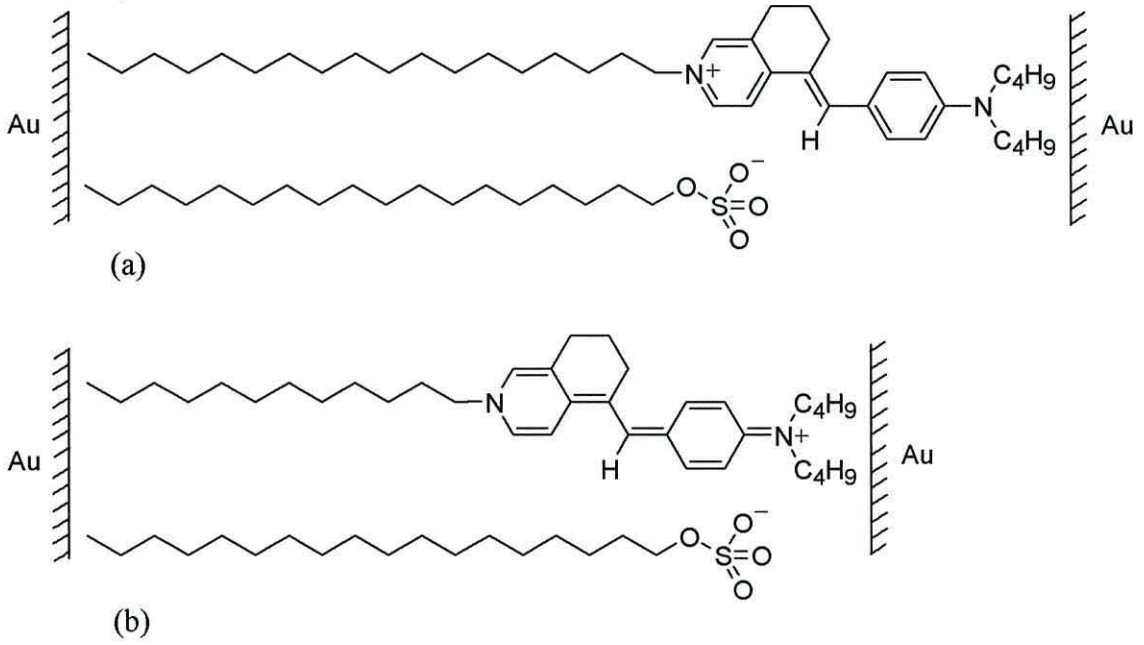

Figure 27 Molecular structures of the isoquinoline hemicyanine showing the length of the (a) octadecyl and (b) dodecyl analogues relative to the octadecyl sulfate conterion. Copied from [157].

Self-assembly has also been used to create rectifying junctions. A truncated S–C_3H_6 link between the gold substrate and chromophore (as shown in Figure 28) negated the effect of asymmetric placement of the D-π-A unit between the electrodes [158]. The films exhibited asymmetric I-V characteristics (see Figure 28) with a rectification ratio of 12 at ± 1 V. This was assigned to Aviram and Ratner type rectification [2].

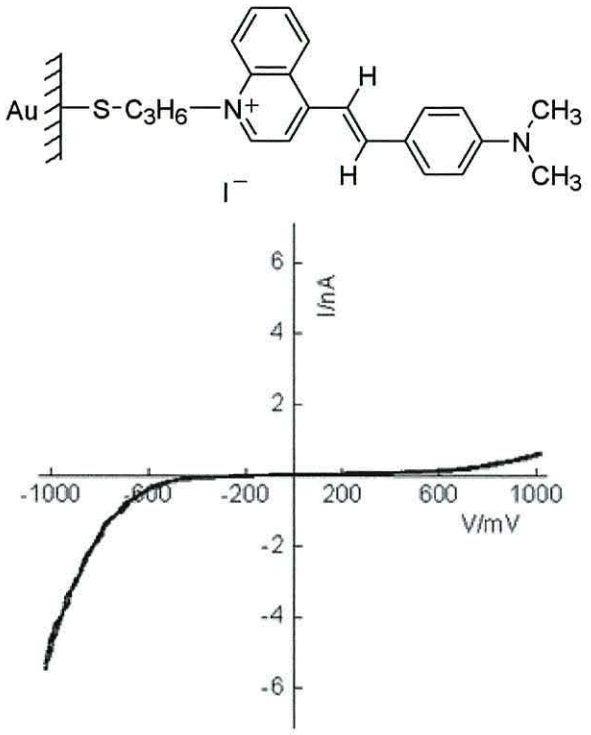

Figure 28 SAM of a cationic dye with a truncated $S–C_3H_6$ group (top), and its I-V characteristics (bottom). Copied from [158].

The characteristics became symmetrical upon exposure of the film to HCl vapour, which interrupted the intramolecular charge-transfer axis by protonation of the donor group. A loss of electrical asymmetry when the dye was protonated suggests that the effect of positional asymmetry on the I-V characteristics is negligible. The electrical asymmetry was then restored by deprotonation upon exposure to ammonia vapour. These studies not only showed that the films may be suitable for the use as acid/base sensors, but also demonstrated useful changes in the change-transfer bands of these dyes when studying their electronic properties.

Rectification of the self-assembled quinolinium hemicyanine ($Au–S–C_{10}H_{20}–D-\pi-A$), an analogue of the dye above, was observed for four types of tip: Au and PtIr, where the active D-π-A part was located between the electrodes and isolated from the substrate by an insulating alkyl tail; and $C_5H_{11}–S–$ and $C_{10}H_{21}–S–$ coated Au tips [159]. Significantly, geometries of the quinolinium analogues showed a dihedral angle of 31° between the planes through the donor and the acceptor moieties [159]. Its analogue, with a long alkyl ($S–C_{10}H_{20}$) link between the Au substrate and chromophore, exhibited

rectification with a ratio from 5 to 18 respectively for different kinds of tip, whereas the pyridinium hemicyanine dye (shown in Figure 29) did not rectify (rectification ratio less than 1.5 at ± 1 V, once reached a rectification ratio of 3) [107],[158]. This confirms the fact that the $-S-C_{10}H_{20}$ tail did not induce the observed rectification effect. It was not expected to rectify due to it possessing a very low twist angle between the planes of the donor and acceptor parts of the molecule, which was estimated by modelling to be ca. 10° [160].

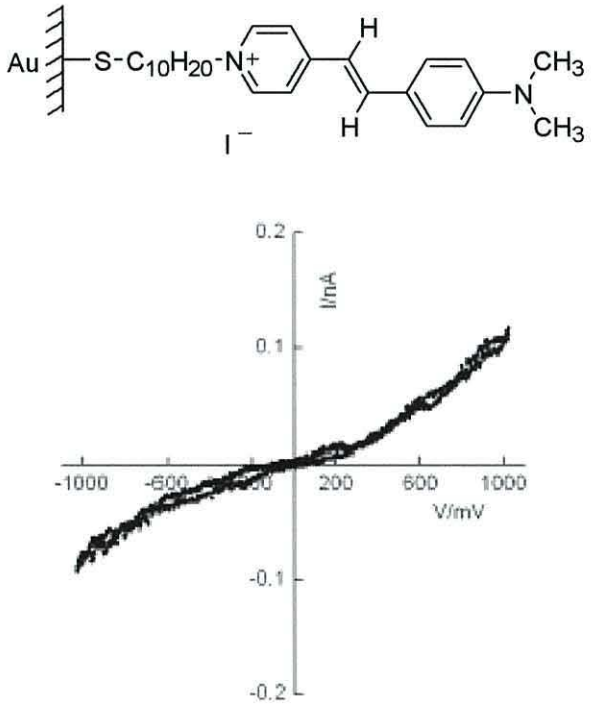

Figure 29 Molecular structure of a SAM of a pyridinium hemicyanine dye (top), and I-V characteristics probed using PtIr tip (bottom). Copied from [158].

The experimental evidence shows the alkyl tail provided no significant rectification effect [161],[162], a statement which conflicts with Metzger's published work [163], [164]. He has argued that the rectifying behaviour is induced, at least in part, by the insulating tail.

In order to improve rectification behaviour, further work was carried out using the sterically hindered dye of 1-(10-acetylsulfanyldecyl)-4-{2-(4-dimethylaminonaphthalen

-1-yl)-vinyl}-quinolinium iodide (see Figure 30a) [165]. This sterically hindered dye with a twist angle between the planes of donor and acceptor parts (estimated by modelling to be of 61°, see Figure 30b), exhibited strong I-V characteristics with a current ratio in the range 50-150 at ± 1 V (see Figure 30c). The improved behaviour was attributed to controlled alignment of the sterically hindered chromophore, Au-S-$C_{10}H_{20}$-A^+-π-D. The behaviour was indistinguishable when studied using Au or PtIr probes. The higher current in the negative quadrant corresponded to electron flow from the gold-coated substrate to the acceptor and from the donor to the STM tip. Therefore, this direction of electron transfer was attributed to the Aviram-Ratner model.

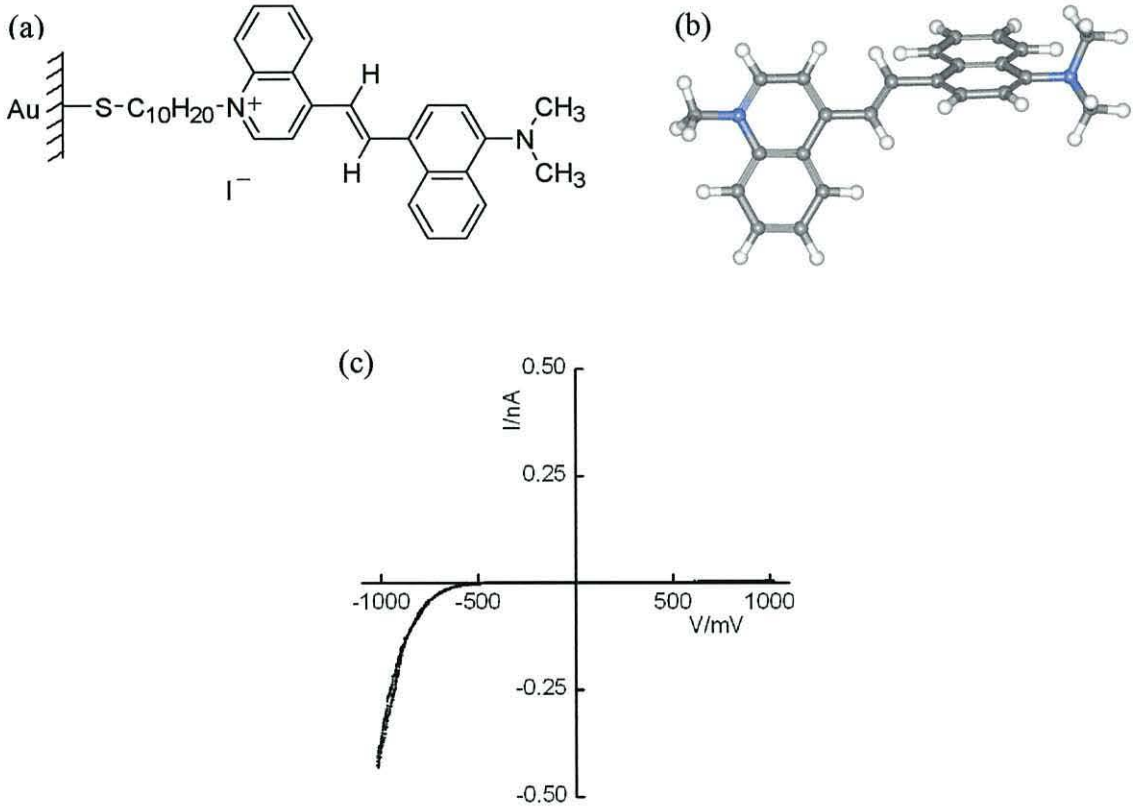

Figure 30 (a) Molecular and (b) geometrical optimised structure of a SAM of dye of 1-(10-acetylsulfanyldecyl)-4-{2-(4-dimethylaminonaphthalen-1-yl)-vinyl}-quinolinium iodide, and (c) I-V characteristics probed using PtIr tip. Taken from [165],[166].

This structure/property relationship highlights the dependence of the rectification upon steric hindrance; the D-π-A^+ moiety reported having double-ring substituents on opposite sides of a CH=CH bridge, which induced the nonplanarity. This improved rectification may also be compared to 12-18 at ± 1 V for a less sterically hindered

quinolinium hemicyanine analogue [159], and *ca.* 1.5 at ± 1 V for a pyridinium hemicyanine dye which had an almost planar chromophore.

Ratios as high as 450 at ± 1 V were obtained by ionically coupling cationic molecules on anionic surfaces: $Au–S–C_3H_6–SO_3^- \,|\, A^+–\pi–D$ [167]. The much improved behaviour was attributed to a non planar $D\text{-}\pi\text{-}A^+$ moiety induced by the $CH_2CH_2CH_2$ link between the conjugated part of the heterocycle and π-bridge (see Figure 31a). The higher values were expected for SAMs as this molecules possessed substantial steric hinderance; modelling calculations proved that the twist angle between the planes of donor and acceptor (Q^+ -5,6,7,8-tetrahydroisoquinolinium) was 51° (see Figure 31b). Strong asymmetry with a high current ratio (see Figure 31c) from ultra-thin organic films was reported from structures contacted by non-oxidisable electrodes.

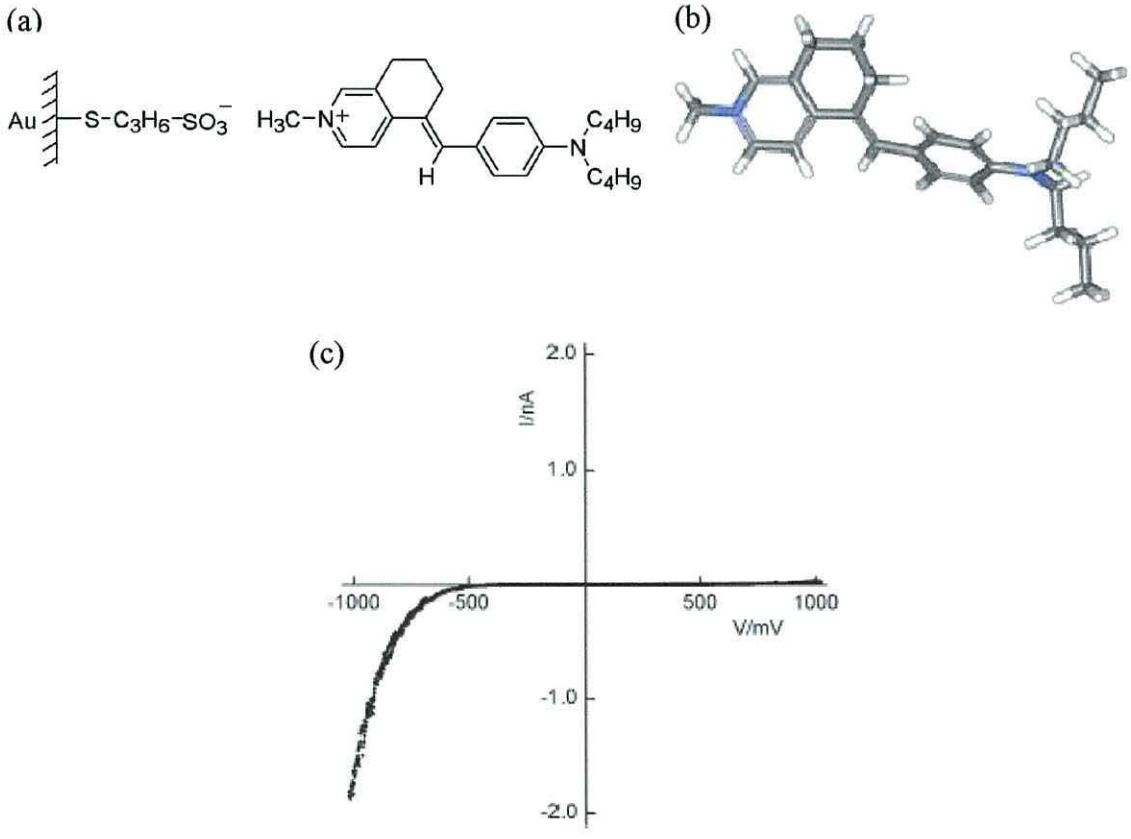

Figure 31 (a) Molecular and (b) geometrical optimised structure of the hybrid containing isoquinolinium-acceptor-based $Q^+\text{-}\pi\text{-}C_6H_4N(C_4H_9)_2$ dye deposited on top of the alkanethiol molecule of $Au–S–C_3H_6–SO_3^-Na^+$, and (c) I-V characteristics contacted by the PtIr probe. Taken from [167],[168].

Nonetheless this rectification ratio was still much higher than previously reported values of 5 at ± 1 V from SAMs where the D-π-A^+ moiety was connected via a decanethiolate link [159] (see Figure 32). Although rectification from the molecule presented in Figure 32 was minor it was expected to be more asymmetric due to the efficient angle of 48° between donor and acceptor planes [159]. The altered properties of both isoquinolinium dyes were attributed to the placement of the iodide counterion [167]. Thus, reduced rectification from SAMs of the dye presented below might be interpreted as arising from a mixed ground state and dipole reversal [157],[167]. However, alignment on the anionic surface, as presented in Figure 31 ruled out this problem.

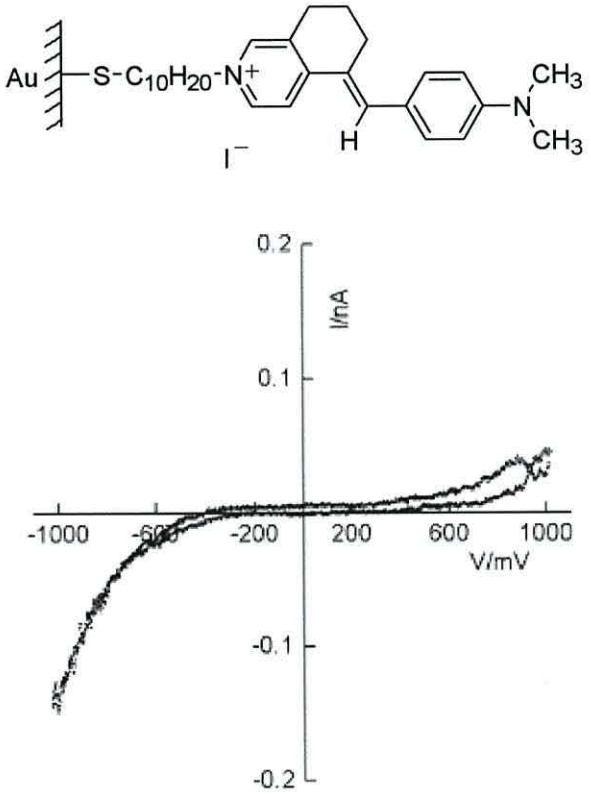

Figure 32 Molecular structure of a SAM of isoquinolinium hemicyanine dye (top), and I-V characteristics probed using a PtIr tip (bottom). Taken from [159].

6.3.2 Rectification from mixed monolayers

Mukherjee and Pal [60] studied a mixed monolayer of donor and acceptor molecules binding electrostatically to fabricate a D and an A assembly. As an example they

presented a monolayer of a phthalocyanine and Rose Bengal as donor and acceptor respectively (see Figure 33).

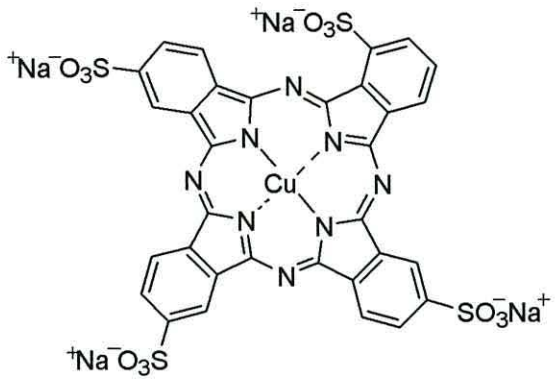

Tetrasulfonated salt of copper phthalocyanine (CuPc)

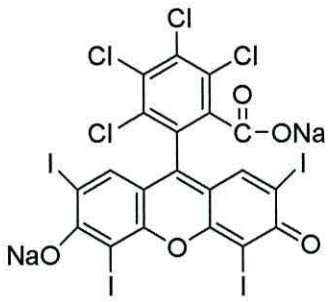

Rose Bengal (RB)

Figure 33 Incorporated molecular structures by Mukherjee and Pal [60], which play the roles of donor and acceptor respectively.

I-V characteristics from the monolayers composed of the individual components of the CuPc and the RB assemblies were found to be almost symmetrical, whereas the mixed CuPc-RB molecular assembly showed asymmetrical characteristics with a current ratio of 30 at ± 1.9 V. The direction of electron flow was from donor to acceptor, thus was not consistent with the Aviram-Ratner proposal. Further research into different kinds of donor-acceptor molecular assemblies [169] confirmed the electron flow was favourable from donor to acceptor in both donor-acceptor and acceptor-donor assemblies. Also, Bryce *et al.* [170] observed the opposite rectification direction in D-σ-A tunnel junctions depending on the electrodes used. The authors explained that the behaviour was due to changing orientations of the molecule. Therefore, the electrical properties presented here have to be verified. However, the donor-acceptor monolayer approach opened possibilities to select a donor and an acceptor material and thus build a desired D-A assembly for molecular rectification.

Ashwell *et al.*[171] also studied the electrical behaviour of an electrostatically coupled junction where cationic acceptors and anionic donors were coupled as separate layers (see Figure 34a). However, they incorporated covalent self-assembly for deposition of the first compound (onto a gold-coated substrate) to assure a well-ordered first layer

(4,4'-bipyridinium) and hence in the whole structure [171]. The second component (copper phthalocyanine-3,4',4'',4'''-tetrasulfonate) was deposited on the top of the first by electrostatic interaction of oppositely charged counterions during immersion. When contacted by STM the system exhibited I-V characteristics in which the bipyridinium molecule acted as an acceptor and controlled the molecular alignment of the donor (copper phthalocyanine) in the junction (see Figure 34b). The asymmetrical behaviour was observed with a rectification ratio in the range 60-100 at ± 1 V, this indicates that the direction of the current flow was in agreement with the Aviram-Ratner model.

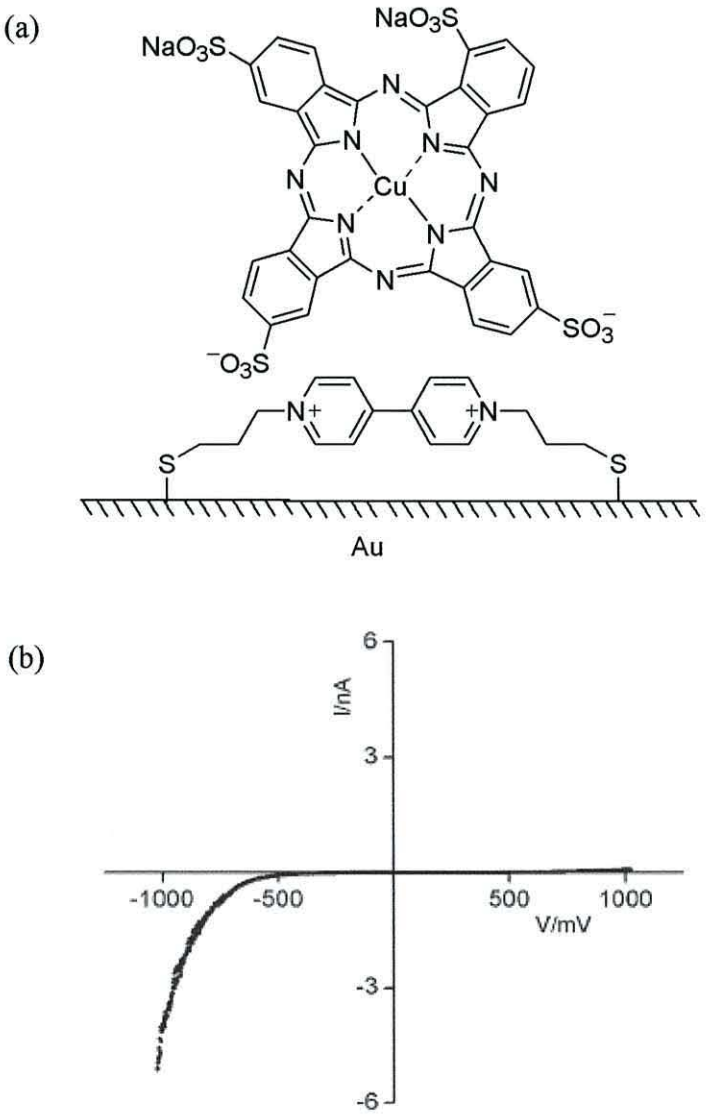

Figure 34 Rectifying junction investigated by Ashwell *et al.* [171] of (a) SAM of a bipyridinium acceptor and electrostatic self-assembled copper phthalocyanine $(CuPc(SO_3^-)_4(Na^+)_n$ where experimental studies suggest $1 \leq n \leq 2$, and (b) I-V curve with a rectification ratio of 60-100 at ± 1 V.

A similar experiment was performed by Ashwell *et al.* a year later [172] but this time the ionically coupled rectifying junction consisted of $TCNQ^-$ as the donor top layer and, the previously described, self-assembled bipyridinium acceptor (see Figure 35a). This acceptor-donor bilayer arrangement exhibited diode-like behaviour with a rectification ratio in the range 20-30 at ± 1 V, as shown in Figure 35b. The tunnelling occurred in the same direction as the previous example, from cathode to bipyridinium acceptor on one side of the device, and from $TCNQ^-$ donor to the anode on the other side.

(a)

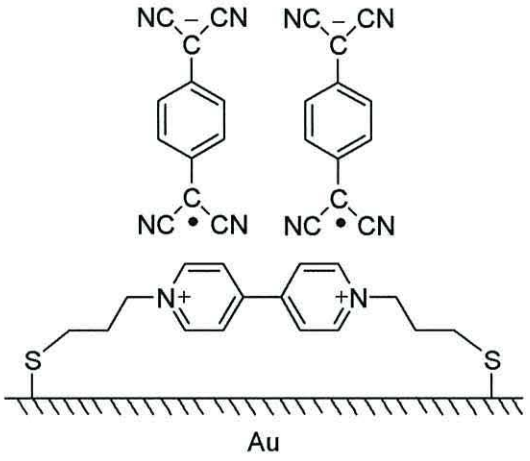

(b)

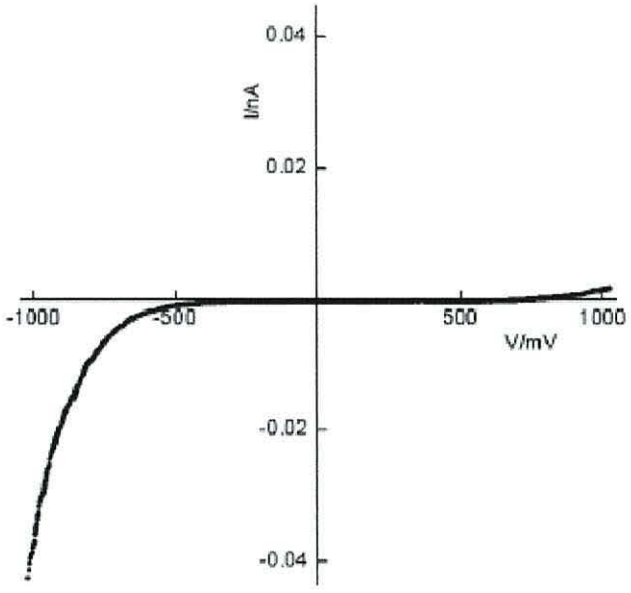

Figure 35 Schematic representation of the rectifying junction showing (a) molecular structures of the self-assembled acceptor and ionically coupled donor, and (b) I-V curve with rectification ratio of 20-30 at ± 1 V, [172].

6.3.3 Rectification from molecular wires

Research on molecular electronics has provided a large number of molecular wire candidates [173],[174]. Features such as a linear chain structure and the electron delocalisation along the chain show why molecular wires are expected to exhibit novel electronic and optical properties, and why they could find applications in future large scale integrated circuits.

Reed *et al.* [21],[99],[175] have developed a novel technique of vapour deposition of metals on to a SAM, to perform direct measurement of the conduction through a small number of molecules. The authors used the molecule 4-thioacetylbiphenyl, as shown in Figure 36a, to construct a sandwich-type structure with a length of about 12 Å. This molecule exhibited strong rectifying behaviour (see Figure 36b), which was thought to arise from the asymmetry of the molecule. The I-V curves of the device presented in Figure 36b were measured at room temperature and correspond to electron flow from Au/Ti top electrode into the SAM, and then to the bottom Au electrode. Moreover, temperature dependence was observed, namely the current decreased monotonically with temperature under both positive and negative biases.

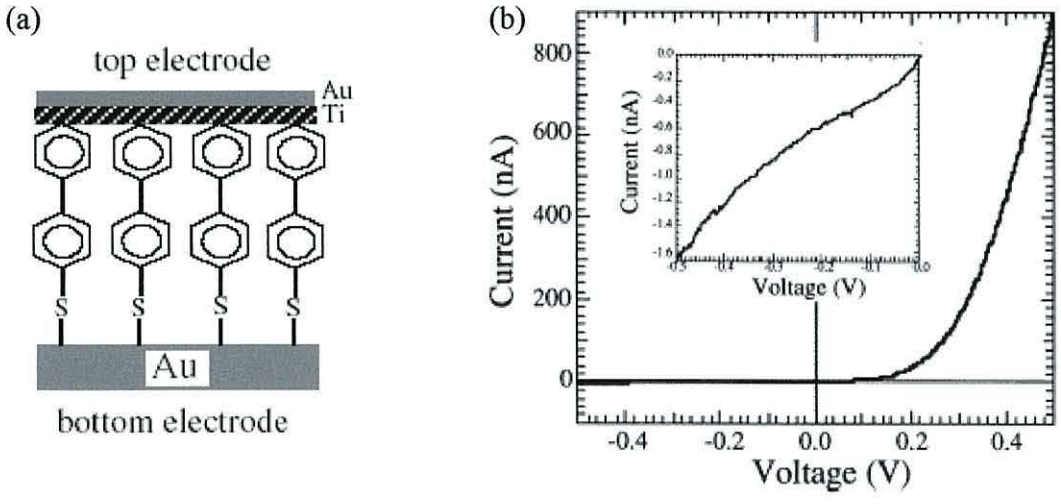

Figure 36 A nanopore device used by Reed and coworkers [99],[175]. (a) Only one side of the molecule used has a thiol for covalent bonding to the Au electrode, and a Ti layer was evaporated on the phenyl end group of the SAM before the Au layer was evaporated, likely reacting with the organic layer. (b) I-V characteristics at room temperature; magnified view of the negative bias part in the inset.

The example presented above concerns the vertical metal-evaporated junction is one of many, where the electrical asymmetry arises from the organic layer being overwhelmed by oxide induced Schottky barrier effect and assignment of the properties could be ambiguous to a large extent. It is the same problem that was also shown in the other experiment [195] where further studies (XPS) showed formation of titanium oxide layers (TiO_2 and TiO_3), as a result of the presence of residual gases in the evaporation chamber.

Kushmerick *et al.* [109],[176],[177] demonstrated current rectification in metal-molecule-metal junctions, through control of the interaction strength of one of the two metal–molecule contacts. It was demonstrated that the thiolate bound conjugated organic molecules with a nitro or pyridine termination (see Figure 37), showed characteristics of a molecular diode. These molecular wires were deposited as SAMs on a gold wire and contacted by a second gold wire.

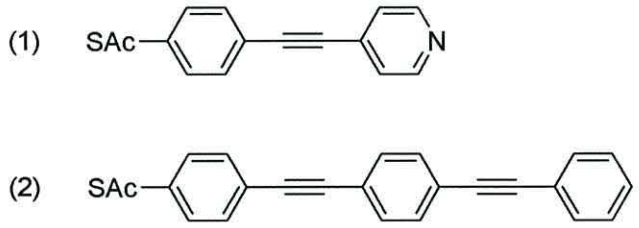

Figure 37 Chemical structures of molecular wires used to make SAMs by Kushmerick *et al.* [109],[176],[177].

Studies of the electrical properties of the compounds presented above were performed along with analogues of compound (1) and (2) with a higher affinity for gold, but they showed no rectification [177],[178]. The junction formed from compound (2), which was only a mechanical phenyl-Au contact, exhibited a rectification ratio of 3.8 at ± 0.9 V. The pyridyl-Au contact of (1) showed a rectification ratio of 1.8 at ± 1 V. The results of (2) were supported by STM measurements performed by Dhiriani and co-workers [179]. They also confirmed the observations of the previous group; that the extent of rectification in the molecular junction correlated well with the extent of coupling between the chemical linker and metal electrode.

Morales *et al.* [180] presented an example of a molecular diode that could reversibly alter the rectifying direction. They proposed a new molecule in which the dipyrimidinyl moiety was connected with diphenyl groups (see Figure 38a). STM studies revealed that this molecule not only yielded rectifying behaviour, but also exhibited a reversible effect – the ability to alter the rectifying direction after protonation on the nitrogen atoms by exposure to a strong acid. The I-V characteristics of the unprotonated assembly molecular wires exhibited asymmetrical behaviour in the positive quadrant, the average rectification ratio was around of 7.4 at ± 1.5 V (see Figure 38b). The most interesting result was the reversible change in the rectifying direction by protonation/deprotonation of the dipyrimidinyl moiety (see Figure 38c). This inverse rectification possessed an average current ratio of around 9.2 at ± 1.5 V (this was the most pronounced rectifying effect observed).

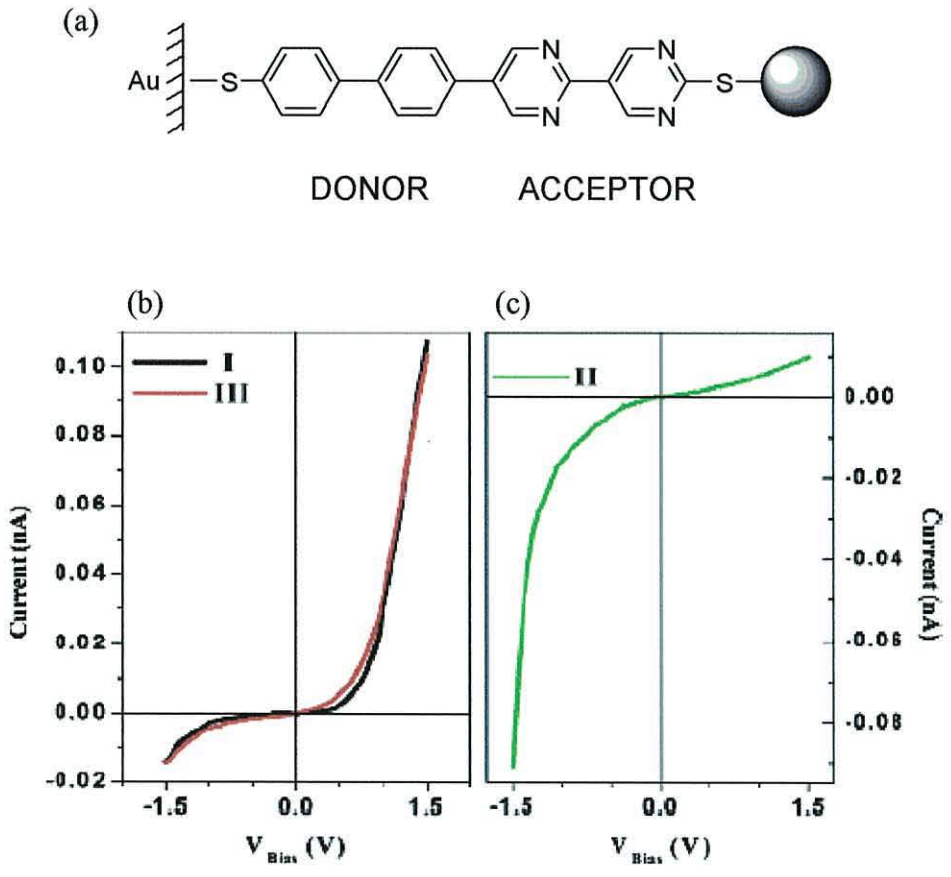

Figure 38 (a) Diblock oligomer proposed by Morales *et al.* [180]. Average I-V curves measured for: (b) deprotonated assembly wire, I-sample before protonation, III-sample after protonation-deprotonation, (c) assembly protonated. Copied from [180].

Ochs *et al.* [181] proposed a molecular rod that consisted of two weakly coupled electronic π-systems with mutually shifted energy levels. This molecule, with its donor and acceptor moiety specially designed to act as a diode, was contacted with gold electrodes from both sides. The authors utilised an MCB junction technique to immobilise the individual molecular rods for investigation of the electronic properties. The molecular rectifiers are presented in Figure 39. The I-V characteristics of the molecule presented in Figure 39a exhibited diode-like behaviour. In contrast to that, control experiments with symmetrical rods (showed in Figure 39b) did not show significant electrical asymmetries.

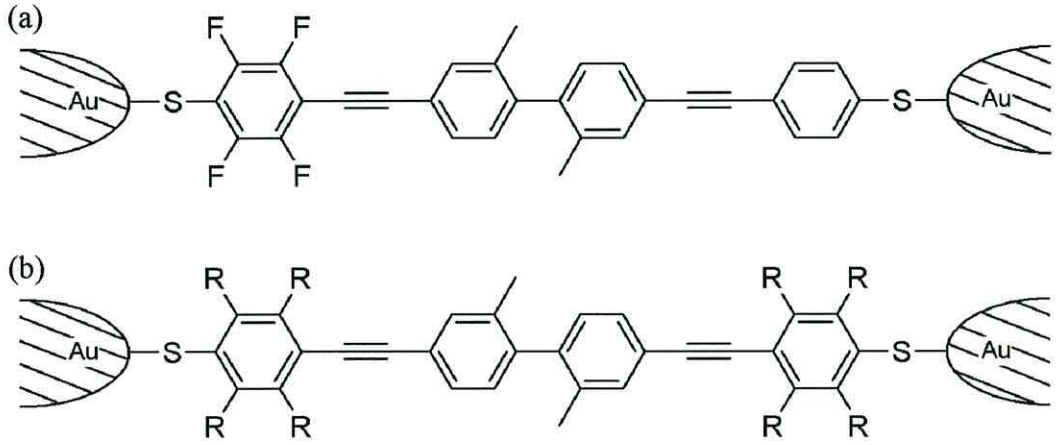

Figure 39 Molecular rods proposed by Ochs *et al.* [181] immobilised between Au electrodes of a MBC technique. R=F or R=H.

In the original work of Aviram and Ratner [2], rectification was a consequence of different step heights of the current at positive and negative bias. Experimental work published by Ochs and co-workers revealed that the fluorine part of the molecule was more conducting than the opposite part. Therefore, the current was higher at forward bias, thus a diode-like shape was observed in the I-V characteristics. Even though this conclusion is in agreement with Aviram and Ratner, the current flow was in the opposite direction, from donor to acceptor.

7. Phthalocyanines

Phthalocyanine (Pc) is an 18 π-electron aromatic macrocycle, which is closely related to the naturally occurring porphyrins. This intensively coloured dye consists of four isoindole rings conjugated by a nitrogen bridge, as shown in Figure 40.

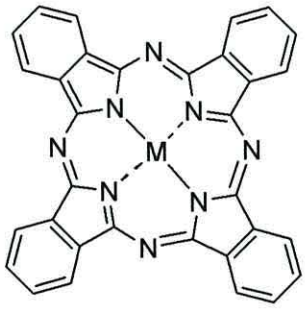

Figure 40 Molecular structure of unsubstituted metalophthalocyanine (MPc), M-metal ion.

Like the porphyrins, the Pc macrocycle can play host to over seventy different metal ions (e.g. Cu^{2+}, Al^{3+}, Zn^{2+}, Fe^{2+}, V^{2+}, Ni^{2+}) in its central cavity. One of the most important advantages of Pc, over other organic materials, is their exceptional thermo- and chemical stability [182]. Since its discovery over eighty years ago by Deisbach and Weid [183], Pc and its derivatives have been extensively used as dyes and pigments [184]. More recently they have been employed in several applications such as the photoconducting material in laser printers and the light-absorbing layer in recordable CDs [185]. They are also used as photosensitisers in photodynamic therapy (PDT) [186],[187], (publication V in Chapter 12.). Most of these applications require the use of phthalocyanines in the form of thin films [188],[189],[190]. The synthesis and application of Pc materials is a very dynamic and multidisciplinary field of research.

The tetrasulfonated salt of copper(II) phthalocyanine (structure was presented earlier in Chapter 6.3.2., Figure 33), along with a different MPc, was the object of intensive studies and demonstrated different electrical properties.

Dekker *et al.* [82] published topographic STM images and the electrical properties of CuPc. The authors used an evaporation technique to deposit molecules on a liquid nitrogen-cooled (at about 200 K) graphite substrate, which avoided clustering of individual molecules at random positions. The I-V curves taken for CuPc were almost symmetrical and did not differ much from those on the bare substrate for tip voltages ranging from −0.8 to +0.3 V. However, a reproducible step was observed in the I-V curves of CuPc, where the tip voltage varied between 0.3 and 0.5 V. The peak observed in the STM studies, and also displayed from the calculated derivative dI/dV versus V, was attributed to resonant tunnelling through a molecular level of CuPc.

Zhang *et al.* [191] proposed a binuclear cobalt-phthalocyanine (CoPc–CoPc) system (see Figure 41), which might have had a potential application as a unimolecular rectifier.

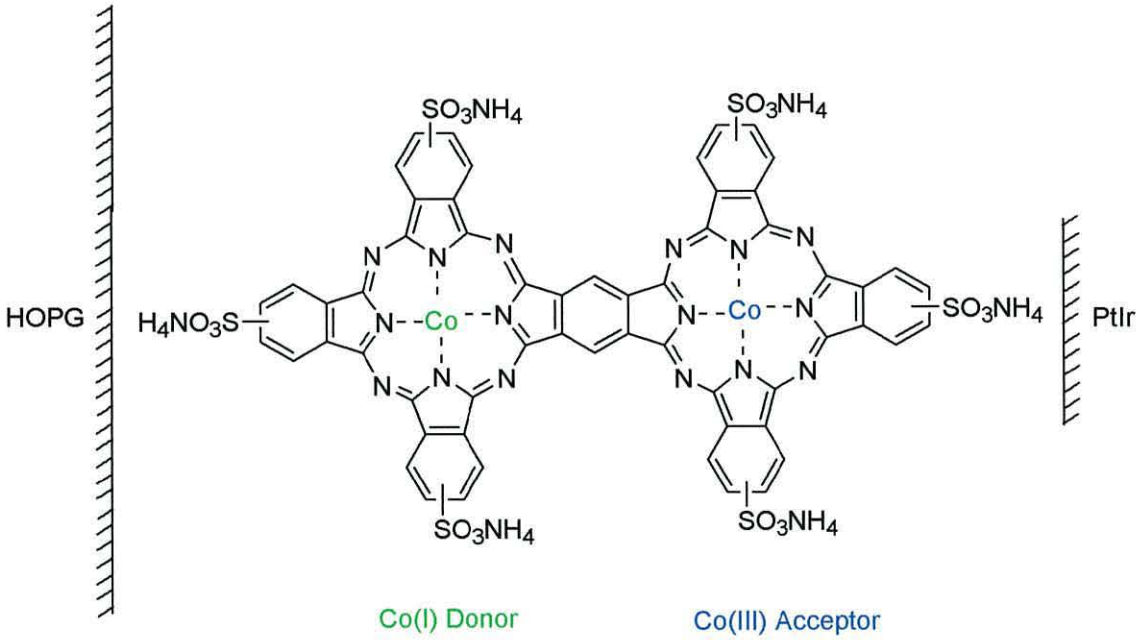

Figure 41 The chemical structure of CoPc–CoPc studied by Zhang *et al.* [191].

The molecules were deposited on HOPG and then studied by STM using a PtIr tip in air at 22 °C. The STM experiments indicated asymmetrical I-V curves for both the mono and double layer planar binuclear phthalocyanine systems. XPS data confirmed that the CoPc–CoPc molecule existed in the configuration of Co(I)Pc–Co(III)Pc and that it aligned with the Co(I) section adjacent to the HOPG surface as shown in Figure 41. The

authors showed that the I-V curves which indicated rectification behaviour arose from the material asymmetry. Co(I)Pc–Co(III)Pc is an asymmetrical molecule because the valency of the two coupled ions within the molecule are different to each other. The asymmetry creates a dipole moment and leads to intermolecular, one-direction charge transfer. In this case rectification was believed to be of the Aviram-Ratner type in such that the Co(I)Pc and Co(III)Pc were considered as donor and acceptor respectively. Moreover, if the coupling between the acceptor and donor was too strong, the asymmetry of the I-V characteristics would be broken, thus charge transfer would be possible in both directions.

One potential application of molecular nanotechnology is the integration of molecular electronic functions with advanced current technology. One step towards this process is the manipulation of individual molecules at specific locations on a surface. Hersam *et al.* [192] reported the fabrication of arrays of individual isolated CuPc molecules on Si(100) surfaces patterned with ultrahigh vacuum STM. The STM analysis was performed via constant topography images and tunnelling conductance imaging. The fourfold symmetry and central copper atom of CuPc were clearly observed at positive sample bias. Spatial tunnelling conductance maps of CuPc illustrated charge transfer from the surrounding substrate, when the molecule was bound to the surface via its central copper atom. On the other hand, when the CuPc molecule interacted with the substrate via an outer benzene ring, molecular rotation was observed. Overall, the wealth of molecular scale information generated by this initial experiment performed by Hersam and co-workers [192], suggests the suitability of this experimental technique for empirically screening molecules for various applications. Electrical interfaces open many possibilities for fabrication of molecular electronic devices.

8. Experimental

8.1 Substrate preparation and apparatus

The 10 MHz AT-cut quartz crystals (for QCM characterisation) were plasma cleaned (using a Plasma Prep 2) and then rinsed with the appropriate solvents depending on the solvent used during monolayer deposition. They were then left to dry in a cool place to avoid any temperature distortion of the quartz crystals. The plasma cleaner apparatus, *Plasma Prep 2* manufactured by *Gala Instrument* used for cleaning quartz crystals is shown in Figure 42.

Figure 42 Plasma cleaner, *Plasma Prep 2* (*Gala Instrument*).

The cleaning procedure for quartz crystals by plasma cleaner consists of the following stages:

1) Quartz crystals were placed into the plasma cleaner;
2) The plasma cleaner was closed and the vacuum pump switched on for 3 minutes;
3) After this time the gas was switched on for 3 minutes;
4) Then the generator was switched on;
5) The generator was automatically turned off by the timer, and the gas along with the pump were switched off as well;

6) This operation was always repeated a second time in order to clean the other side of gold-coated quartz crystals.

Thermal evaporation, under vacuum, for gold coating was used extensively on different substrates. Due to the requirements of this thesis, HOPG substrates coated with gold were used for the formation of SAMs prior to the STM study. This technique is commonly used for deposition of metal layers with a specific thickness, which was ~50 nm for HOPG. The thermal coating of gold was performed using an *Edwards 360A* unit (see Figure 43) in a clean room environment. A pre-determined mass of pure gold (99.99%) purchased from *Sigma-Aldrich Chemicals Ltd.* was put into a heating boat connected to a current circuit. HOPG substrates were attached to a holder and placed in a vacuum chamber above the heating boat (see Figure 44).

Figure 43 A photograph of a coater unit, *Edwards 360A*.

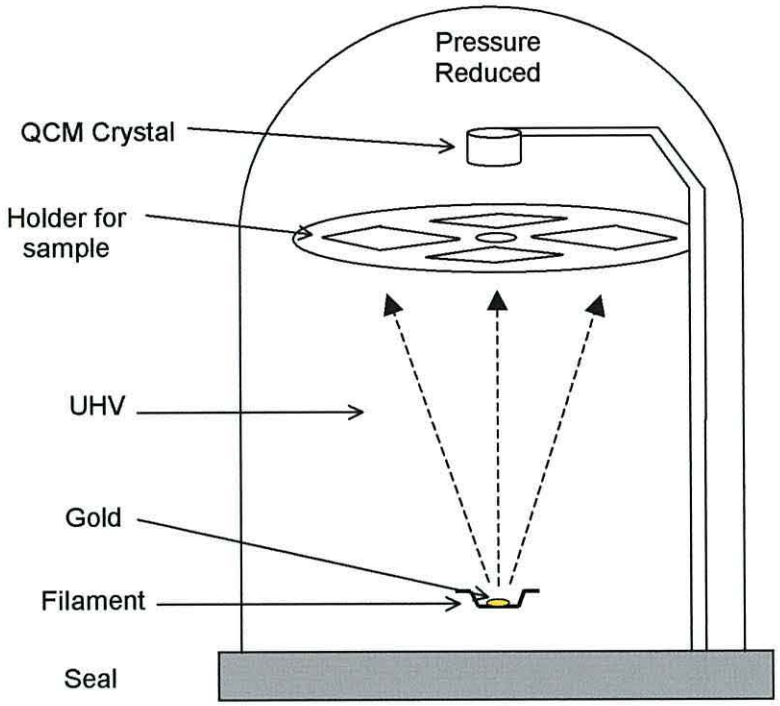

Figure 44 An illustration of a UHV chamber for thermal evaporation process of thin metal films.

When the pressure of the vacuum chamber was reduced to 2×10^{-6} Torr the gold was gently warmed up until melted, then allowed to evaporate onto substrates. The process was controlled by the use of a single quartz crystal monitor until the desired gold thickness was reached. Adjustment of the current going through the molybdenum heating boat allows control of the deposition rate of around 0.5 nm per second.

8.2 Monolayer preparation

A SAM was fabricated by immersion of a substrate, e.g. gold-coated substrates such as quartz crystals or HOPG, or platinum-coated glass slide, into a freshly prepared sample solution (0.05–0.1 mg cm^{-3} in typically ethanol, methanol or tetrahydrofuran) of the compounds of interest for the appropriate period of time. Between immersions the substrates were rinsed with solvents to remove any physisorbed impurities from the surface and left to dry. It was found that immersion of substrates for short periods of time, interrupted by rinsing with solvents, delivered better monolayers than films obtained as a result of a single long immersion.

The thioacetate group, used to protect the sulphur of the deposited molecule, was removed by addition of a few drops of ammonium hydroxide to the solution. When the cyanoethyl protected group was present, sodium methoxide was added to facilitate deposition. Thus, the self-assembly deposition rate was increased.

8.3 Measurement methods and apparatus

8.3.1 Quartz crystal microbalance (QCM)

The International Crystal Manufacturing Co manufactured the gold-coated quartz crystals, with a nominal frequency of 10 MHz and thickness of 0.2 mm used in the experiments. They were used in conjunction with a Thandar TS3021S generator delivering a direct current of 0.01 A and 9 V. An electronic circuit connected to the gold electrodes of the quartz crystal drove the crystal oscillations. The changes in frequency were monitored using a Hewlett Packard 53131A frequency counter (see Figure 45).

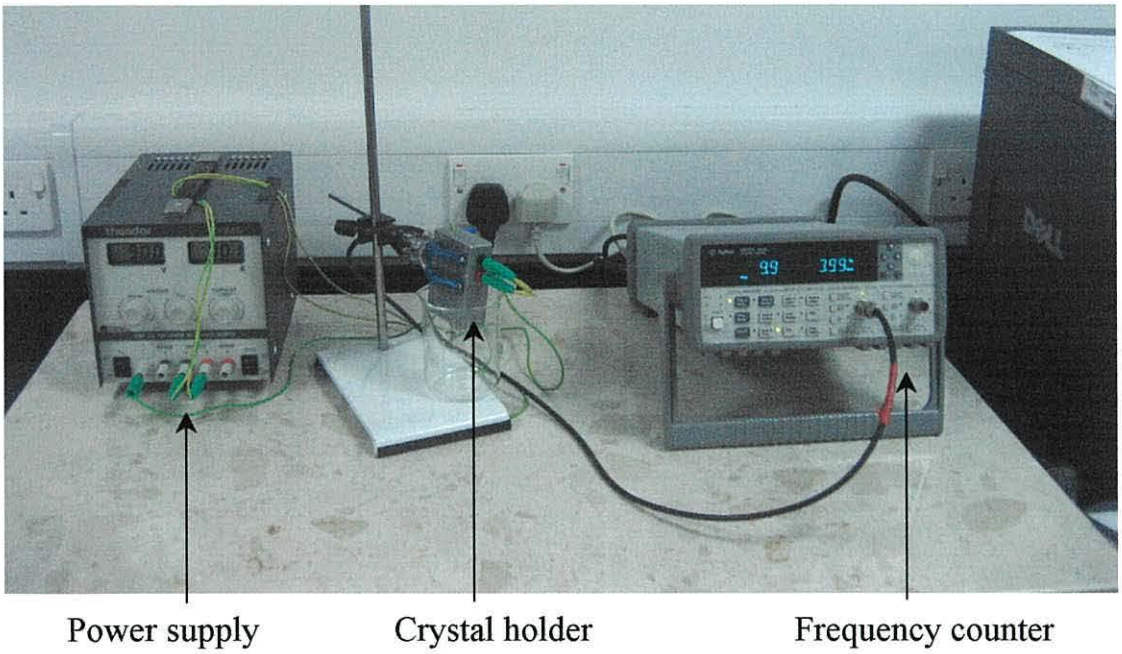

Figure 45 An illustration of QCM apparatus.

For SAM deposition the crystals were repeatedly immersed into sample solution for a determined amount of time, typically 10 minutes intervals, and washed each time.

Throughout the SA process, the frequency was monitored for deposition on the gold-coated 10 MHz quartz crystals. The process was continued until the frequency measurements stabilised, this means that the molecules had created a complete coverage (perfect monolayer).

Calculation of the area was possible after transformation of the basic Sauerbrey relation (equation *(1)*, see Chapter 3.1.) to determine the mass change per unit area, and then the area per molecule of the investigated material. The known parameters are: F_o - fundamental frequency of the crystal (10×10^6 Hz), A - surface area of the resonator (2.059×10^{-5} m^2), ρ_q - density of quartz (2.648×10^6 g m^{-3}), μ_q - the shear modulus of quartz (2.947×10^{13} g/m s^2). The final equation for the change of the adsorbed mass on a quartz resonator is:

$$\Delta m = -(9.09 \pm 0.01)\times10^{-10}\,\Delta F \qquad (4)$$

Knowing the molecular mass of the molecule, and the change in frequency due to the monolayer, the area per molecule can be calculated and is reported in nm^2 $molecule^{-1}$.

8.3.2 UV/visible spectroscopy

UV/visible spectra of the SAMs of studied compounds were obtained on a 10 nm thick platinum-coated glass substrate using a *UV/visible Super Aquarius 9000 spectrophotometer*. Measured spectra were used for identification of the investigated compounds that absorb the light in UV and visible regions of the electronic spectrum, and to analyse the transitions resulting from them. A schematic diagram of the UV/visible spectrophotometer is presented in Figure 46.

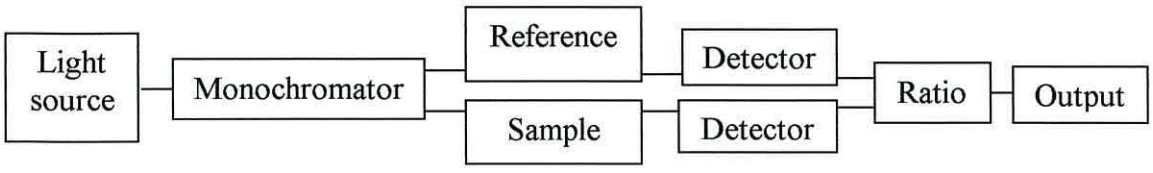

Figure 46 Schematic diagram of a UV/visible spectrophotometer.

8.3.3 X-ray photoelectron spectroscopy

The XPS analyses were obtained from an *AXIS Ultra* spectrometer with a monochromatic Al X-ray source at 150 W, manufactured by *Kratos Analytical Co* (see Figure 47). Each analysis started with a survey scan from 0 to 1200 eV with a dwell time of 100 ms, pass energy of 160 eV at steps of 1 eV (with 1 sweep). For the higher-resolution scans, the pass energy was lowered to 80, 40, or 20 eV (depending on the intensity of peaks) at steps of 400, 200, and 100 meV respectively. The dwell time was also changed to 250 ms and the number of sweeps was increased to 5. The spectra of SAMs on gold were referenced to the Au $4f_{7/2}$ line at 84.0 eV. Data was collected using *CasaXPS Version* 1.1 software. The XPS studies were performed by Dr Barry Wood at University of Queensland in Brisbane, Australia.

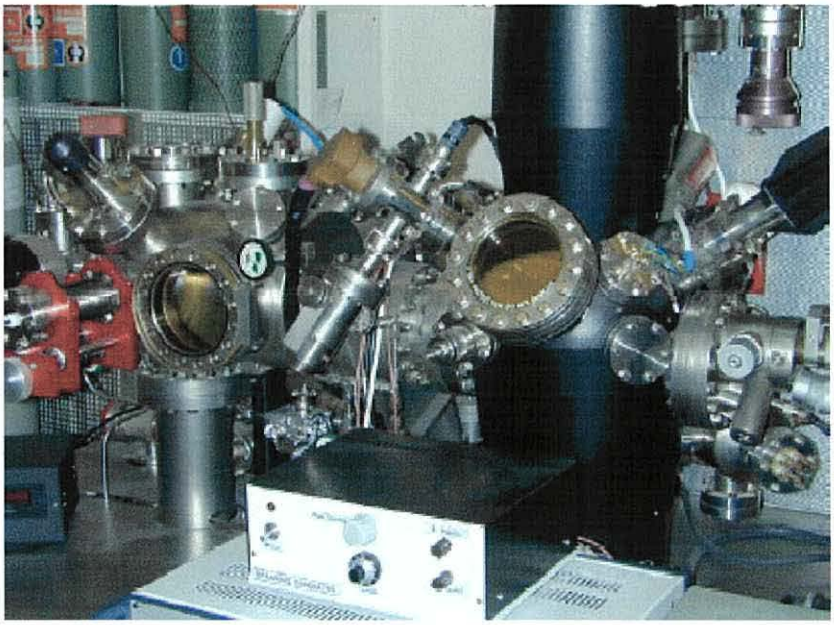

Figure 47 An illustration of X-ray photoelectron spectrometer, *Kratos*.

8.3.4 Scanning tunnelling spectroscopy

STM studies were performed with a *Digital Instruments Multimode* instrument using a *Nanoscope IV* control box. Additionally the STM apparatus was connected to a vibration isolation control unit. A schematic representation of the STM is presented in Figure 48.

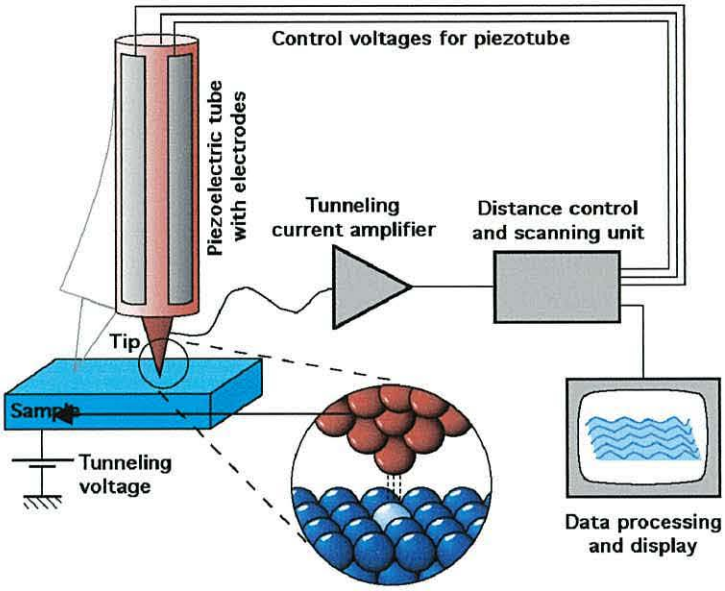

Figure 48 Schematic representation of STM [193].

Photographs of the STM head that was utilised for electrical measurements can be seen in Figure 49.

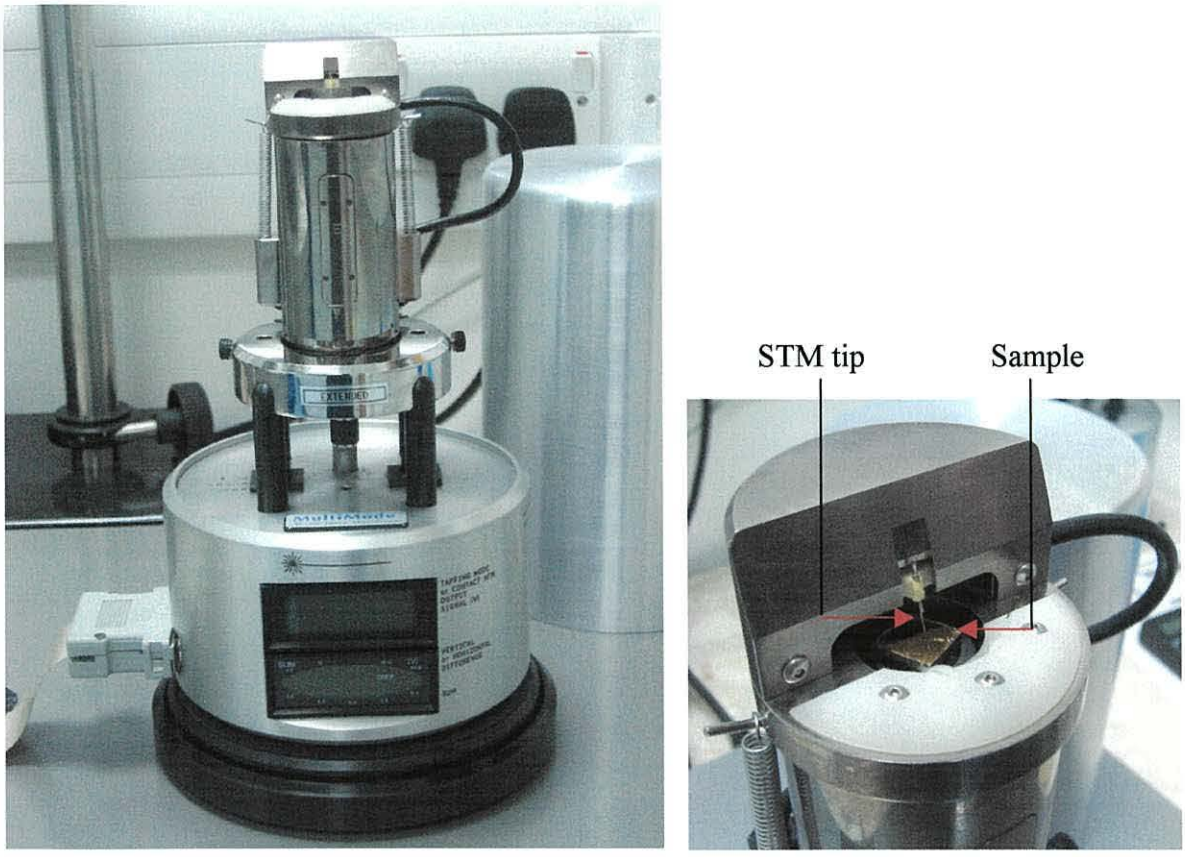

Figure 49 Digital Instruments Multimode STM.

For the studies described in this thesis, commercially available PtIr tips (Vecco *International*), and also plain gold tips were used, but only after prior plasma cleaning and rinsing with standard solvents. When the tip had been successfully landed and was scanning the surface, an even part of the substrate was located, and the tip was switched to the current-voltage (I-V) mode. A study of a gold surface, which was in contact with the HOPG, is presented in Figure 50.

(a)

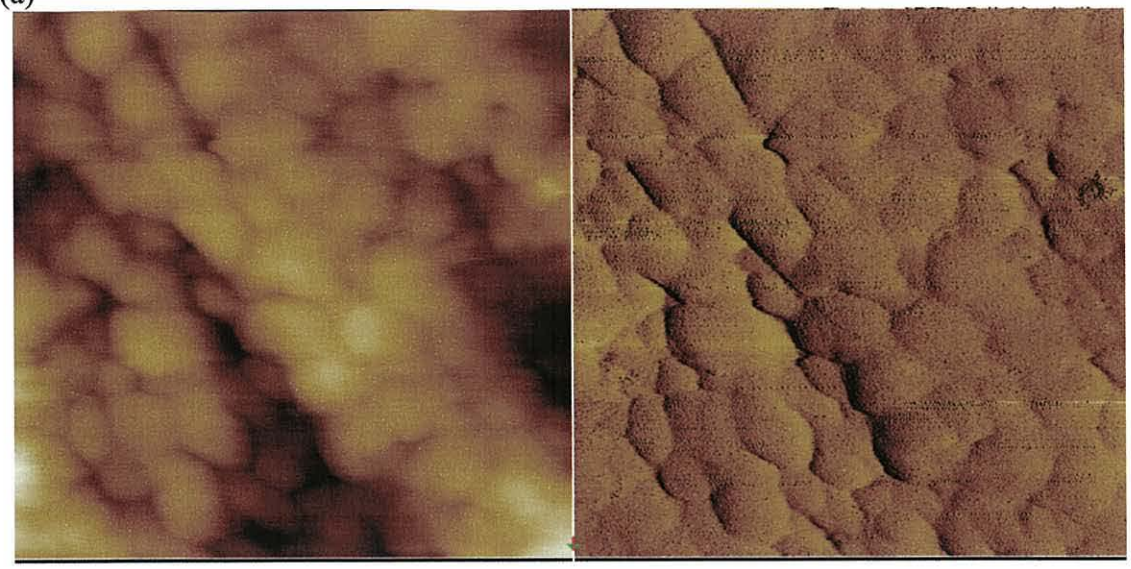

(b)

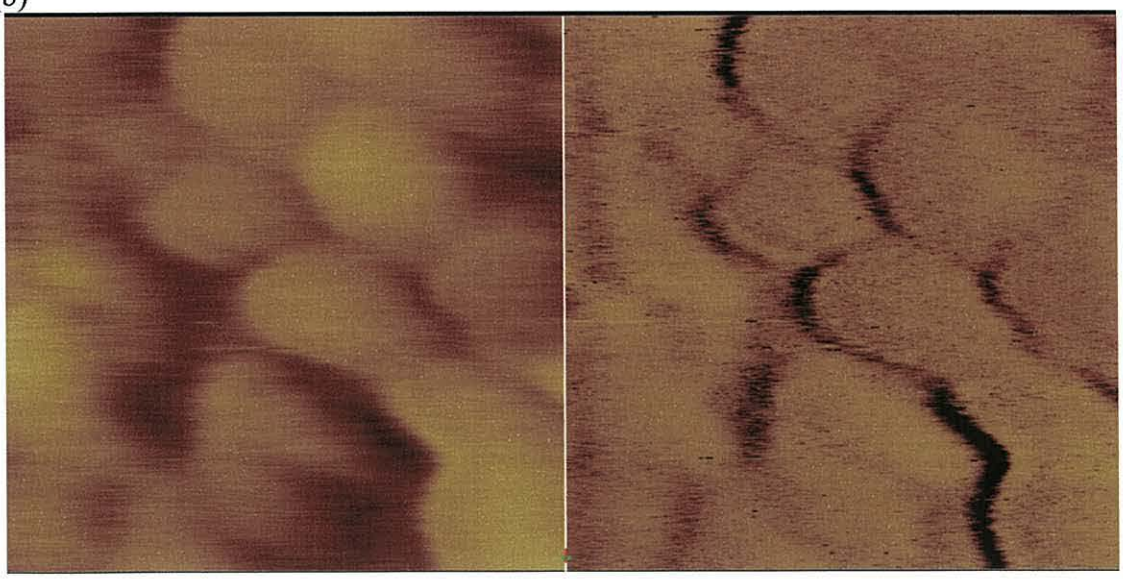

Figure 50 (a) 157 nm x 157 nm and (b) 58.8 nm x 58.8 nm surface of gold film coated on HOPG. The image was obtained with a PtIr tip at a set point current of 800 pA and a substrate bias of –1 V.

There are many parameters that influence operation of the STM and they are controlled by a computer. Parameters were adjusted for I-V studies, in order for the tip to reach a stable position at an adequate distance from the sample; in the range of 20–300 mV for the bias and 0.2–2 nA for the set point current. The I-V curves were an average of 10–30 single scans performed within a voltage range of –1.024 V to 1.024 V. All STM results presented in this thesis were obtained in the constant current mode.

8.4 Studied materials

Overall, this thesis contains the study of:

1) Molecular diodes (A–π–D | D);
2) Rectifying junctions (A | D);
3) Molecular wires.

The first part of the experimental work, which was performed during the first year of study is concerned with measurements of a new type of films in which a SAM of a cationic moiety was coupled with anionic donors: $Au–S–C_{10}H_{20}–A^{+}–\pi–D|D^{-}$ and $Au–S–C_3H_6–A^{+}–\pi–D|D^{-}$. SAMs of cationic donor–(π-bridge)–acceptor molecules and a strong donor, the copper(II) phthalocyanine-3,4',4'',4'''-tetrasulfonate salt (purchased from Sigma-Aldrich Chemical Co., Gillingham,UK), have resulted in highly rectifying devices. The cationic dyes were synthesised at Cranfield University by Dr Anne J. Whittam (Figure 51, 52, 53) and Dr Abdul Mohib (Figure 54). The electrical properties of these chromophores were studied before [158],[159],[165] but, in this dissertation, they are presented as molecular systems ionically coupled with a strong donor.

The second part of this thesis concerns single-molecule electrical studies of different length molecular wires, synthesised at the University of Durham by Changsheng Wang (Figure 55, 58) and Richard Jones (Figure 59 - 62). Moreover, this dissertation presents the measurements of a new type of organic rectifying junctions. Protonated cationic wires are electron accepting components in combination with an adjacent electron donating layer of the aforementioned copper(II) phthalocyanine or LiTCNQ (also purchased from Sigma-Aldrich Chemical Co., Gillingham,UK).

8.4.1 Hemicyanine dyes

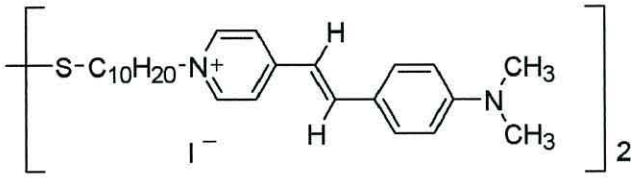

Figure 51 Molecular structure of bis-[1-(10-decyl)-4-(2-(4-dimethylaminophenyl)vinyl)pyridinium iodide]- disulfide (dye **1**).

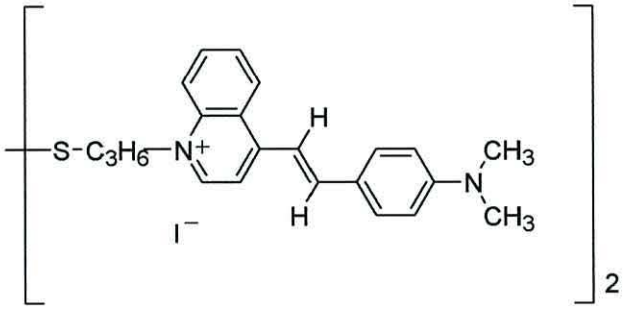

Figure 52 Molecular structure of bis-[1-{(3-propyl)-4-(2-(4-dimethylaminophenyl) vinyl) quinolinium}]disulfide diodide (dye **2**).

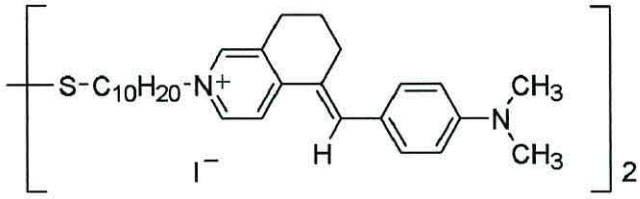

Figure 53 Molecular structure of bis-[1-(10-decyl)-5-(4-dimethylaminobenzylidene)-5,6,7,8-tetrahydroisoquinolinium iodide]disulfide (dye **3**).

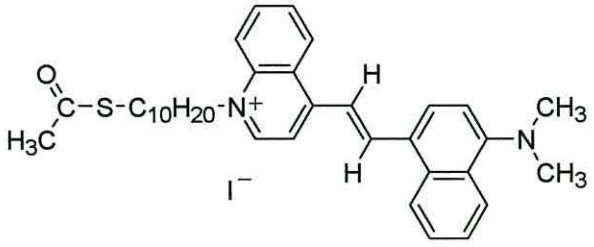

Figure 54 Molecular structure of 1-(10-acetylsulfanyldecyl)-4-{2-(4-dimethylaminonaphthalen-1-yl)-vinyl}-quinolinium iodide (dye **4**).

8.4.2 Arylene-ethynylene molecular wires with fluorene unit

5

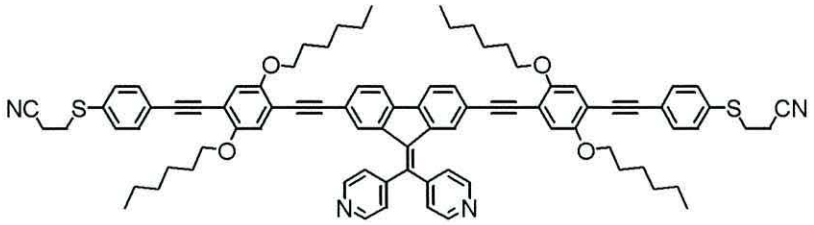

6

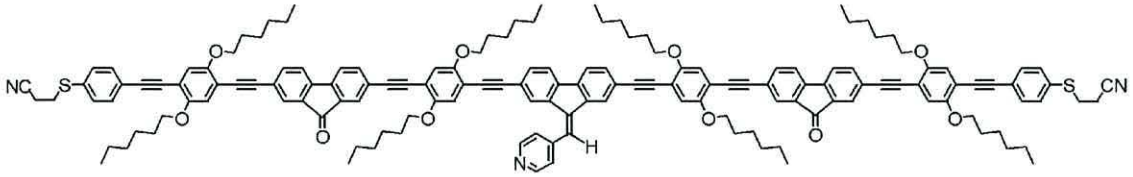

7

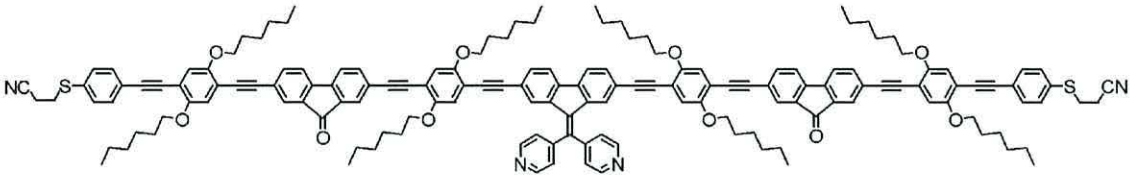

8

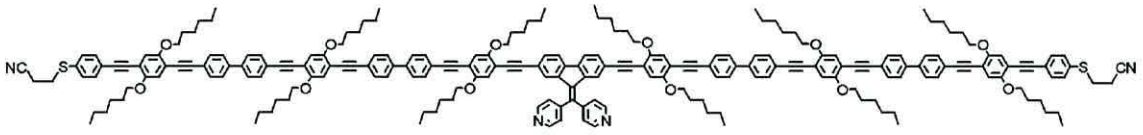

Figure 55 Molecular structure of the: **(5)** 4 nm, **(6, 7)** 7 nm and **(8)** 10 nm long molecular wires with the terminal sulphur showing the cyanoethyl group.

8.4.3 Molecules used as a strong donor in rectifying junctions

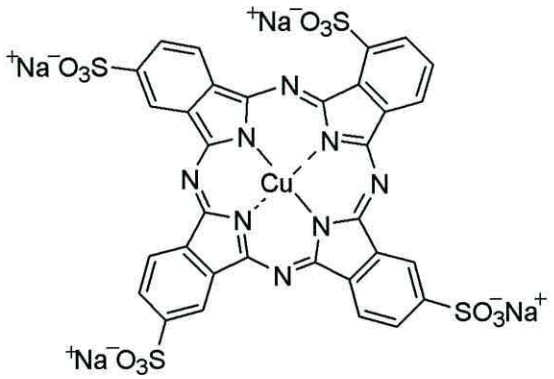

Figure 56 Molecule of copper(II) phthalocyanine-3,4',4'',4'''-tetrasulfonate salt, ($CuPc(NaSO_3)_4$).

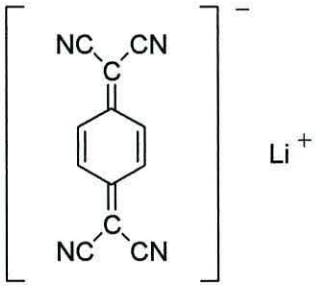

Figure 57 Molecule of lithium tertacyanoquinodimethane (LiTCNQ), TCNQ = 7,7',8,8'-tertacyanoquinodimethane.

8.4.4 Structures of 2 nm long thiol terminated oligo(phenylene-ethynylene) oligomers

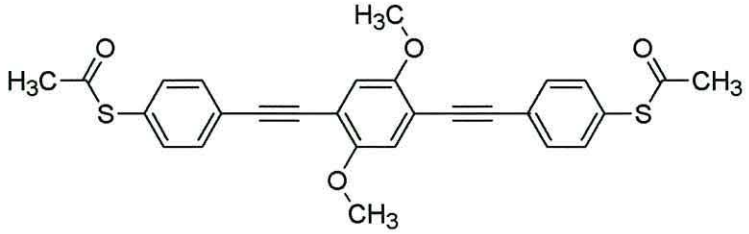

Figure 58 Molecule of 1,4-bis[4-(acetylsulfanyl)phenylethynyl)]-2,5-dimethoxbenzene, (molecule **9**).

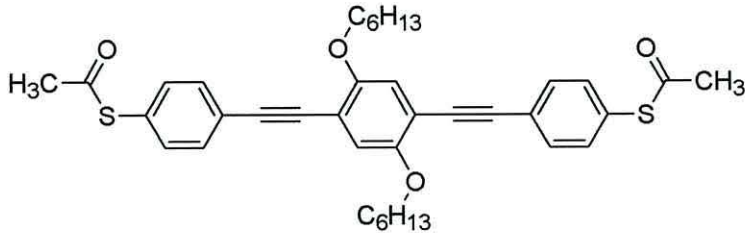

Figure 59 Molecule of 1,4-bis[4-(acetylsulfanyl)phenylethynyl)]-2,5-dihexyloxybenzene, (molecule **10**).

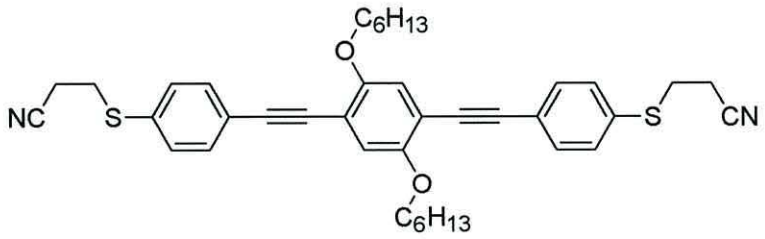

Figure 60 Molecule of 1,4-bis[4-(cyanoethylsulfanyl)phenylethynyl]-2,5-dihexyloxybenzene, (molecule **11**).

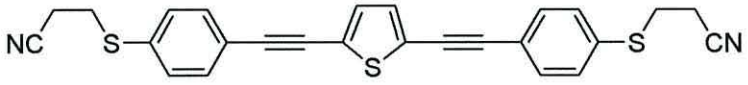

Figure 61 Molecule of 1,4-bis[4-(cyanoethylsulfanyl)phenylethynyl]-thiophene, (molecule **12**).

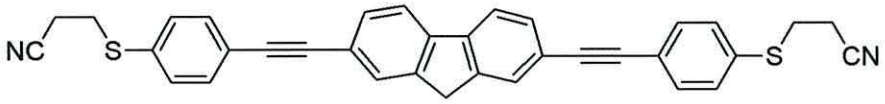

Figure 62 Molecule of 1,4-bis[4-(cyanoethylsulfanyl)phenylethynyl]-1,8-fluorene, (molecule **13**).

9. Results and discussion

9.1 Hemicyanine dyes

Four types of cationic donor–(π-bridge)–acceptor molecules (dye **1**, **2**, **3** and **4**) in a solution of the tetrasodium salt of copper(II) phthalocyanine-3,4',4'',4'''-tetrasulfonate were studied (see Figure 56). In each case, the films of the compound under study were prepared in the same way, using a one-stage process in which the gold-coated substrates were immersed in solutions of both the cationic and anionic dyes. Initial attempts at deposition of the films, which focused upon a two-stage process, were unsuccessful as the iodide probably located between the chemisorbed molecules and was inaccessible. During the deposition process the films were rinsed with a sequence of solvents to remove physisorbed material and with copious volumes of water to remove sodium iodide.

A SAM of the cationic moiety was coupled with that of a strong anionic donor ($CuPc(SO_3)^-_4$) and formed $Au–S–C_3H_6–A^+–\pi–D|D^-$ or $Au–S–C_{10}H_{20}–A^+–\pi–D|D^-$ structures. The inorganic ions, Na^+ from $CuPc(NaSO_3)_4$ and I^- from the cationic donor-(π bridge)-acceptor molecules, were displaced during the deposition process as NaI salt. All results were obtained by locating an anionic donor adjacent to the electron-donating end of a cationic $D–\pi–A^+$ dye, the latter being connected to, and aligned by, the gold substrate. Evidence of the deposition process was provided by XPS analysis for two of the complete systems, additional verification was also provided by the UV/visible spectra for each ionically coupled structures.

9.1.1 Deposition of a self–assembled pyridinium hemicyanine dye ($D–\pi–A^+$) and the tetrasodium salt of copper(II) phthalocyanine (D^-)

The cationic dye with a $S–C_{10}H_{20}$ group was deposited from a disulfide precursor (dye **1**) with the tetrasodium salt of copper(II) phthalocyanine dye. It was assumed that the S–S bond breaks when the molecules were adsorbed to the gold surface to form Au–S

bonds. Figure 63 presents a SAM deposited on a gold substrate of ionically coupled cationic dye **1** with anionic strong donor $CuPc(SO_3^-)_4$.

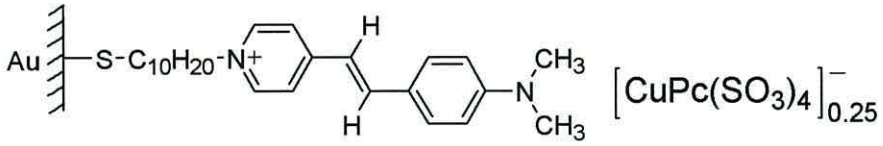

Figure 63 Dye **1** assembled to gold ionically coupled with copper(II) phthalocyanine.

A SAM of both dyes (see Figure 63) was successfully deposited on gold-coated substrates in an ethanol solution of pyridinium hemicyanine dye (1.7×10^{-5} M) and copper(II) phthalocyanine (9.0×10^{-6} M). The optimum deposition on QCM was obtained by short immersion times (5 minutes each) and thorough rinsing sequentially with chloroform, methanol, distillated water and ethanol to remove any physisorbed material. The deposition of a complete monolayer of the investigated mixture was seen at 100 minutes. The area per molecule was calculated by means of the Sauerbrey equation to be 2.89 ± 0.10 nm^2 molecule^{-1} for $[Au–S–C_{10}H_{20}–A^+–\pi–D]_4[CuPc(SO_3^-)_4])$, (see Figure 64). For other possible combinations of molecules, the area per molecule amounted to:

2.47 nm^2 molecule^{-1} for $[Au–S–C_{10}H_{20}–A^+–\pi–D]_3[CuPc(SO_3^-)_4\ Na^+]$,

2.00 nm^2 molecule^{-1} for $[Au–S–C_{10}H_{20}–A^+–\pi–D]_2[CuPc(SO_3^-)_4\ (Na^+)_2]$,

1.59 nm^2 molecule^{-1} for $[Au–S–C_{10}H_{20}–A^+–\pi–D]\ [CuPc(SO_3^-)_4\ (Na^+)_3]$.

A Sauerbrey analysis of the data, that yielded the above-mentioned values of the molecular area, is only an estimation of the real values, and it is difficult to assess which combination of the molecules would be the most probable. On the basis of the previous research, molecular areas of the self-assembled pyridinium hemicyanine dye and copper phthalocyanine dye, deposited on gold, amounted to 0.3 and 0.9 nm^2 molecule^{-1} respectively. Comparison of the obtained molecular areas with the van der Waals cross-section of the components indicates that there is sufficient space for coexistence of both dyes in the same layer.

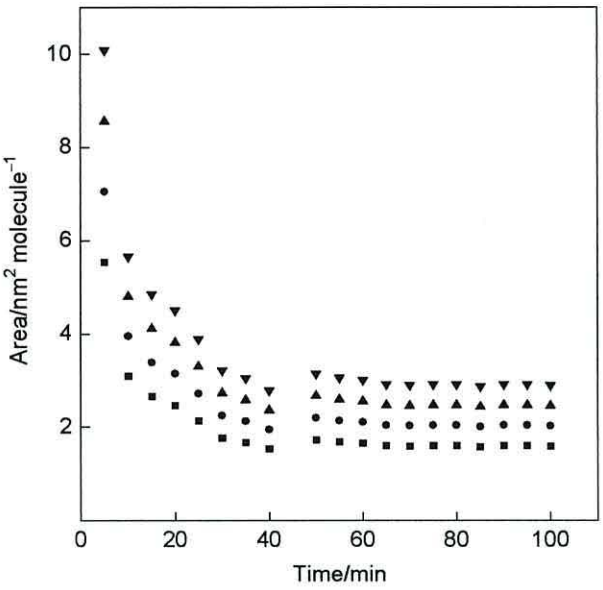

Figure 64 Variation of the molecular area versus the total period of immersion of quartz crystal in a mixture of ethanol solution of pyridinium hemicyanine dye and copper(II) phthalocyanine. Molecular area was calculated for different molecular mass depending on how many Na^+ and I^- ions were eliminated. Individual sign means molecular mass for: one cationic and one anionic dye (■), two cationic and one anionic dye (●), three cationic and one anionic dye (▲), four cationic and one anionic dye (▼).

The UV/visible spectrum, which is shown in Figure 65, consists of two absorption bands. The first of which is characteristic of the charge-transfer band of the D–π–A^+ chromophore, with a maximum at 490 nm, the second is within the range 593-700 nm, which is characteristic of $CuPc(SO_3^-)_4$.

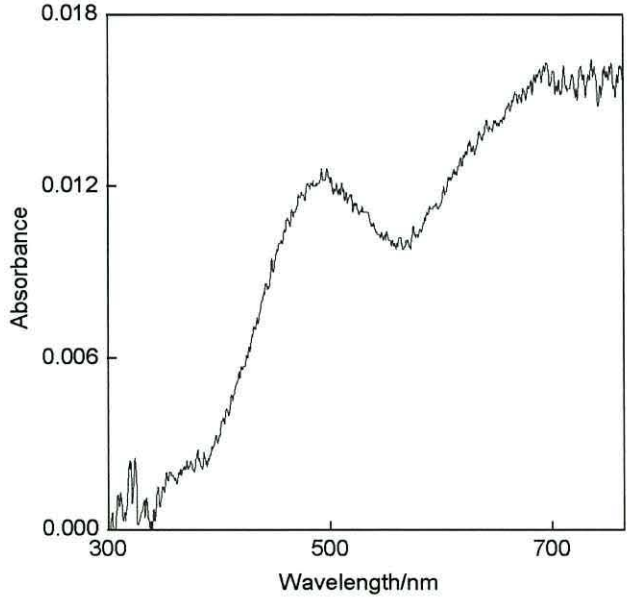

Figure 65 UV/visible spectrum of the self-assembled structures on platinum-coated glass.

Asymmetric I-V curves for self–assembled films of pyridinium hemicyanine dye and a tetrasodium salt of copper(II) phthalocyanine dye (Au–S–$C_{10}H_{20}$–A^+–π–D|D^-) were measured at many points on the sample (gold-coated HOPG). Data was obtained with a PtIr tip and exhibited a higher current in the negative quadrant as expected (see Figure 66), which corresponds to electron flow from the gold substrate (cathode) to the LUMO of the acceptor (cationic dye) and from the HOMO of the donor (anionic dye) to the tip (anode). The calculated rectification ratios were from 17 to 70 at ± 1 V in the range from 2.5 nA to 800 pA for the current set point (see Figure 66). It is necessary to emphasise that this value was significantly higher than that obtained for SAMs of the same iodide pyridinium hemicyanine dye studied at Cranfield University. This almost planar pyridinum analogue with an iodide counter ion exhibited symmetrical I-V characteristics with a rectification ratio less than 1.5 ± 1 V [159].

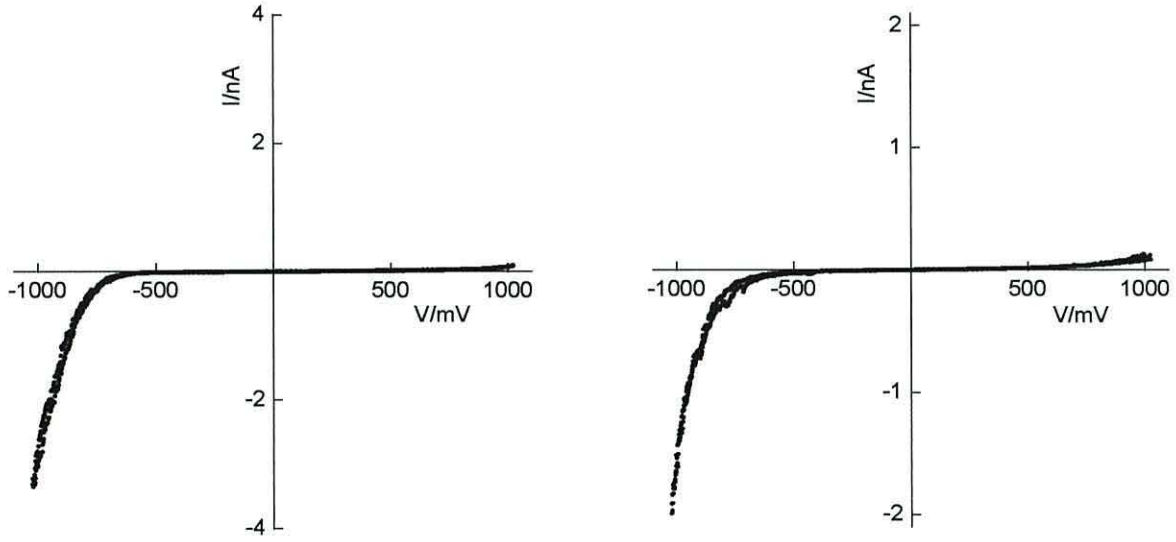

Figure 66 Typical I–V characteristics of a SAM of the ionically coupled dyes: pyridinium hemicyanine (D–π–A^+) and copper(II) phthalocyanine (D^-).

9.1.2 Deposition of SAMs of D–π–A^+ chromophore connected via Au–S–$(CH_2)_3$ bridge and the tetrasodium salt of copper(II) phthalocyanine

The cationic dye with a truncated S–C_3H_6 group was deposited from a disulfide precursor (dye **2**) with the tetrasodium copper(II) phthalocyanine (see Figure 67). A shorter alkyl chain was used in order to decrease the resistance of the linking group, but

the advantage obtained from having a reduced insulation may be counteracted by the inevitably less ordered nature of the SAMs of these structures [194].

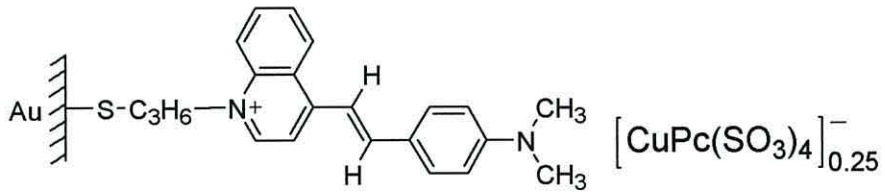

Figure 67 Molecular structure of SAM of dye **2** linked to the gold substrate and adjacent quarter part of copper(II) phthalocyanine.

Molecules were assembled on gold via immersion of a gold substrate into a mixture of 2×10^{-4} M cationic dye and 1×10^{-4} M copper(II) phthalocyanine. After 100 minutes total immersion of a QCM, in an ethanol solution of a quinolinium hemicyanine dye and copper(II) phthalocyanine dye, the frequency stabilised. The area occupied by ionically coupled molecules was calculated to be:

1.66 nm^2 $molecule^{-1}$ for $[Au–S–C_3H_6–A^+–\pi–D]_4[CuPc(SO_3^-)_4]$,

1.42 nm^2 $molecule^{-1}$ for $[Au–S–C_3H_6–A^+–\pi–D]_3[CuPc(SO_3^-)_4\ (Na^+)]$,

1.18 nm^2 $molecule^{-1}$ for $[Au–S–C_3H_6–A^+–\pi–D]_2[CuPc(SO_3^-)_4\ (Na^+)_2]$,

0.94 nm^2 $molecule^{-1}$ for $[Au–S–C_3H_6–A^+–\pi–D]\ [CuPc(SO_3^-)_4\ (Na^+)_3]$, (see Figure 68).

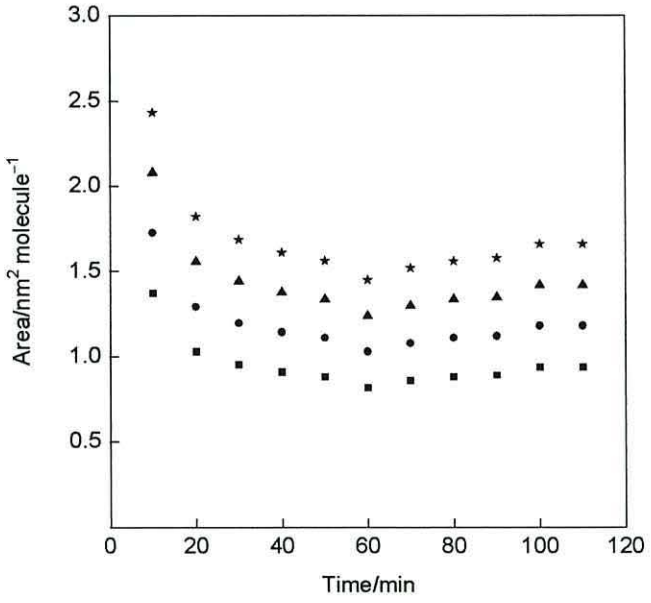

Figure 68 The area per molecule versus immersion time graph for the $Au–S–C_3H_6–A^+–\pi–D\,|\,D^-$ monolayer. Molecular area was calculated for different molecular masses depending on how many Na^+ and I^- ions were eliminated. Individual sign means molecular mass for: one cationic and one anionic dye (■), two cationic and one anionic dye (●), three cationic and one anionic dye (▲), four cationic and one anionic dye (*).

Comparison of the molecular areas obtained on the basis of Sauerbrey analysis with the van der Waals cross-section of the components indicates that there is insufficient space for coexistence in the same layer for both the cationic and anionic dyes. It is assumed that the film structure comprises a chemisorbed cationic species with its anions located at the surface.

The UV/visible spectrum exhibited a transition in the range 600-650 nm, characteristic of the charge-transfer band of $D–\pi–A^+$, and another at 680 nm that corresponds to the Q–band of $CuPc(SO_3^-)_4$ (see Figure 69).

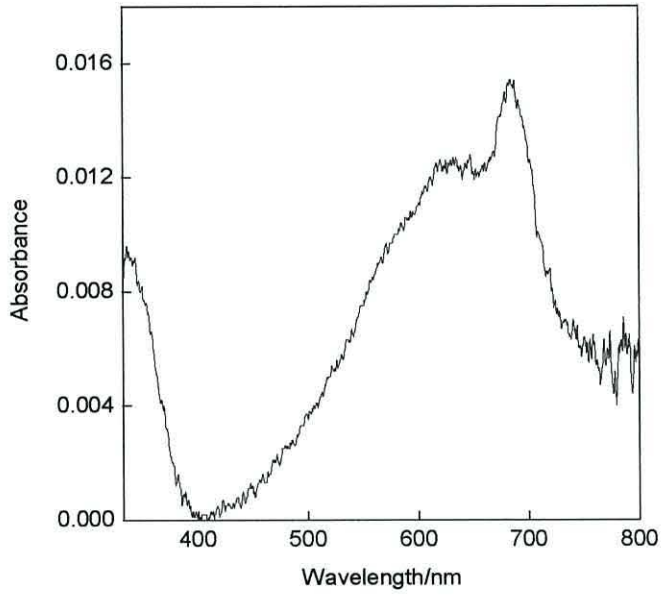

Figure 69 UV/visible spectrum of the SAM on platinum-coated glass substrate.

The asymmetric I-V characteristics of the film on gold-coated HOPG were investigated by STM with a PtIr tip and a typical plot is shown in Figure 70. The I-V characteristics obtained for the $Au–S–C_3H_6–A^+–\pi–D\,|\,D^-\,|\,Au$ exhibited higher current in the negative quadrant (see Figure 70), which would suggest that the preferred movement of electrons was from the gold surface through the molecule then to the PtIr tip. This is consistent with the Aviram-Ratner theory of rectification [2]. The calculated rectification ratios amount to 30–40 at ±1 V, which is almost four times higher than that obtained from SAMs of the same dye but with an iodide counter ion (the highest value of RR amounted to 12 at ±1 V [158]), which was also tested at Cranfield University.

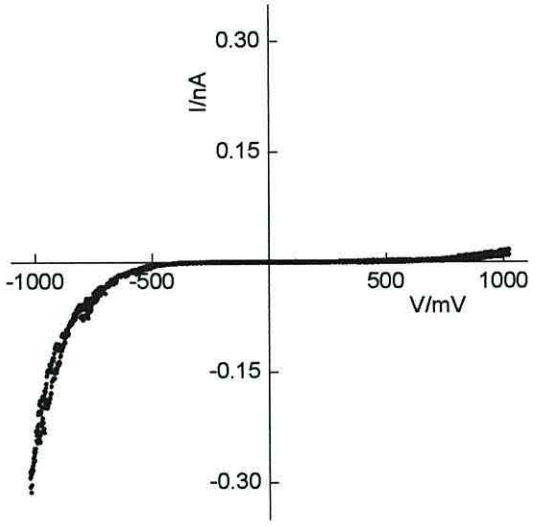

Figure 70 Typical I–V characteristics from a SAM of the $CuPc(SO_3)^-_4$ salt and the quinolinium hemicyanine dye. Electrons tunnel from the substrate (cathode) to acceptor on one side of the device, and from the donor to probe (anode) on the other.

9.1.3 Deposition of a SAM of isoquinolinium hemicyanine dye and the tetrasodium salt of copper(II) phthalocyanine

Films of the rectifying material were obtained by molecular self-assembly of bis-[N-(10-decyl)-5-(4-dimethylaminobenzylidene)-5,6,7,8-tetrahydroisoquinolinium]disulfide diiodide (2.4×10^{-4} M), (dye **3**) and the tetrasodium salt of copper(II) phthalocyanine (1×10^{-4} M), (see Figure 71).

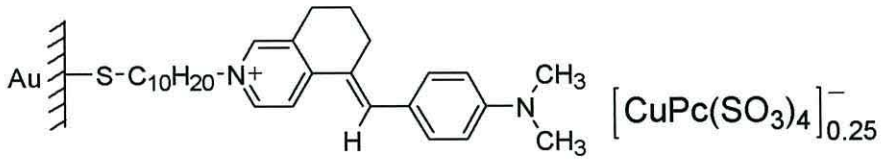

Figure 71 Molecular structure of SAM of dye **3** linked to the gold substrate and adjacent quarter part of copper(II) phthalocyanine.

The monitored frequency of the gold-coated quartz crystal stabilised to a constant value after *ca.* 65 minutes with data which correspond to a limiting area of *ca.* 1.57 ± 0.10 nm^2 molecule^{-1} for $[Au–S–C_{10}H_{20}–A^+–\pi–D]_4[CuPc(SO_3^-)_4]$, (see Figure 72). For other combinations of molecules the molecular area amounted to:

1.33 nm^2 molecule^{-1} for $[Au–S–C_{10}H_{20}–A^+–\pi–D]_3[CuPc(SO_3^-)_4\ Na^+]$,

1.10 nm^2 $molecule^{-1}$ for [Au–S–$C_{10}H_{20}$–A^+–π–D]$_2$ [CuPc(SO_3^-)$_4$ (Na^+)$_2$],

0.85 nm^2 $molecule^{-1}$ for [Au–S–$C_{10}H_{20}$–A^+–π–D] [CuPc(SO_3^-)$_4$ (Na^+)$_3$].

The values of the molecular area specified above confirm insufficient space for both ionically coupled components, to occupy the same layer and it is assumed that, the film structure comprises a chemisorbed cationic dyes with its anions located at the surface.

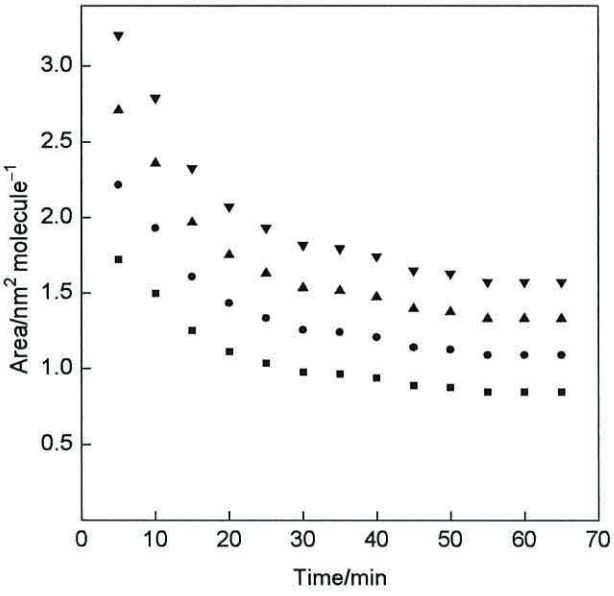

Figure 72 Variation of the molecular area versus the total period of immersion of quartz crystal in a mixture of methanol solution of isoquinolinium hemicyanine dye and copper(II) phthalocyanine. Molecular area was calculated for different molecular masses depending on how many Na^+ and I^- ions were eliminated. Individual sign means molecular mass for: one cationic and one anionic dye (■), two cationic and one anionic dye (●), three cationic and one anionic dye (▲), four cationic and one anionic dye (▼).

Comparison with the van der Waals cross-section of the components indicated that the self-assembled and ionically coupled species formed separate layers. This was also confirmed by SPR studies. A two-layer analysis of the SPR data yielded a thickness of 2.8 ± 0.2 nm, this is consistent with the anion forming a separate layer. This contrasts with 1.9 nm obtained for SAMs of the iodide salt in which spherical anions probably located between the D–π–A^+ moieties (Chapter 12, publication II). The area and thickness suggest a vertical arrangement of self-assembled cationic chromophores with the planar counterions being on edge and tilted towards the substrate.

Confirmation of metathesis was provided by XPS. The spectrum exhibited peaks at 162 and 167 eV, which are distinctive of the binding energies of the two types of sulphur (S 2p, Figure 73a) present in the gold thiolate link and sulfonate groups of the cationic and anionic species, respectively. The areas under the curves are in a ratio of ca. 1:1, which is consistent with the described molecular structure. Moreover, the peak at 399–401 eV corresponds to the nitrogen (N 1s, Figure 73b) of the isoquinolinium dye and phthalocyanine dye. Peaks that correspond to the Na^+ and I^- ions are either weak or not evident from spectra obtained, whereas those at 533 eV (O 1s, Figure 73c) and 935 eV (Cu 2p, Figure 73d) are unique to the $CuPc(SO_3^-)_4$ counterion that replaces the iodide.

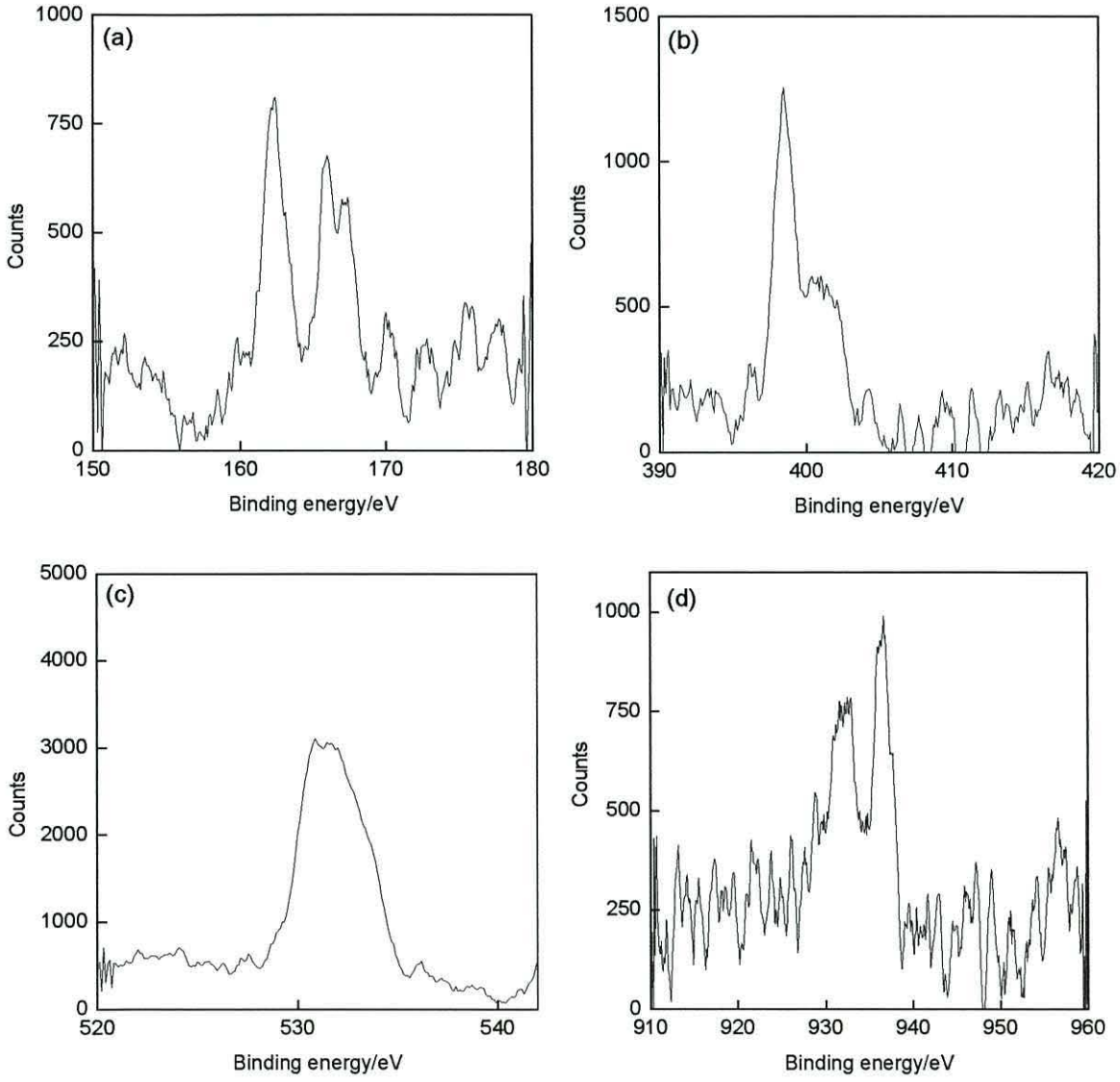

Figure 73 XPS spectra of the sulphur (2p), nitrogen (1s), oxygen (1s), copper (2p) core levels from a SAM of isoquinolinium hemicyanine dye and copper(II) phthalocyanine on gold.

Verification of metathesis was also provided by the UV/visible spectrum of the SAM on a platinum-coated glass substrate. The spectrum exhibited a transition at 480 nm, characteristic of the charge-transfer band of D–π–A^+, and two other bands which come from $CuPc(SO_3)^-_4$: Soret band at 340 nm and a broad Q-band in the range of 600–730 nm with a maximum intense peak at 690 nm, which is due to the $\pi \rightarrow \pi^*$ transition (see Figure 74).

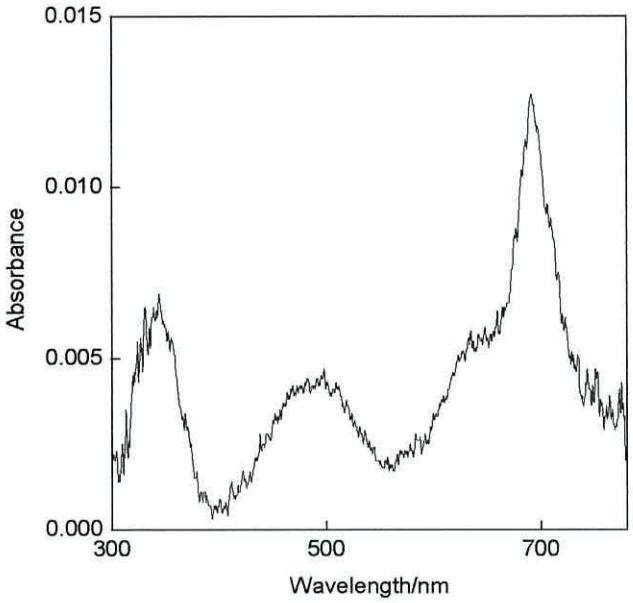

Figure 74 UV/visible spectrum of the SAM of a isoquinolinium hemicyanine dye and the copper(II) phthalocyanine on platinum-coated glass.

I-V characteristics of the organic film, on gold-coated HOPG measured by the STM, were reproducibility confirmed by varying the set point current and voltage for multiple scans. Each of four films was investigated and without exception every one exhibited electrical asymmetry unparalleled by any other organic diode. They exhibit strong asymmetry with rectification ratio in excess of 3000 at ± 1 V when contacted by either PtIr or Au probes (see Figure 75a,b). The rectification ratio is almost three orders of magnitude higher than obtained from SAMs of the same iodide salt of the same dye (RR≈5 at ± 1 V [159]). The much improved rectification is attributed to two key factors: (a) a non planar D–π–A^+ moiety induced by the $CH_2CH_2CH_2$ link between the heterocycle and π-bridge, this is vital as out of plane rotations of the donor and acceptor disrupt the conjugation but maintain the integrity of the electroactive end groups (see Chapter 12, publication II); (b) the location of the $CuPc(SO_3^-)_4$ anion at the surface

increases the electron donating capability of the electroactive device, which is represented here as Au–S–$C_{10}H_{20}$–A^+–π–D|D^-|Au.

STM images of the ionically coupled molecular structures on gold-coated HOPG were obtained using a gold probe and a set point current of 0.1 nA at a sample bias of –1 V, all films exhibited "streaks" approximately 2 nm long, as shown in Figure 75c. These streaks probably correspond to the van der Waals dimension of the edge of the phthalocyanine anion. This is consistent with a surface arrangement indicated by the thickness and area from SPR and QCM studies respectively. The STM images revealed a highly disordered surface arrangement, as the positive charges of the underlying cationic lattice are not ideally placed to locate the four SO_3^- groups of $CuPc(SO_3^-)_4$.

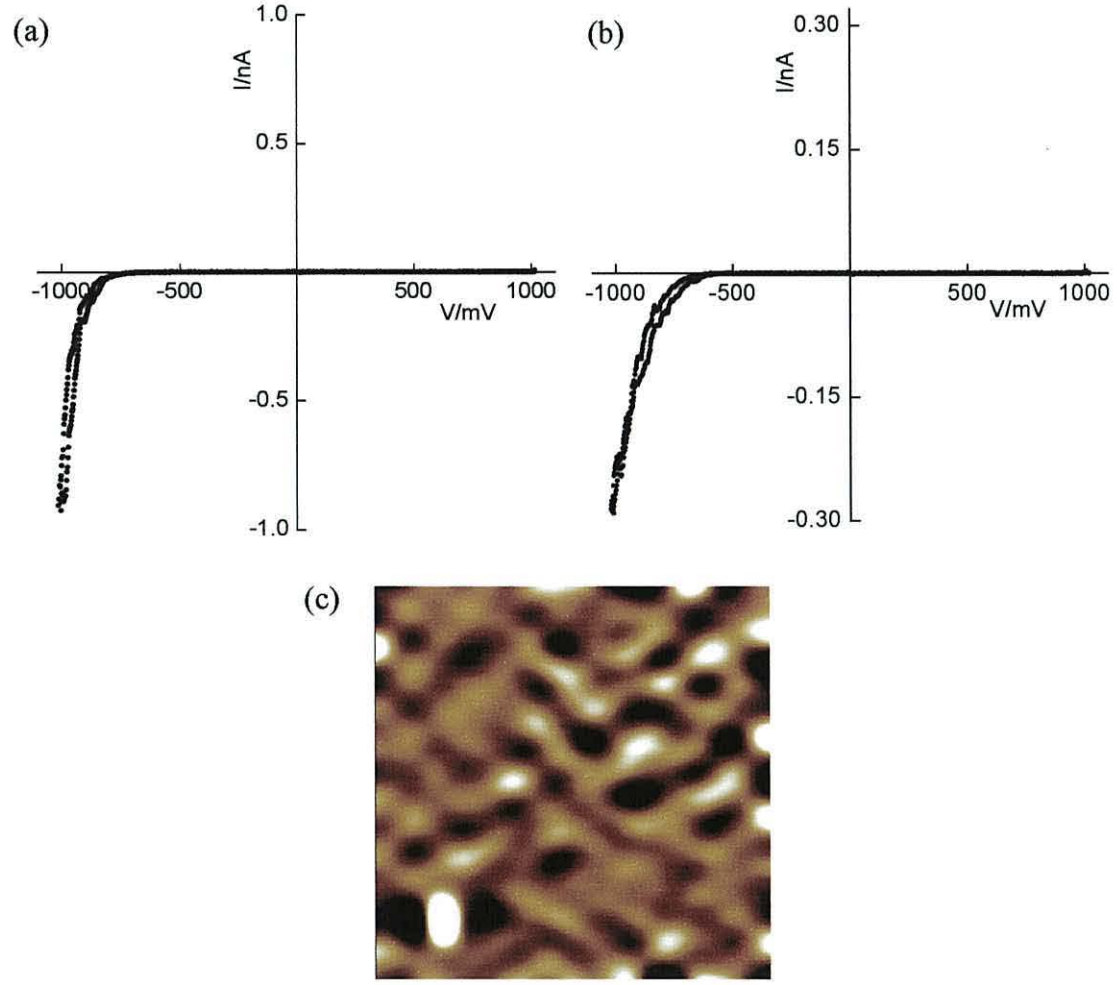

Figure 75 (a) and (b) Typical I–V characteristics from a SAM of the $CuPc(SO_3)^-_4$ salt and the isoquinolinium hemicyanine dye studied using PtIr and Au probe respectively. (c) A 10 nm × 10 nm STM image of the hughly disordered surface structure of SAM on Au.

This rectification is substantially higher than ratios reported from other organic films to date. This high value of the current ratio is on par with characteristic ratios from metal-insulator-metal structures obtained by McCreery [83],[195], where the behaviour arises from oxide-induced Schottky contacts.

9.1.4 Deposition of cationic dye (1-(10-acetylsulfanyldecyl)-4-{2-(4-dimethylamino-naphthalen-1-yl)-vinyl}-quinolinium iodide) and the tetrasodium salt of copper(II) phthalocyanine

Films were obtained by immersing HOPG, quartz crystal and platinum-coated glass in a mixture of ethanol solutions of 1×10^{-4} M dye **4** and 4×10^{-5} M tetrasulfonated salt of copper(II) phthalocyanine. Figure 76 presents a SAM of the ionically coupled compounds.

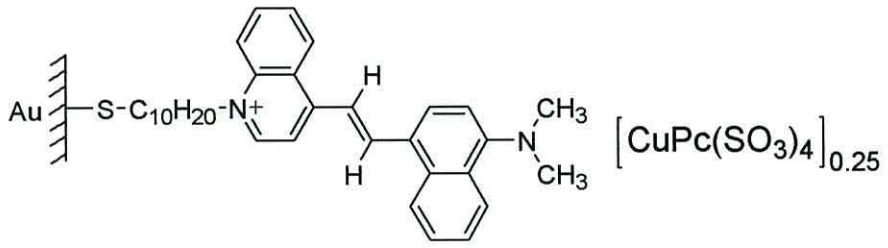

Figure 76 Molecular structure of a SAM of quinolinium cationic dye linked to the gold substrate and adjacent quarter part of copper phthalocyanine.

Optimum conditions for chemisorption were obtained by monitoring the frequency of the quartz crystals, which stabilised to a constant value after an immersion period of 200 minutes, the calculated molecular area amounted to 1.64 ± 0.10 nm^2 molecule^{-1} for: $[Au–S–C_{10}H_{20}–A^+–\pi–D]_4[CuPc(SO_3^-)_4]$, (see Figure 77). For other combinations of molecules, molecular area amounted to:

1.37 nm^2 molecule^{-1} for $[Au–S–C_{10}H_{20}–A^+–\pi–D]_3[CuPc(SO_3^-)_4\ Na^+]$,

1.10 nm^2 molecule^{-1} for $[Au–S–C_{10}H_{20}–A^+–\pi–D]_2[CuPc(SO_3^-)_4\ (Na^+)_2]$,

0.82 nm^2 molecule^{-1}for $[Au–S–C_{10}H_{20}–A^+–\pi–D]\ [CuPc(SO_3^-)_4\ (Na^+)_3]$.

The calculated areas by means of Sauerbrey equation suggest that the cationic moieties are closely packed with insufficient space for the iodide counterions to be located

between. It also may indicate the self-assembled and ionically species form separate layers.

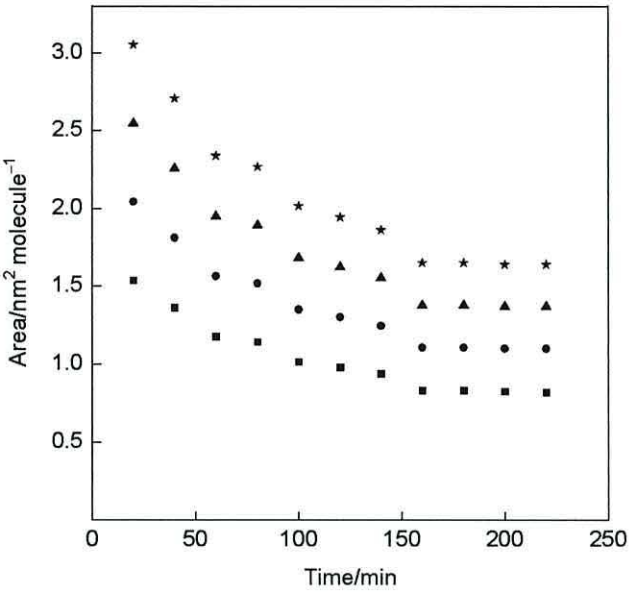

Figure 77 Variation of the molecular area versus the total period of immersion of quartz crystal in a mixture of ethanol solution of 1-(10-acetylsulfanyldecyl)-4-{2-(4-dimethylaminonaphthalen-1-yl)-vinyl}-quinolinium iodide and copper(II) phthalocyanine. Molecular area was calculated for different molecular mass depending on how many Na^+ and I^- ions were eliminated. Individual sign means molecular mass for: one cationic and one anionic dye (■), two cationic and one anionic dye (●), three cationic and one anionic dye (▲), four cationic and one anionic dye (*).

Evidence of metathesis was provided by the XPS studies and the UV/visible spectrum (see Figure 78). The distinctive binding energies of the two types of sulphur occurred at 126 eV, for the Au–S link of the cationic dye, and at 167 eV, for the SO_3^- groups of the counterion.

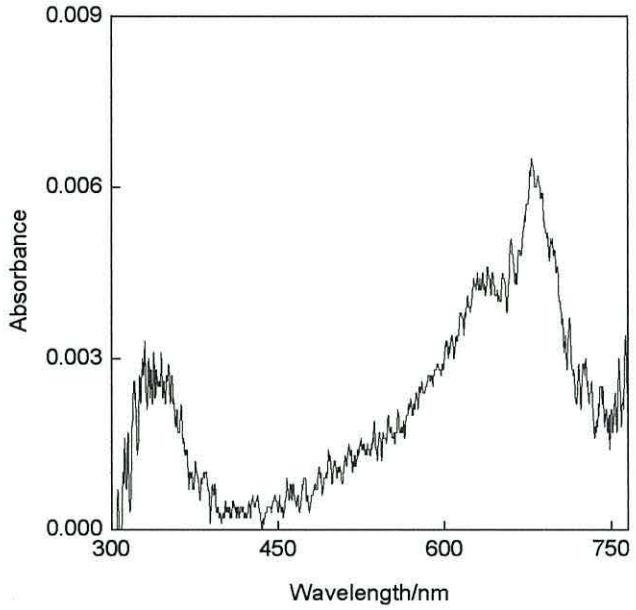

Figure 78 UV/visible spectrum of the self-assmebled dyes on platinum-coated glass.

Spectroscopic studies exhibited (see Figure 78) two absorption bands centered at 340 nm and 680 nm, which are characteristic for copper(II) phthalocyanine, and one broad band from the cationic dye in the range 500-655 nm, with a maximum at 630 nm.

Asymmetric I-V characteristics were obtained for $Au–S–C_{10}H_{20}–A^{+}–\pi–D|D^{-}$ using Au and PtIr probes for three different films. For these films 80% provided rectification ratios in excess of 90 at ± 1 V (Figure 79a), of which 40% exhibited values in the range 200-500 at ± 1 V (Figure 79b,c), some exhibited values in the range from 600 to 900 at ± 1 V (Figure 79d). The previous study, for the iodide salt of the compound, gave rectification ratios in the range 50–150 at ± 1 V [165].

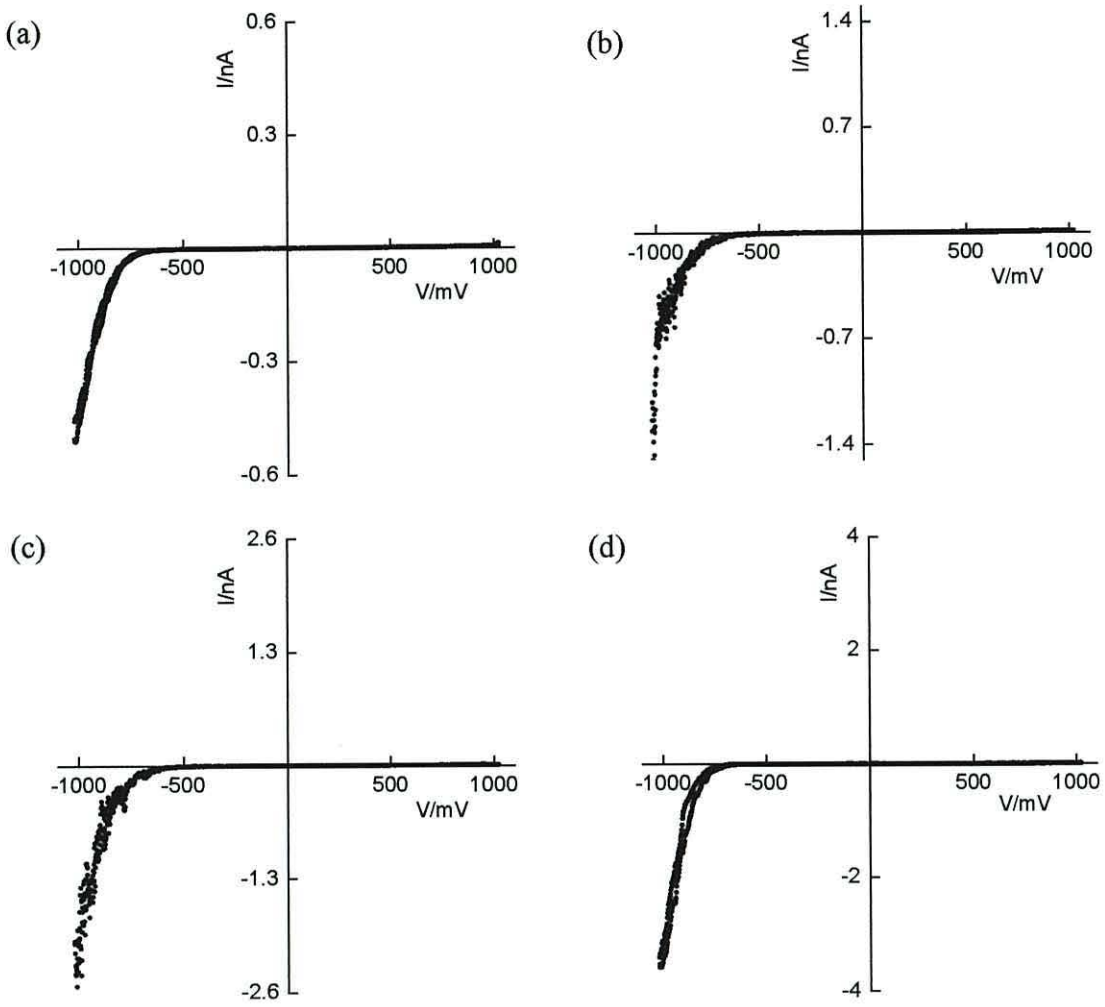

Figure 79 Typical I–V characteristics of Au–S–$C_{10}H_{20}$–A^+–π–D|D^- obtained for set point currents of 0.8-1.0 nA and a substrate voltage of 0.04-0.05 V studied using PtIr (a,d), and Au (b,c) probes.

9.1.5 Summary

The I-V characteristics for the iodide salts of the same D–π–A dyes (presented in Chapter 6.3.1.) showed rectification that was dependent upon the extent of the twist of the bridge (the molecule being sterically hindered to enforce a non-planar D–π–A structure). These results are not sufficient to have any practical significance; therefore, fabricating molecular systems with improved electrical asymmetries has become the new challenge.

Electrical behaviours obtained by measuring the I-V characteristics, were observed for all Au–S–C_nH_{2n}–A^+–π–D | D^- systems. High rectification ratio values were obtained by locating an anionic donor adjacent to the electron-donating end of a cationic D–π–A^+ dyes, the latter being connected to, and aligned by a gold substrate. The SAM measurements revealed higher current in the negative quadrant of the I-V plots. It follows that the direction of the electron flow, for all rectifying structures, was in accordance with the Aviram and Ratner model; this was from the cathode (substrate) to the acceptor of the cationic dye, and from the anionic donor to the anode (tip). The rectification was expected for the SAMs as the cationic molecules alone possessed varied steric hinderance. However, much higher rectification ratios were observed for Au–S–C_nH_{2n}–A^+–π–D | D^- systems as a result of ionic-electrostatic interactions of the cationic dyes with an anionic strong donor. Rectification ratios in a wide range of 20-500 at ±1 V and even in excess of 3000 at ±1 V (in case of the isoquinolinium hemicyanine dye **3**) are the highest to date for molecular diodes. These revelations have been published and are of great scientific importance in the field of molecular rectification. The details about publication can be found in Chapter 12, publication II.

9.2 Electrical studies on arylene-ethynylene molecular wires with a central fluorene unit

Four arylene-ethynylene oligomers **5**, **6**, **7**, **8** were studied (also presented before in Figure 55), which had 4, 7 and 10 nm (S·····S distances) long linear backbones, hexyloxy side-chains to ensure solubility in organic solvents and terminal thiol groups for chemisorption protected by cyanoethyl. They also incorporate a central 9-[(4-pyridyl)methylene]fluorene unit (compound **6**) or 9-[di(4-pyridyl)methylene]fluorene (compounds **5**, **7**, **8**) moiety. Additionally, both 7 nm long wires (**6**, **7**) incorporated 9-fluorenone units in its backbone to impart electron-accepting characteristics despite being separated by weak dialkoxyphenyl donors. SAMs of wires **5**, **6**, **7** and **8** were fabricated by immersion of gold-coated substrates (QCM and HOPG) in a tetrahydrofuran (THF) solution to which sodium methoxide was added to facilitate removal of the cyanoethyl groups. Substrates were repeatedly immersed into solutions of studied compounds and washed each time with THF to remove physisorbed material from the surface.

9.2.1 Single-molecule electrical studies

9.2.1.1 A 4 nm long conjugated molecular wire

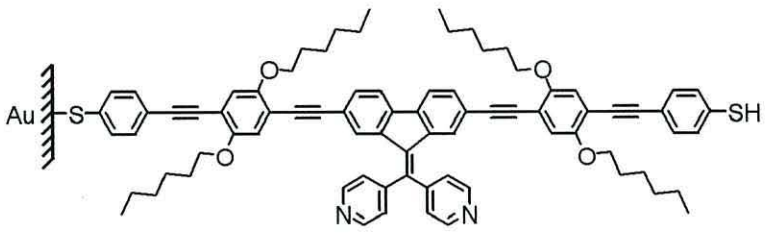

Figure 80 The assembled structure of the deprotected wire **5**.

A monolayer of compound **5** (see Figure 80) was prepared from a 0.08 mg ml^{-1} solution in THF using a sequence of 10 minutes immersions. Optimum deposition for wire **5** was achieved after ca. 120 minutes (see Figure 81). The resultant monolayer had an area per molecule of 1.5 ± 0.2 nm^2 $molecule^{-1}$ for deposition from solution with or without deprotecting agent. In the absence or presence of sodium methoxide, the immersion time

was similar. The area is consistent with the calculated values from the van der Waals dimensions of the molecular wire.

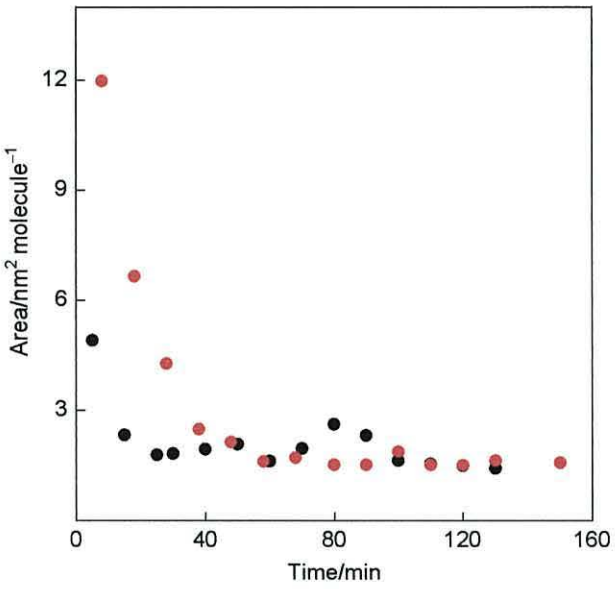

Figure 81 Variations of the molecular area with the combined period of immersion of a gold-coated 10 MHz quartz crystal in a THF solution of the self-assembling molecular wire **5** (0.08 mg ml^{-1}) to which sodium methoxide was added (•), and without deprotection (•).

SAMs of the 4 nm long molecular wire exhibited symmetrical I-V characteristics (see Figure 82), although slight electrical asymmetries were observed albeit infrequently. Symmetrical I-V characteristics have been obtained for both Au and PtIr tips, which is not unexpected as their work functions are similar (-5.5 eV for PtIr [196] and -5.3 eV for Au [197]). This is a common feature from STM studies on wire-like molecules. The set point current and voltage had very little effect on the profile of the I-V curves, but they did affect the magnitude of the tunnelling current by influencing the distance between the probe and the surface. The curves presented in Figure 82 were obtained using a set point current and voltage of 0.6-0.9 nA and 0.04-0.3 V, respectively.

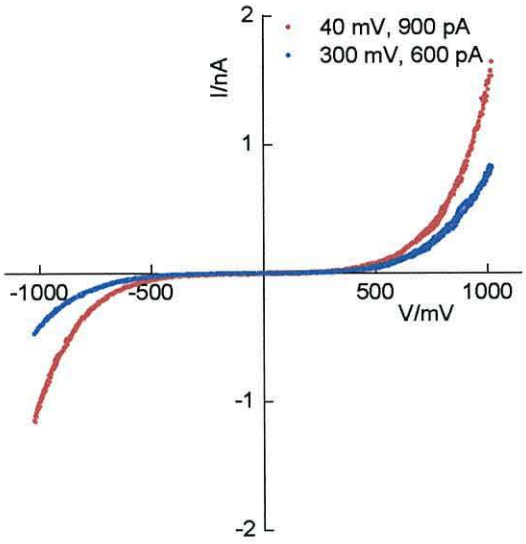

Figure 82 I-V characteristics of the molecular wire **5** deposited with the deprotecting agent as a SAM on gold-coated quartz crystal and contacted by a gold tip.

Using the methods of Haiss *et al.* [114],[115],[118], to measure the electrical conductivity of single molecules, the electronic properties of single 4 nm long arylene-ethynylene wire **5** were studied. Both methods were based on trapping molecules between an STM tip and a substrate. The spontaneous adsorption and desorption of wires, with abrupt changes in the tunnelling current, was easy to observe within the time frame and the tip-sample distance domains used. Each adsorption/desorption of wire **5** persisted for *ca.* 110 ms (see Figure 83a) with almost 25 % of all current jumps within the range 0.15-0.20 ± 0.05 nA for a surface bias of –0.3 V (see Figure 83b). The single molecule current of *ca.* 0.2 nA at –0.3 V is about one order of magnitude larger than the value displayed by the I-V plot at this voltage (see Figure 82). This can be explained by the latter being dependent upon the set point conditions which influenced the distance between the probe and the surface, whereas the former is independent of the set point current [114] as the molecule is chemisorbed by both electrodes. However, the upper limiting current exhibited by I-V curves of thiol-terminated molecules approached the corresponding single-molecule value obtained from the current-jump method as the set point conditions were altered to minimise the gap between the surface and probe.

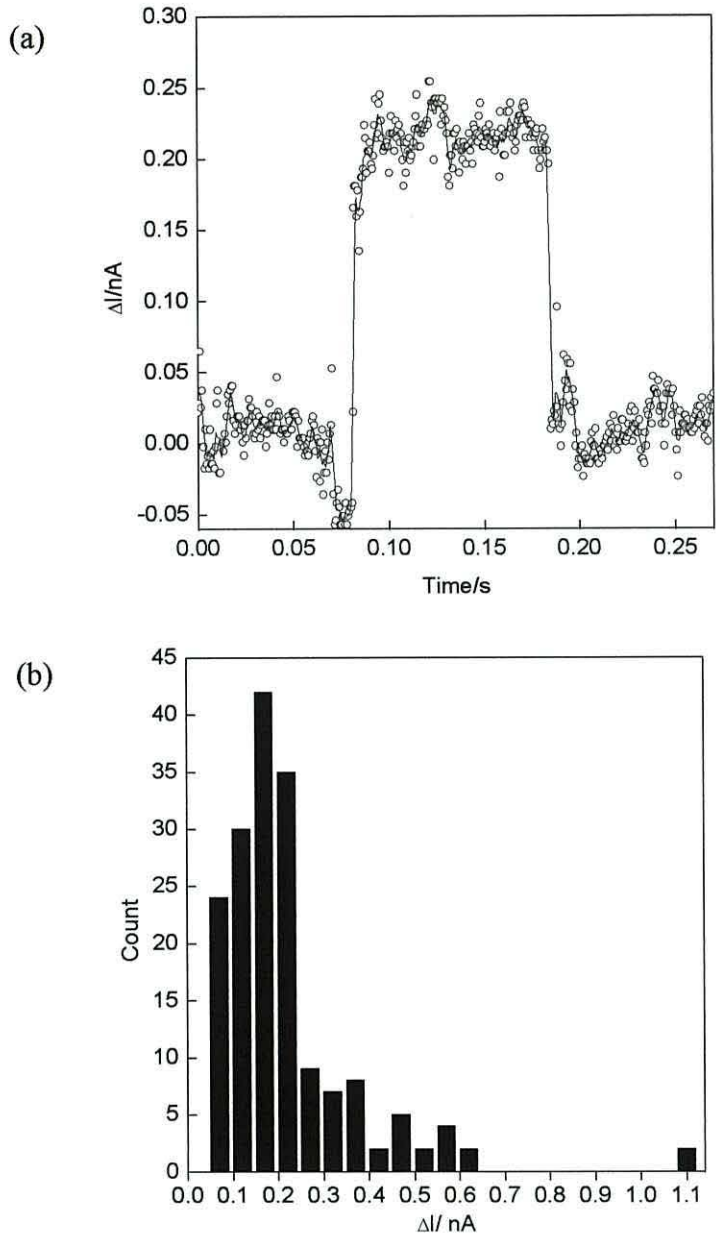

Figure 83 (a) Current jump with the gold STM probe located at a fixed height above the SAM with a sample bias of –0.3 V. (b) Histogram of 172 recorded current jumps at a sample bias of –0.3 V.

The I(s) relation was measured in two ways; first relied on slowly bringing the STM tip close enough to the Au surface, then quickly lifting the tip while keeping the X-Y position constant; the second relied on quickly bringing the tip to the surface and slow lifting. Results of the spontaneous formation of a stable molecular wire of **5** between the gold STM tip and the sample, obtained using the second method, better illustrated the

studied phenomenon. Figure 84 presents some typical examples of I(s) scans obtained for molecular wire **5**.

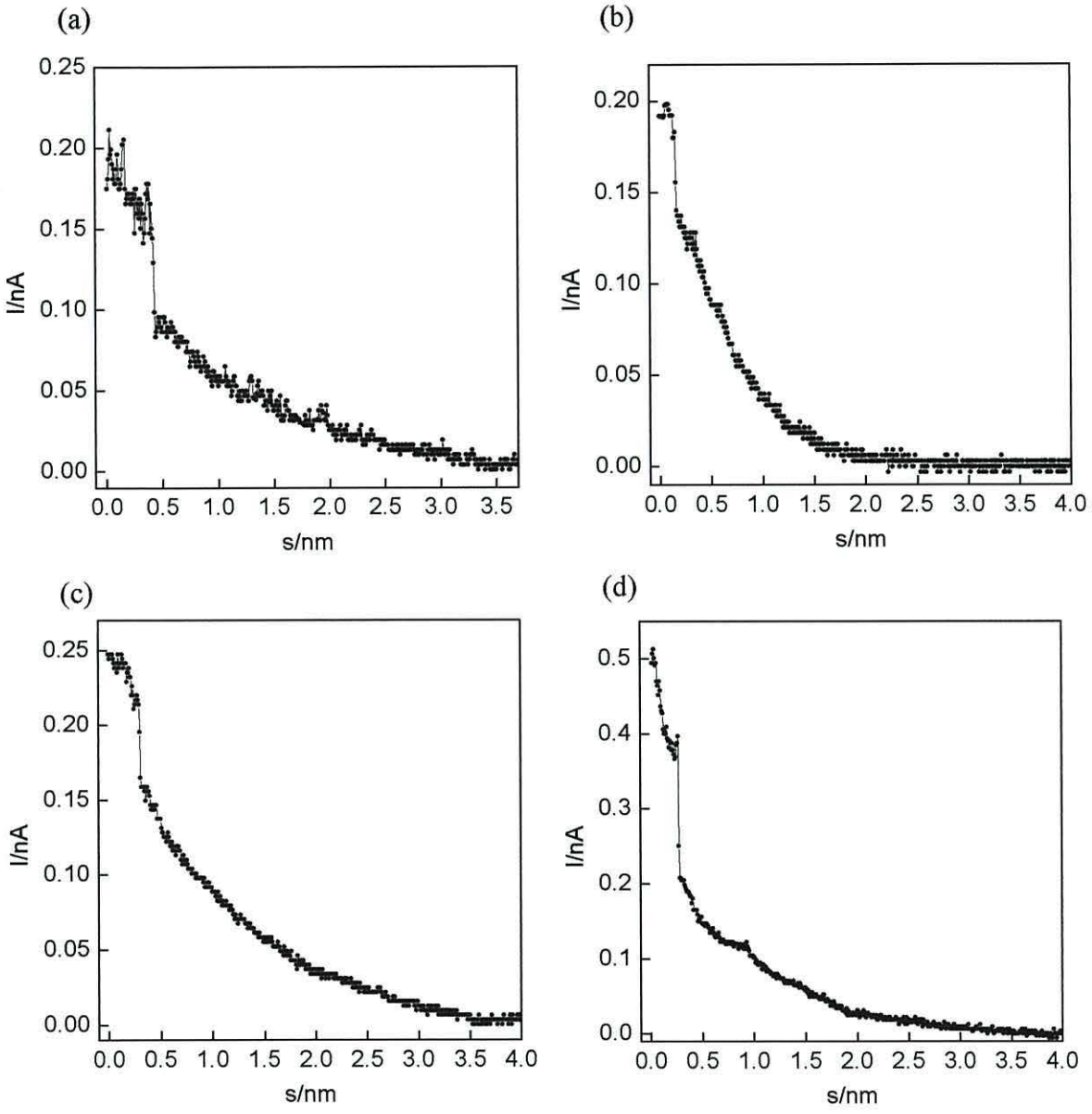

Figure 84 Current decay scans (I(s) scans) for molecule **5** on Au in air measured at 0.3 nA and 0.03 V. (a), (b) and (c) present current pletau at lower values of I (*ca.* 0.18, 0.19 and 0.25 nA) that corresponds to the conductance through the single molecule wire, (d) current pletau at higher value of I (*ca.* 0.39 nA) that corresponds to the conductance through the few molecules.

The current plateau that could be observed in the I(s) curves for many contact events have clear maxima in the range 0.18–0.39 nA (see Figure 84a,b,c,d). The comparison of the results of the I(t) and I(s)methods shows an important feature: the current corresponding to the basic conductance unit is the same for both techniques.

9.2.1.2 A 7 nm long conjugated molecular wire with one central pyridyl unit

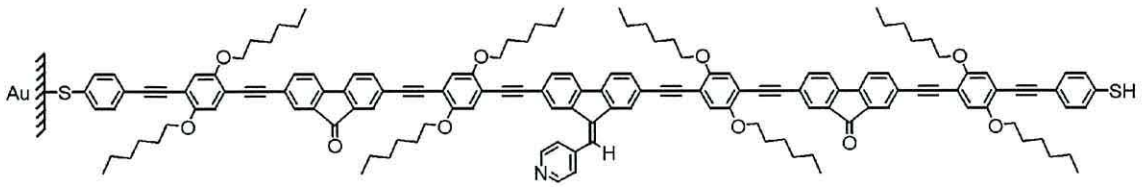

Figure 85 The self assembled structure of the deproteced wire **6**.

A monolayer of compound **6** (see Figure 85) was prepared from a 0.05 mg ml^{-1} solution in THF using a sequence of 10 minutes immersions. Substrates were repeatedly immersed for 15 minutes intervals and washed with THF to remove physisorbed material from the surface. Throughout this process, self-assembly was monitored from the frequency change on a gold-coated 10 MHz quartz crystals. The frequency stabilised to a constant value after 2 hours, and a Sauerbrey analysis of the data provided a mean area of 1.7 ± 0.4 nm^2 $molecule^{-1}$ for the chemisorbed wire (see Figure 86). The same value was also obtained by omitting the deprotecting agent - sodium methoxide, but the timescale for assembly was considerably longer (Chapter 12, publication I). However, the area was consistent with the van der Waals dimensions of the molecular wire but only if partial overlap of these highly tilted molecules was assumed.

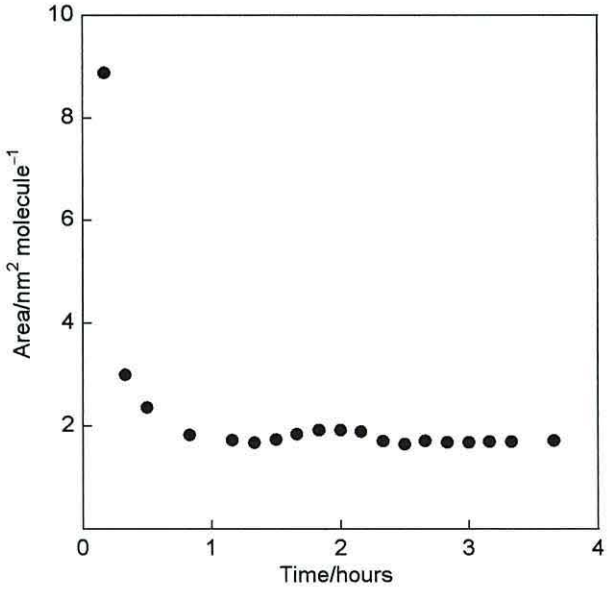

Figure 86 Variations of the molecular area with the combined period of immersion of a gold-coated 10 MHz quartz crystal in a THF solution of the self-assembling molecular wire **6** to which sodium methoxide was added.

UV/visible spectra on a platinum-coated glass slide, which exhibited a peak at 400 nm in both cases (*cf.* 400 nm in THF solution), confirmed the self-assembly of the studied compound. UV/visible spectra are presented in Figure 87.

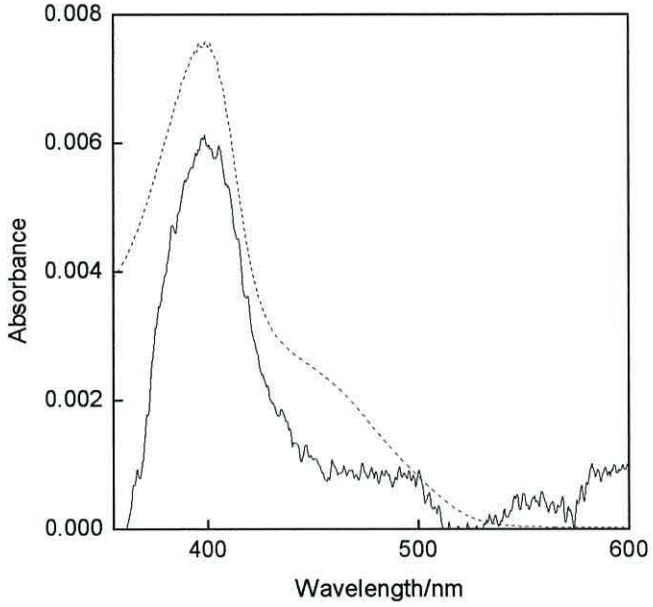

Figure 87 UV/visible absorption spectrum of SAMs of **6** on a platinum-coated glass (solid line) and the spectrum of **6** in THF solution (dotted line).

SAMs of the 7 nm long molecular wire **6** (Figure 85) exhibited symmetrical I-V characteristics (see Figure 88), although slight electrical asymmetries were observed, albeit infrequently. The subtle difference in the shape of I-V curves is a result of the varied parameters, e.g. the set point current was varied from 0.5 to 0.8 nA at a constant bias 0.05 V. Symmetrical I-V characteristics have been obtained for both Au and PtIr tips, and do not seem to be anything unusual as their work functions are similar.

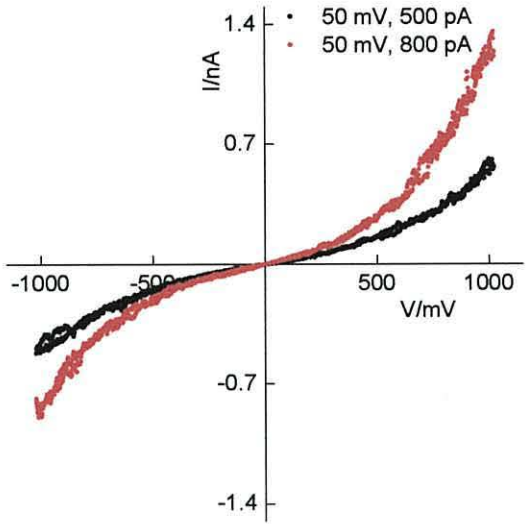

Figure 88 I-V characteristics of molecular wire **6** deposited as a SAM on gold-coated HOPG and contacted by a gold tip.

Single molecule studies were performed by monitoring the single molecule current as a function of time. Measurements were performed at a surface bias of –0.3 V and a tunnelling current jump, via a single molecule contacted by –SH groups to both Au contacts, is shown in Figure 89.

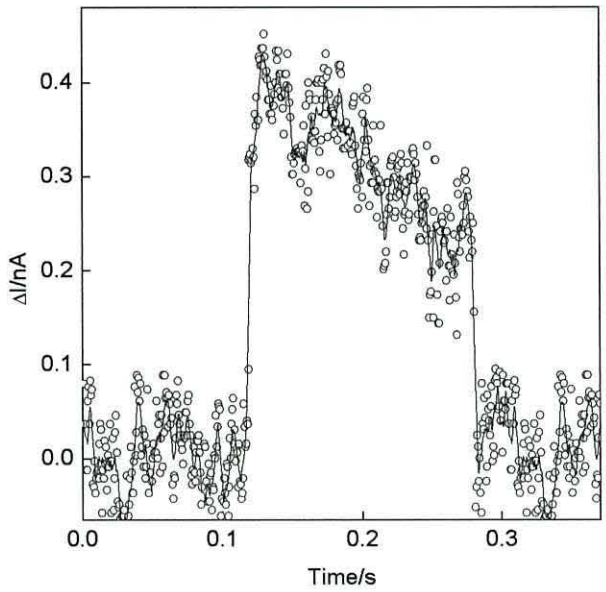

Figure 89 Typical current jump of molecular wire **6** with the gold STM tip located at a fixed height above the SAM with a sample bias of –0.3 V.

The spontaneous adsorption/desoprtion process was easy to observe, and persisted for 160 ms for the clearest observable current jumps. The current jumps were reproducible for each point that was probed by an Au tip. Almost 50 % of all current jumps were within the range 0.35-0.4 ± 0.05 nA, for a surface bias of -0.3 V (Figure 90). This was attributed to the single molecule current, with adsorption via a single thiolate link to the tip. Observations of current jumps allowed the construction of a histogram showing eighty-one recorded events of **6** (see Figure 90). Six events of **6** exhibited current jumps of 0.7 ± 0.05 nA, which were almost double the aforementioned values and probably corresponded to the probe contacting two molecules. There is also evidence of higher numbers of molecules, with four events centred about 1.0 ± 0.05 nA, these being indicative of three-molecule contact, and another about 1.3 nA and even 1.6 nA.

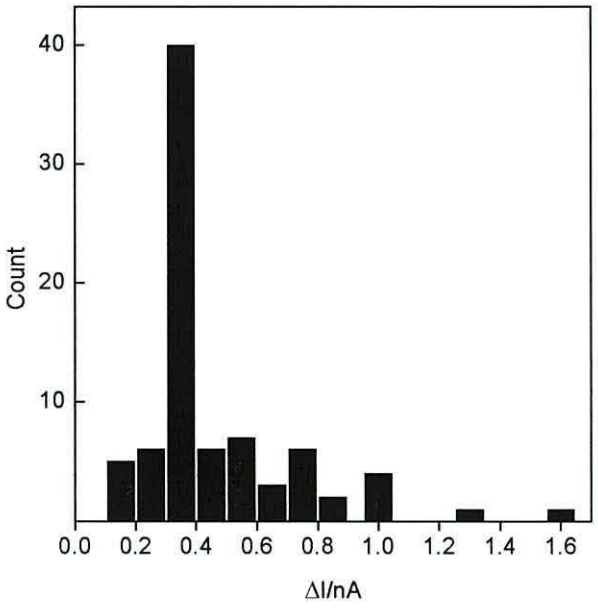

Figure 90 Histogram of 81 recorded current jumps at a sample bias of –0.3 V for molecular wire **6**.

9.2.1.3 A 7 nm long conjugated molecular wire with two central pyridyl units

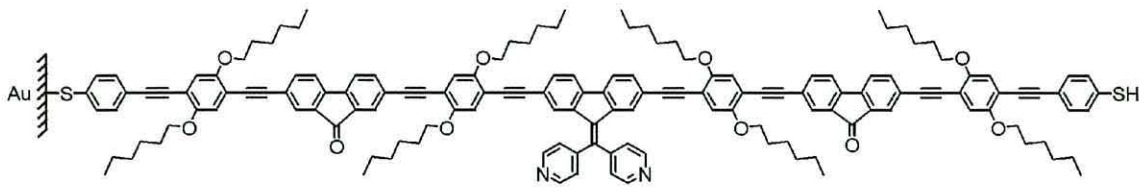

Figure 91 The self assembled structure of the deproteced wire **7**.

Gold-coated substrates were immersed in a THF solution of **7** (0.05 mg ml^{-1}) containing sodium methoxide, and the formation of a SAM (see Figure 91) was monitored from the frequency changes following depositions on a gold-coated crystal. The frequency stabilised after about 0.5 hour to a constant value of about 1.30 ± 0.06 nm^2 $molecule^{-1}$ for the chemisorbed wire (see Figure 92). In the absence of deprotecting agent the immersion time increased to 4 hours The area is consistent with the calculated value from the van der Waals dimensions of the molecular wire, assuming partial overlap of the highly tilted molecules in the SAM.

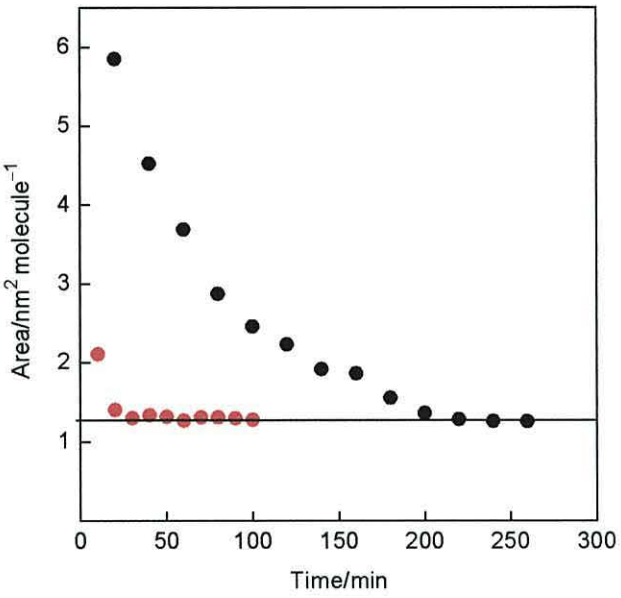

Figure 92 Variation of the molecular area with the period of immersion of a gold-coated crystal in a THF solution of **7** (0.05 mg ml^{-1}) to which sodium methoxide was added (•), and without deprotection (•).

Evidence of self-assembly of **7** was provided by XPS study, which revealed an S dublet at 162.1 and 163.5 eV (S 2p) corresponding to the binding energy of the gold thiolate link. Another doublet characteristic for a surface-based terminal thiol group was observed at 163 and 164.6 eV. The UV/visible spectrum of the SAM on platinum-coated glass exhibited a peak at about 400 nm when corrected for the absorbance of the substrate. The characteristic peak from the SAM of **7** is similar to the solution spectrum in THF of the same compound (λ_{max} 402 nm), (see Figure 93).

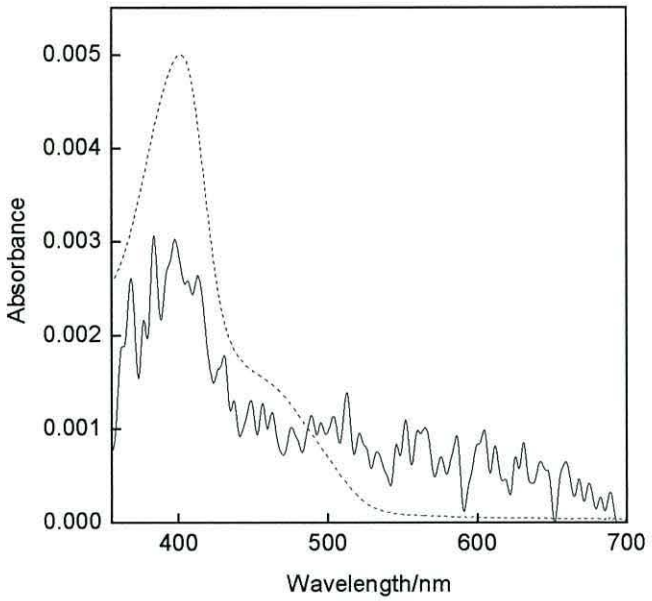

Figure 93 UV/visible absorption spectrum of a SAM of **7** on platinum-coated glass (solid line) and the spectrum of **7** in THF solution (dotted line).

STM investigation of SAMs of the molecular wire on gold-coated HOPG yielded symmetrical I-V characteristics, as expected from symmetrical wire-like molecules located between gold contacts (see Figure 94). The set point current and voltage had very little effect on the profile of the I-V curves but they affected the magnitude of the tunnelling current between the surface and the probe. STM studies were performed for a set point current in the range of 0.5 to 0.8 nA, and a voltage bias of 0.035 to 0.3 V, and each time symmetrical characteristics were obtained.

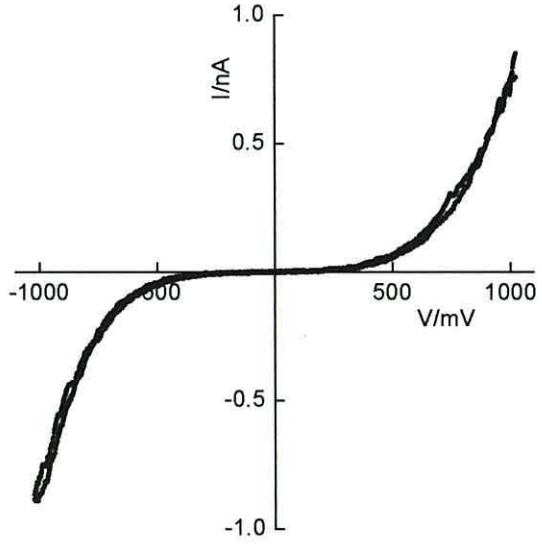

Figure 94 I-V characteristic of molecular wire **7** deposited as a SAM on gold-coated HOPG and contacted by a PtIr tip.

Single molecule electrical conductivity studies of wire **7** were performed, and the observed current jumps were reproducible at each point that was probed by an Au tip. Usually the adsorption/desorption process persisted for *ca.* 10 to 300 ms, and the most observable current jumps were within the range 0.35 ± 0.05 nA at –0.3 V. The effect of tip-single molecular wire contact via an –SH group, as a tunnelling current in the time domain is shown in Figure 95.

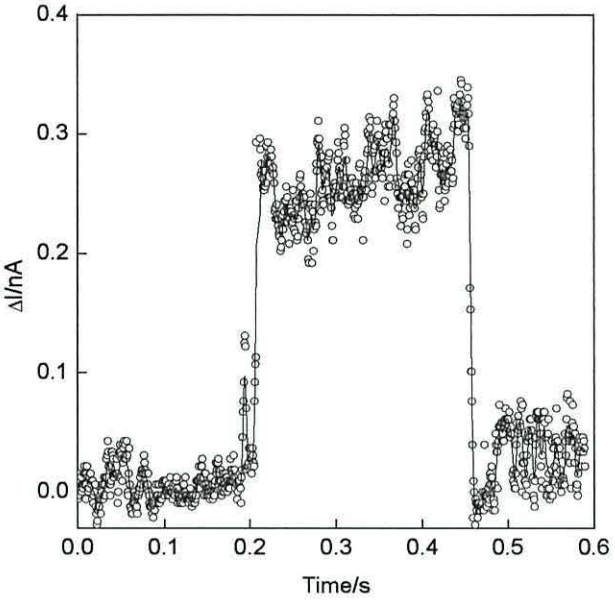

Figure 95 Typical current jump of molecular wire **7** with the gold STM probe located at a fixed height above the SAM with the sample bias of –0.3 V. the increased current, which was attributed to adsorption of the terminal thiol group to the gold probe, persisted for *ca.* 260 ms in this case.

A large number of current jumps, recorded at different locations on the substrate were analysed to yield the histogram that is shown in Figure 96. The most intensive column lies within the range 0.35 ± 0.05 nA, and represents almost 50 % of all current jumps and as mentioned above it was attributed to the single molecule current. Significantly, thirteen of the recorded events exhibited current jumps of 0.65 ± 0.05 nA (see Figure 96), which are almost double the aforementioned values, and probably correspond to the probe contacting two molecules. There is also tentative evidence of higher *e.g.* three and four molecule contacts with two events centred about 1.0 nA, and another centred about 1.4 nA (Figure 96).

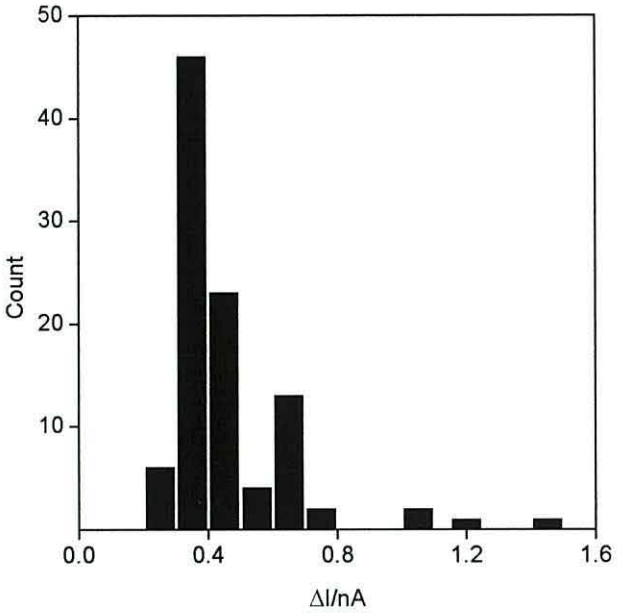

Figure 96 Histogram of 99-recorded current jumps at a sample bias of –0.3 V for molecular wire **7**.

The experimental results of the wire were compared with a detailed *ab inito* simulation of electron transport through the non-protonated self-assembled molecule. To compute the conductance a combination of the density functional theory (DFT) code SIESTA and Green's function scattering approach was used [200],[201], as encapsulated in the non-equilibrium molecular electronics SMEAGOL code. The studies were done by Iain Grace at Lancaster University, and the molecular model is presented in Figure 97.

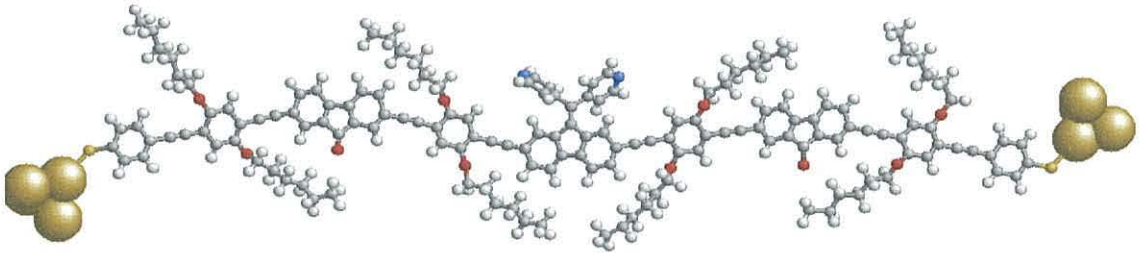

Figure 97 Molecular structure of arylene-ethynylene molecular wire **7** with 7 nm long backbone and thiolated termini.

9.2.1.4 A 10 nm long conjugated molecular wire

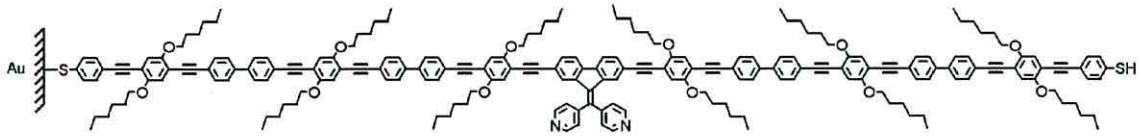

Figure 98 The self assembled structure of the deproteced wire **8**.

The molecular wire **8** was prepared as a SAM on gold (see Figure 98) using a sequence of 10 minutes immersions into a 0.05 mg ml^{-1} solution in THF. Throughout this process, SA was monitored from the frequency change for deposition on gold-coated quartz crystal. The frequency stabilised to a constant value after *ca.* 90 and 300 minutes for deposition from solution in which deprotecting agent was used and not respectively. A Sauerbrey analysis of the data provided a mean consistent area of 2.90 ± 0.04 nm^2 $molecule^{-1}$ for the chemisorbed wire (see Figure 99).

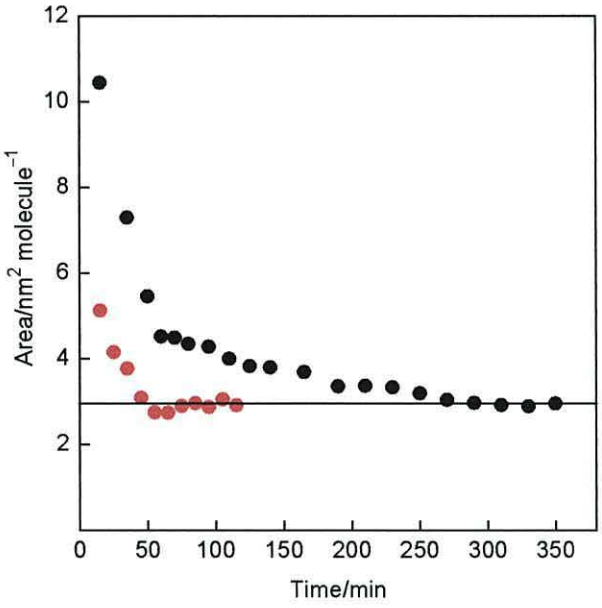

Figure 99 Variation of the molecular area with the period of immersion of a gold-coated crystal in THF solution of **8** (0.05 mg ml^{-1}) to which sodium methoxide was added (•), and without deprotection agent (•).

Confirmation of this SAM was observed in the UV/visible spectrum, on a platinum-coated glass slide, which exhibited a peak at λ_{max} 398 nm indicatives of the wire **8** (*cf.* 404 nm in THF solution), (see Figure 100).

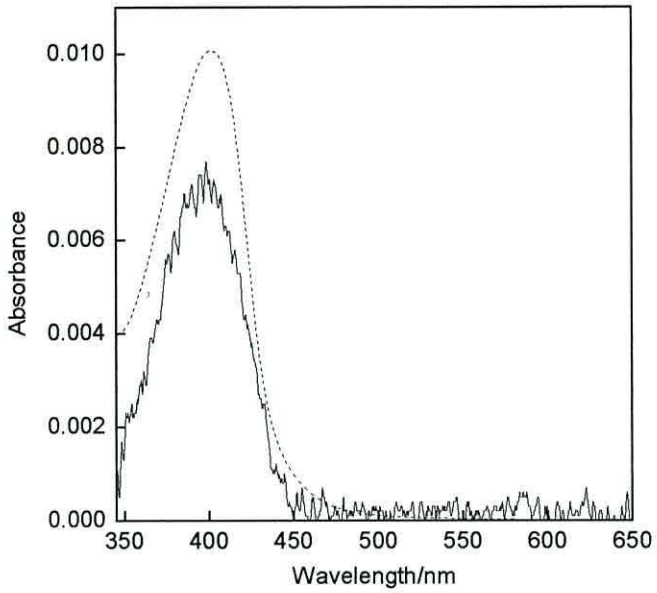

Figure 100 UV/visible absorption spectrum of a SAM of **8** on a platinum-coated glass slide (solid line) and the spectrum of **8** in THF solution (dotted line).

I-V characteristics of the 10 nm long molecular wire **8** exhibited symmetrical or slightly asymmetrical behaviour (see Figure 101). The symmetry was unaffected as the conditions to land the probe were varied. The substrate bias was varied by an order of magnitude, from 0.05 to 0.5 V at a constant set point current 0.4 nA, and similar shape of I-V curves was observed each time.

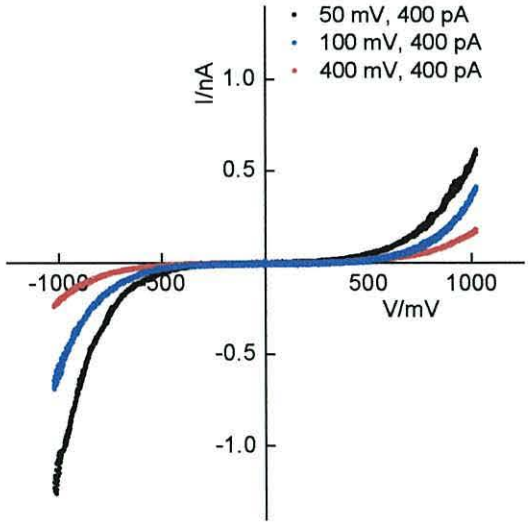

Figure 101 I-V characteristic of molecular wire **8** deposited as a SAM on gold-coated HOPG and contacted by a gold tip.

Characteristic jumps in the tunnelling current were observed by placing the tip at different locations on the substrate surface. A typical current jump, recorded on gold covered with a small surface concentration of molecular wire **8,** is presented in Figure 102. These large current fluctuations, consistent with fast formation and breaking of thiol-gold contacts of the molecular wire, were analysed to yield the histogram shown in Figure 103. This exhibits a pronounced maximum (about 40 % of all current jumps) in the range 0.10–0.15 ± 0.05 nA at a sample bias of –0.3 V, and this may correspond to the probe contacting one molecule. Eight of the 104 recorded events exhibited current jumps in the range 0.20–0.25 ± 0.05 nA, which was double the aforementioned value, and probably corresponds to the probe contacting two molecules. There was also evidence of higher multiples, which might be indicative of several molecule contacts. These events correspond to only 10 % of the total, and therefore the histogram reveals a current for a single molecule of **8** (see Figure 103).

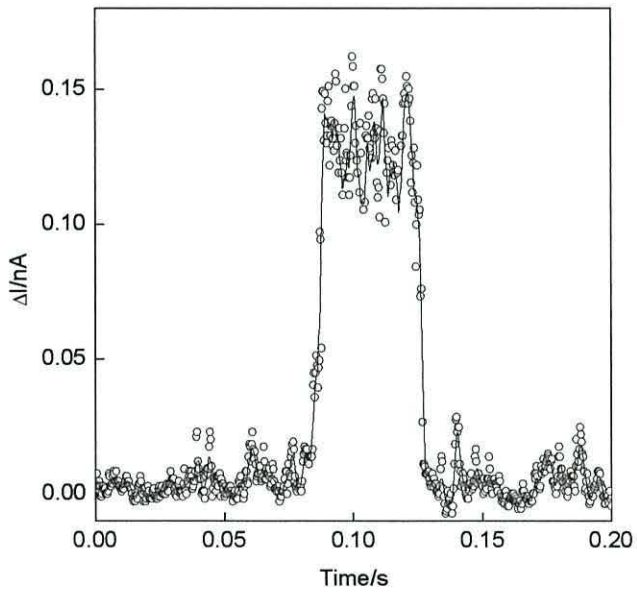

Figure 102 Typical current jump of molecular wire **8** with the gold STM probe located at a fixed height above the SAM with the sample bias of –0.3 V. The increased current was attributed to the attachment of the terminal thiol group to the gold probe.

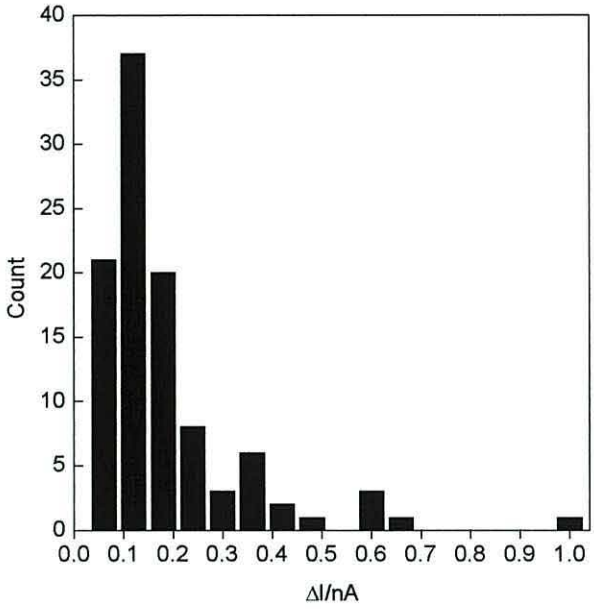

Figure 103 Histogram of the 104 current jumps for molecular wire **8**, recorded at a sample bias of –0.3 V.

The presence of molecular wire **8** was also observed directly as a function of decay of the current with distance (see Figure 104). The plateau observed at a current I was attributed to the conduction through the studied molecular wire **8** formed between the tip and the substrate by chemical bonding of the –SH groups to the gold contacts. The current plateau that could be observed in the I(s) curves for many contact events have clear maxima in the range 0.12–0.5 nA and are shown in, a, b and c of Figure 104.

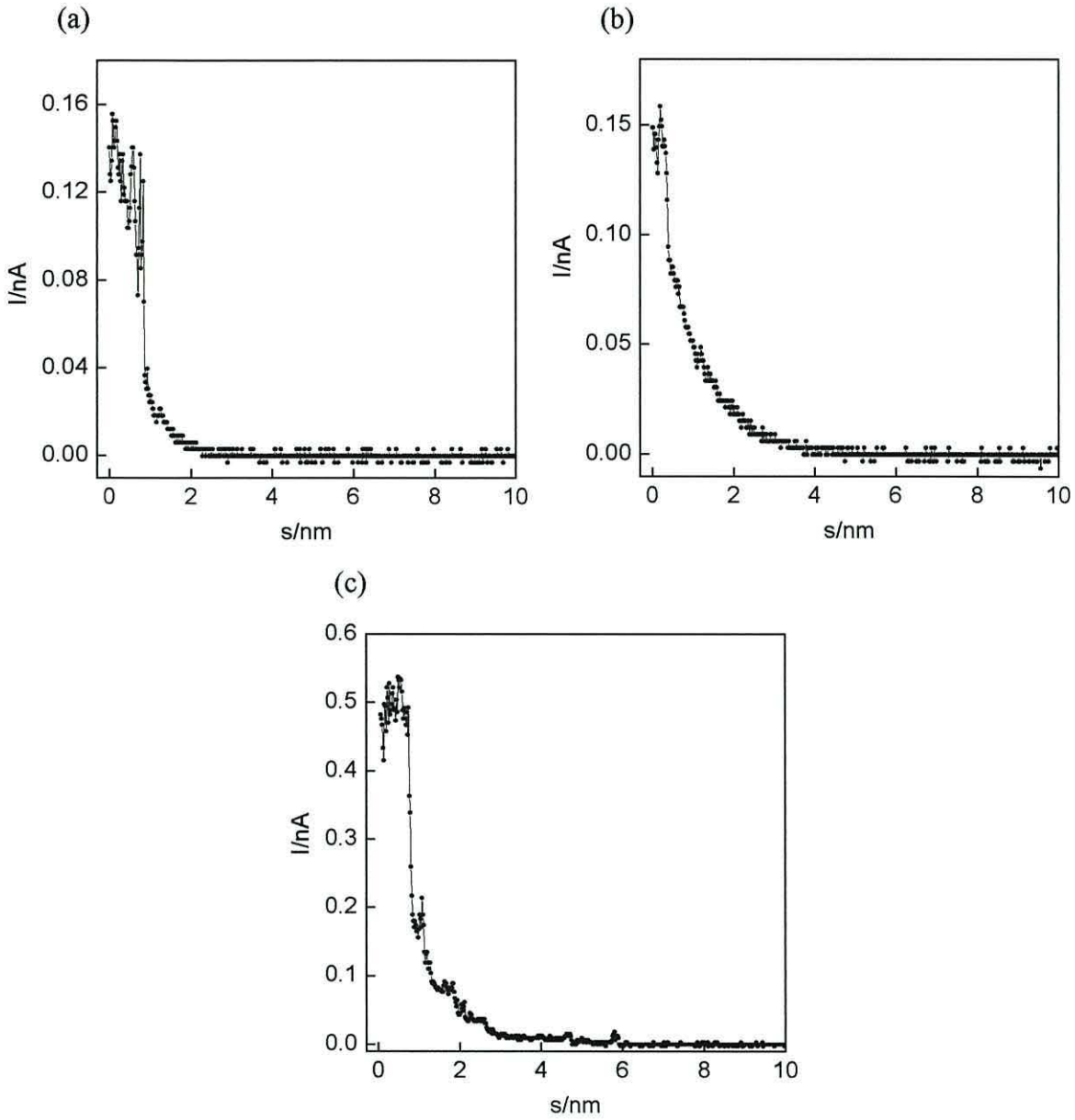

Figure 104 Typical I(s) scans performed in air in the presence of molecular wire **8** between tip and substrate at 0.3 nA and 0.03 V. (a) and (b) present current pletau at lower values of I (*ca.* 0.12 and 0.14 nA) and (c) current pletau at higher value of I (*ca.* 0.50 nA) that correspond to the conductance through a few molecules.

The comparison of the results of the I(t) method which correspond to the I(s) method, shows an important feature: the current corresponding to the basic conductance unit is the same for both techniques.

9.2.2 Organic rectifying junctions from an electron-accepting molecular wire and an electron-donating layer of $CuPc(SO_3^-)_4(Na^+)_4$ or Li^+TCNQ^-

The pyridyl functionality of wire molecules **5**, **6**, **7** and **8** has been utilised to obtain a rectifying junction in which the cationic wire was the electron accepting component, which was used in combination with an adjacent anionic electron-donating layer. To achieve this, SAMs of molecular wires were modified by protonation of the pyridyl units to provide the following forms: [Au–$\mathbf{5}H_2^{2+}(Cl^-)_2$], [Au–$\mathbf{6}H^+Cl^-$], [Au–$\mathbf{7}H_2^{2+}(Cl^-)_2$] and [Au–$\mathbf{8}H_2^{2+}(Cl^-)_2$]. Exposure of the SAMs to HCl vapour did not affect the I-V characteristics. These protonated SAMs of the studied molecular wires were immersed in an aqueous acetone solution of $CuPc(SO_3^-)_4(Na^+)_4$ or in an aqueous ethanol solution of Li^+TCNQ^- for an appropriate time, and washed with ultra-pure water (deposition interrupted by sequential rinsing with water) to remove NaCl or LiCl from the lattice (depending on the donor used). All bilayer structures were investigated in the same manner, as ionically coupled accepting and donating layers seemed to have a great potential in molecular assembly.

The molecular structure of the system after exchanging the chloride counterion of the protonated 4 nm wire **5** with Li^+TCNQ^- is schematically presented in Figure 105.

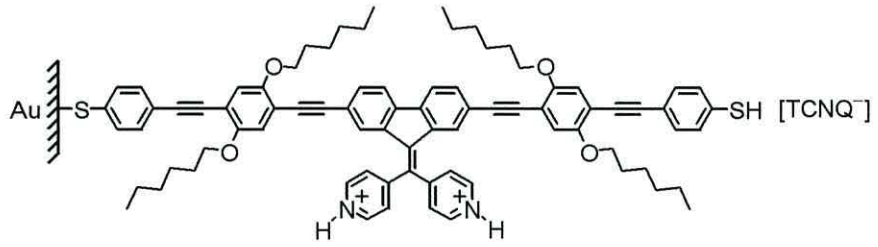

Figure 105 SAMs of protonated wire **5** ionically coupled with $TCNQ^-$.

The metathesis process was monitored with QCM apparatus and the deposition process of the second monolayer (on the SAM of the protonated wire **5**) was interrupted by sequential rinsing with water and ethanol, and stabilised to a constant value after 100 minutes to provide a mean area of 0.26 ± 0.01 nm^2 $molecule^{-1}$ for the negatively charged TCNQ (see Figure 106).

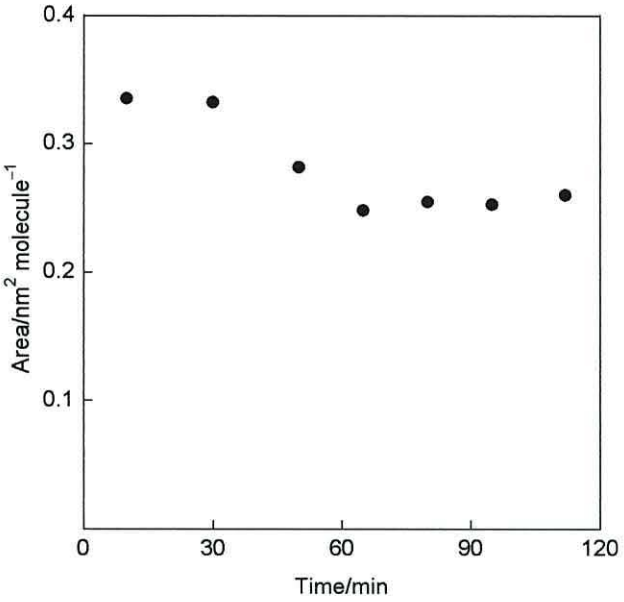

Figure 106 Variation of the mean molecular area with the combined period of immersion time of quartz crystal in an aqueous ethanol solution of the self-assembling Li^+ $(TCNQ)^-$ (0.1 mg ml^{-1}) onto the prior deposited and protonated wire **5**.

Electrical studies of the protonated molecular wire **5** ([Au–**5**$H_2^{2+}(Cl^-)_2$]) showed symmetrical I-V characteristics (Figure 107a), whereas I-V characteristics of ionic bilayer assemblies exhibited rectifying curves with a current ratio of 7 at ± 0.9 V for Au–**5**$H_2^{2+}[(TCNQ)^-]$ and typical curve is shown in Figure 107b. I-V characteristics were obtained for both SAMs of the protonated wire and for the ionically coupled system with $TCNQ^-$ by using a gold probe, and by varying the set point current of 0.3-0.6 nA and voltage throughout the range 0.02-0.3 V. The higher current was observed in the negative quadrant of the I-V plot (Figure 107b), which corresponds to electron flow from the substrate (cathode) to the LUMO of the protonated wire **5** on one side of the device, and from the HOMO of the $TCNQ^-$ to the probe (anode) on the other side.

(a)

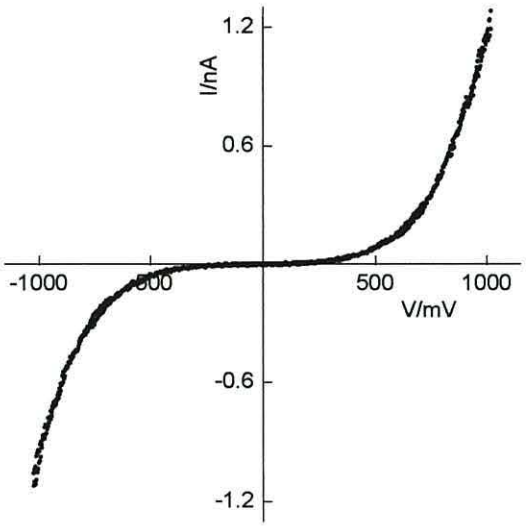

(b)

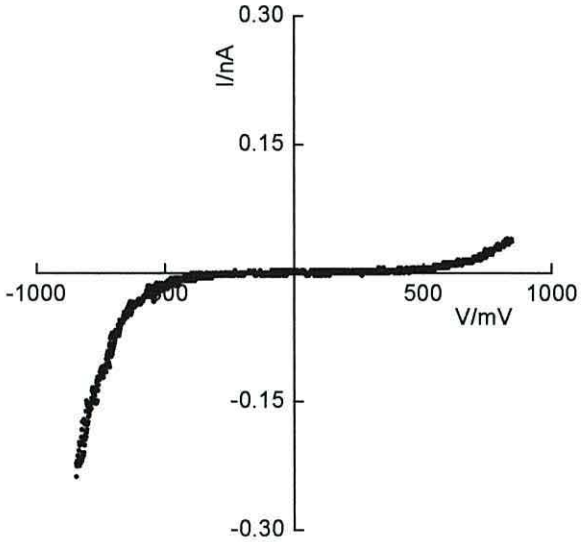

Figure 107 (a) I-V characteristic of protonated form of **5** contacted by an Au probe, the data being obtained for a set point current of 0.3 nA and bias of 0.3 V. (b) I-V characteristic of protonated wire **5** ionically coupled with $TCNQ^-$ obtained using a set point current of 0.6 nA and sample bias of 0.02 V.

The next formation of an organic rectifying junction was obtained by protonating the 9-[(4-pyridyl)methylene]fluorene unit of the molecular wire **6** by exposure to HCl and exchanging the chloride counterion with an electron-donating phthalocyanine (Figure 108).

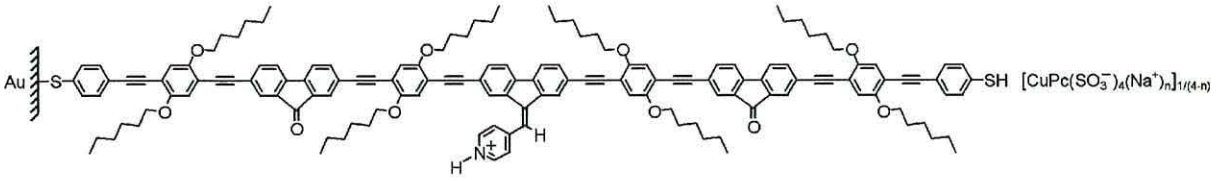

Figure 108 The assembled structure of the protonated wire **6** ionically coupled with $CuPc(SO_3^-)_4(Na^+)_n$.

This was achieved by immersion of the protonated SAMs in an aqueous acetone solution of the $CuPc(SO_3^-)_4(Na^+)_n$ for an appropriate time, and washing with water to remove NaCl from the lattice. To assess the effectiveness of this process, XPS analysis was performed for the system presented in Figure 106. XPS confirmed the presence of the most characteristic atoms. For example, a copper peak at 936 eV (Cu 2p) and sodium at 1074 eV (Na 1s) correspond to the binding energies of atoms unique to the anionic layer of the phthalocyanine component.

UV/visible spectroscopy also provided essential information about the presence of the assembled bilayer films on a platinum-coated glass. The spectrum exhibited a peak at λ_{max} 450 nm indicative of the wire **6** (*cf.* 400 nm in THF solution), and the broad transition with a maximum at *ca.* 700 nm was attributed to the Q band of the phthalocyanine (Figure 109).

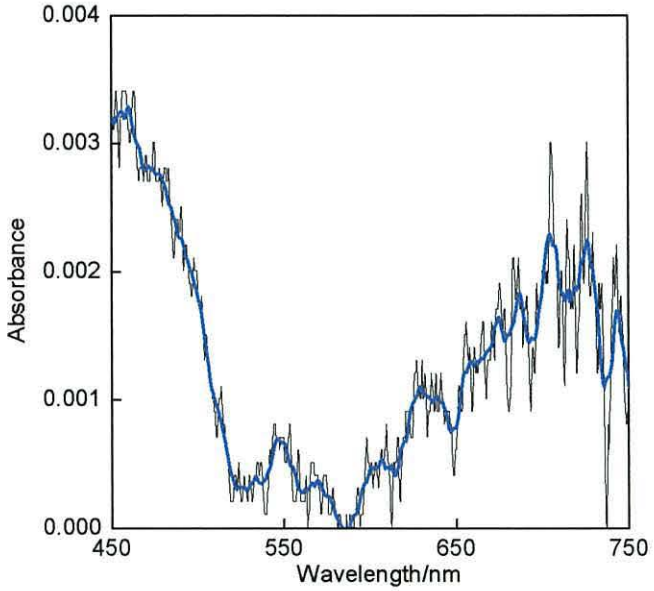

Figure 109 Visible absorption spectrum of the rectifying structure $\mathbf{6}H^+[CuPc(SO_3^-)_4(Na^+)_n]_{1/(4-n)}$ on a platinum-coated glass substrate.

However, the peak (absorbance) at the longer wavelength that was attributed to the Q band of the phthalocyanine had less intensity, compared to the peak at the shorter wavelength characteristic of molecular wire **6** (see Figure 109), and also to the SAMs of phthalocyanine in the other systems. This could be caused by a smaller amount of the anionic dye being present in the molecular structure.

The SA process of the second monolayer of phthalocyanine was also monitored with QCM apparatus. Deposition of the anionic dye revealed a value of 0.69 ± 0.02 nm^2 $molecule^{-1}$ for $[CuPc(SO_3^-)_4(Na^+)_3]$ after 120 minutes of immersion time, which was interrupted by sequential rinsing with water, ethanol and acetone (see Figure 110). For other possible combinations of the phthalocyanine molecule the area amounted to 0.64, 0.60 and 0.56 ± 0.02 nm^2 $molecule^{-1}$ for $[CuPc(SO_3^-)_4(Na^+)_2]$, $[CuPc(SO_3^-)_4Na^+]$ and $[CuPc(SO_3^-)_4]$ respectively, (Figure 110).

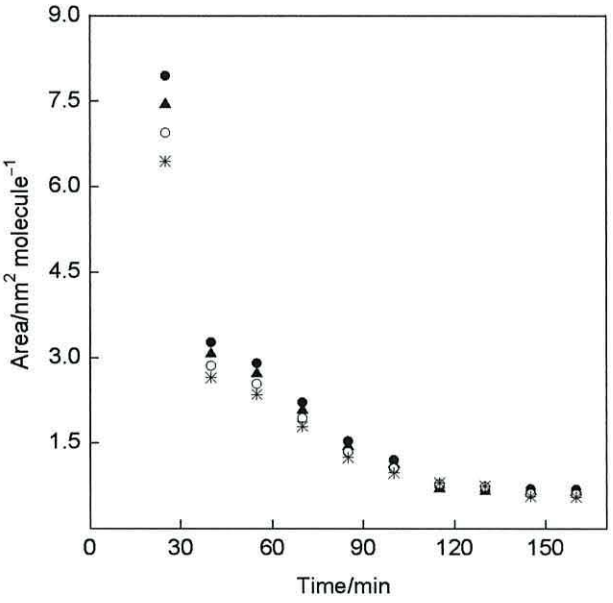

Figure 110 Variation of the mean molecular area with the combined period of immersion time of quartz crystal in an aqueous acetone solution of the self-assembling $CuPc(SO_3^-)_4(Na^+)_4$ (0.02 mg ml^{-1}) onto the prior deposited wire **6.** The individual signs relate to how many sodium cations and chloride anions were eliminated from the bilayer (● NaCl, ▲ 2NaCl, ○ 3NaCl, * 4NaCl).

The area is consistent with the molecules standing on edge and comparison with data obtained for the initially formed SAM yielded a wire **6** to $CuPc(SO_3^-)_4(Na^+)_n$ ratio of

about 1:2.8. Electrical studies of the STM junction containing the molecular wire ionically coupled with the copper(II) phthalocyanine ($\mathbf{6}H^+[CuPc(SO_3^-)_4(Na^+)_n]_{1/(4-n)}$) showed reproducible electric behaviour for the system with the higher current in the negative quadrant of the I-V plot (see Figure 111a). The I-V characteristics of the bilayer assemblies of protonated wire **6** with phthalocyanine counterions in the upper layer exhibited rectifying curves with current ratios in the range of 20-80 at ± 1 V, a typical curve is shown in Figure 111a. However, the protonated form of the deposited wire with chloride counterion [Au–$\mathbf{6}H^+Cl^-$] exhibited symmetrical I-V characteristics (see Figure 111b).

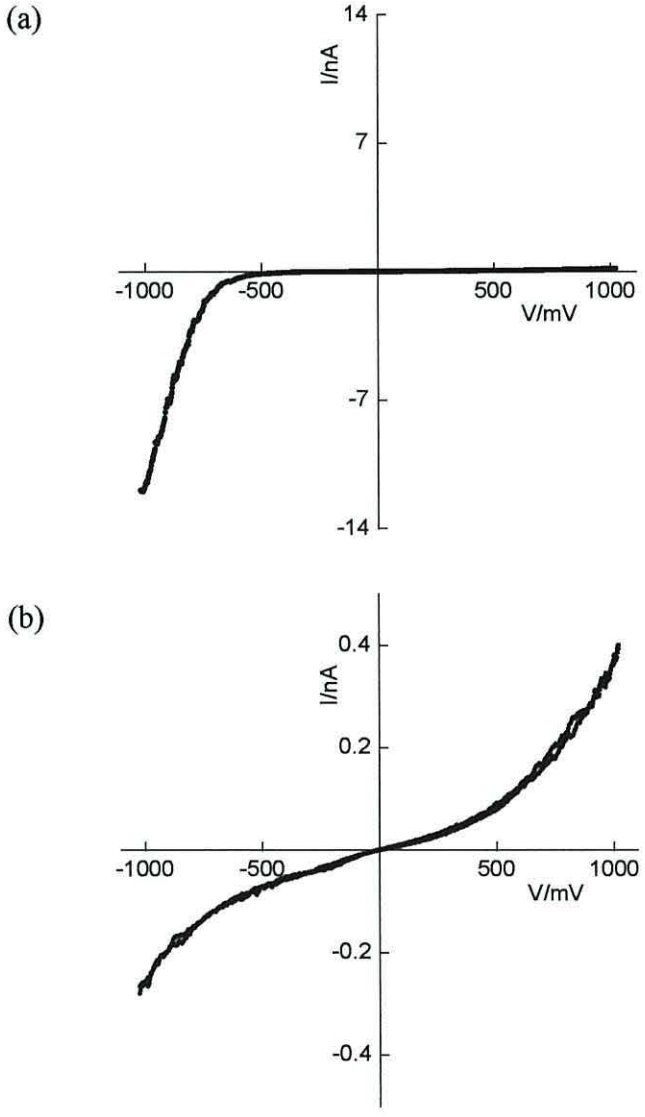

Figure 111 I-V characteristics of (a) Au–$\mathbf{6}H^+[CuPc(SO_3^-)_4(Na^+)_n]_{1/(4-n)}$, and (b) protonated form of wire [Au–$\mathbf{6}H^+Cl^-$]. SAMs contacted by a gold probe for set point current and sample bias of (a) 0.5 nA, 0.05 V, (b) 1 nA, 0.04 V respectively.

I-V characteristics were obtained, as for SAMs of the protonated wire by using a gold probe and by varying the set point current and voltage throughout a broad range. High current in the negative quadrant (Figure 109a) corresponded to electron flow from the substrate (cathode) to the LUMO of the wire on the one side of the device, and from the HOMO of the phthalocyanine to the probe (anode) on the other side. The rectification simply arises from an energy mismatch between these orbitals and the Fermi levels of the contacting electrodes when the bias is reversed.

An STM image of the Au–**6**$H^+[CuPc(SO_3^-)_4(Na^+)_n]_{1/(4-n)}$ bilayer structure on gold-coated HOPG was obtained using a gold tip at the set point current of 0.5 nA and a sample bias of 0.05 V. The bilayer film is highly disordered with dimensions that probably correspond to an edge on arrangement of phthalocyanine anions (see Figure 112).

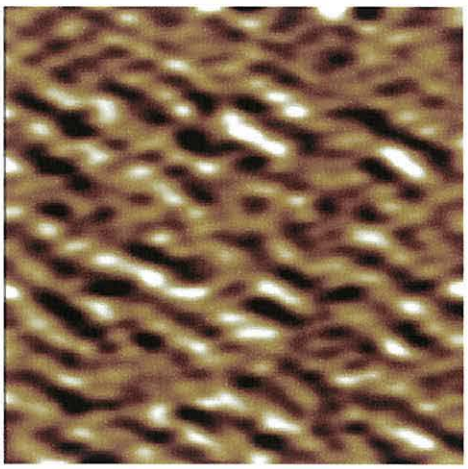

Figure 112 7.7 nm x 7.7 nm STM image of the upper surface of the bilayer structure: Au–**6**$H^+[CuPc(SO_3^-)_4(Na^+)_n]_{1/(4-n)}$.

The next organic rectifying junction, in which the cationic wire **7** was the electron accepting component is one in which it was used in combination with an adjacent anionic donating layer of copper(II) phthalocyanine, see Figure 113.

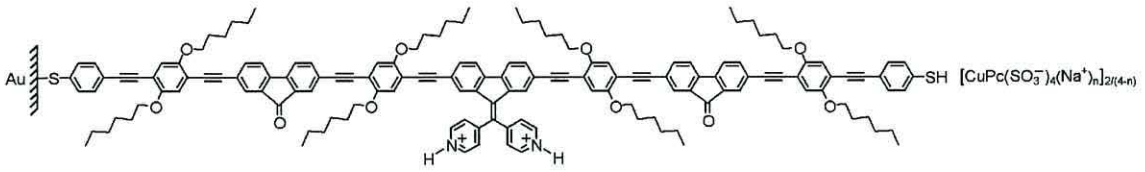

Figure 113 The assembled structure of the protonated wire **7** ionically coupled with $CuPc(SO_3^-)_4(Na^+)_n$.

Evidence of the presence of the bilayer structure presented above was provided by UV/visible spectroscopy. The spectrum of the SAMs on platinum-coated glass exhibited a peak at a λ_{max} of 400 nm was indicative of wire **7**. The broad transition with the highest intensity of absorbance at *ca.* 700 nm was attributed to the Q band of the phthalocyanine (see Figure 114).

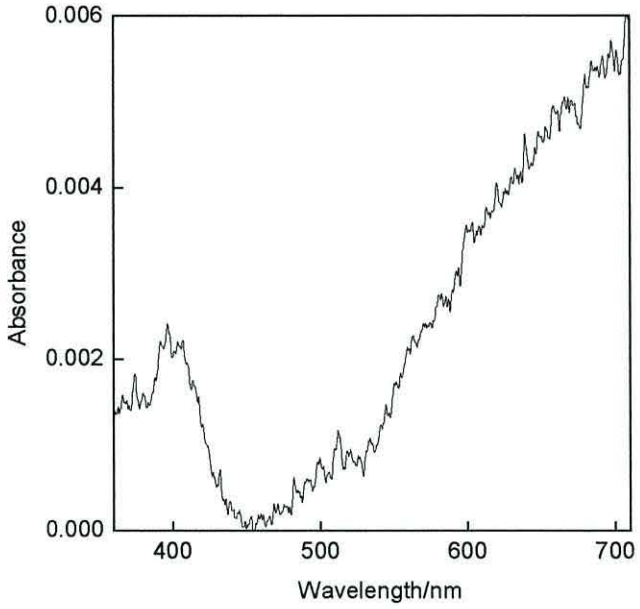

Figure 114 UV/visible absorption spectrum of the rectifying structure $\mathbf{7}H_2^{2+}[CuPc(SO_3^-)_4(Na^+)_n]_{2/(4-n)}$ on a platinum-coated glass substrate.

The process was monitored from the frequency changes of the quartz crystal, which stabilised after about 70 minutes provided an area of about 0.82 ± 0.03 nm^2 $molecule^{-1}$ for $[CuPc(SO_3^-)_4(Na^+)_3]$. For other possible combinations of the phthalocyanine molecule the area amounted to 0.78, 0.73 and 0.67 ± 0.03 nm^2 $molecule^{-1}$ for $[CuPc(SO_3^-)_4(Na^+)_2]$, $[CuPc(SO_3^-)_4\,Na^+]$ and $[CuPc(SO_3^-)_4]$ respectively, (see Figure

115). The area is consistent with the molecules standing on edge. Comparison with data obtained for the initially formed SAM yielded a wire to $[CuPc(SO_3^-)_4(Na^+)_n]$ ratio of about 1:1.6.

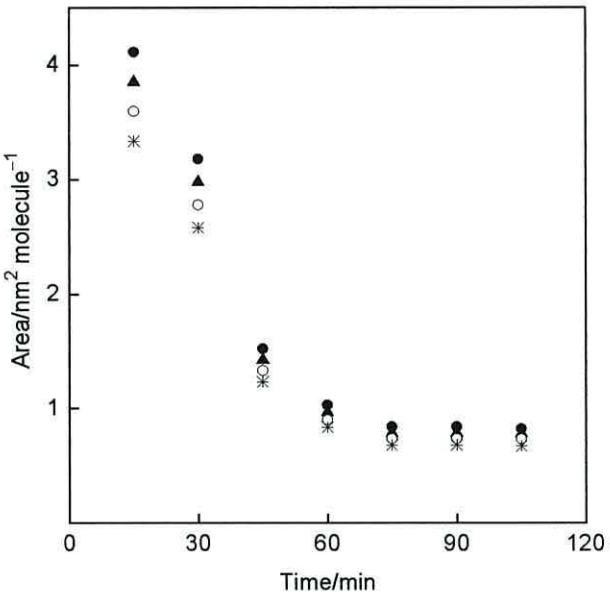

Figure 115 Variation of the mean molecular area with the combined period of immersion time of quartz crystal in an aqueous acetone solution of the self-assembling $CuPc(SO_3^-)_4(Na^+)_4$ (0.02 mg ml^{-1}) onto the prior deposited wire **7**. The individual signs relate to how many sodium cations and chloride anions were eliminated from the bilayer (● NaCl, ▲ 2NaCl, ○ 3NaCl, * 4NaCl).

As expected, the diprotonated wire with chloride counterions $[Au–7H_2^{2+}(Cl^-)_2]$ exhibited symmetrical I-V characteristics (like the neutral wire **7**), (Figure 116a), whereas the bilayer film with phthalocyanine counterions in the upper layer exhibited rectifying curves with current ratios of 15-50 at ± 1V (Figure 116b). These arise from the designated donor/acceptor sequence whereby the favourable direction of electron flow was from substrate to electron-accepting molecular wire, and from the electron-donating phthalocyanine to the probe. In this direction the substrate and probe are the cathode and anode respectively. Moreover, at forward bias, the observed current was significantly higher than for the wire alone, this probably results from the more closely aligned energies of the Fermi levels with the HOMO and the LUMO of the donor and acceptor respectively.

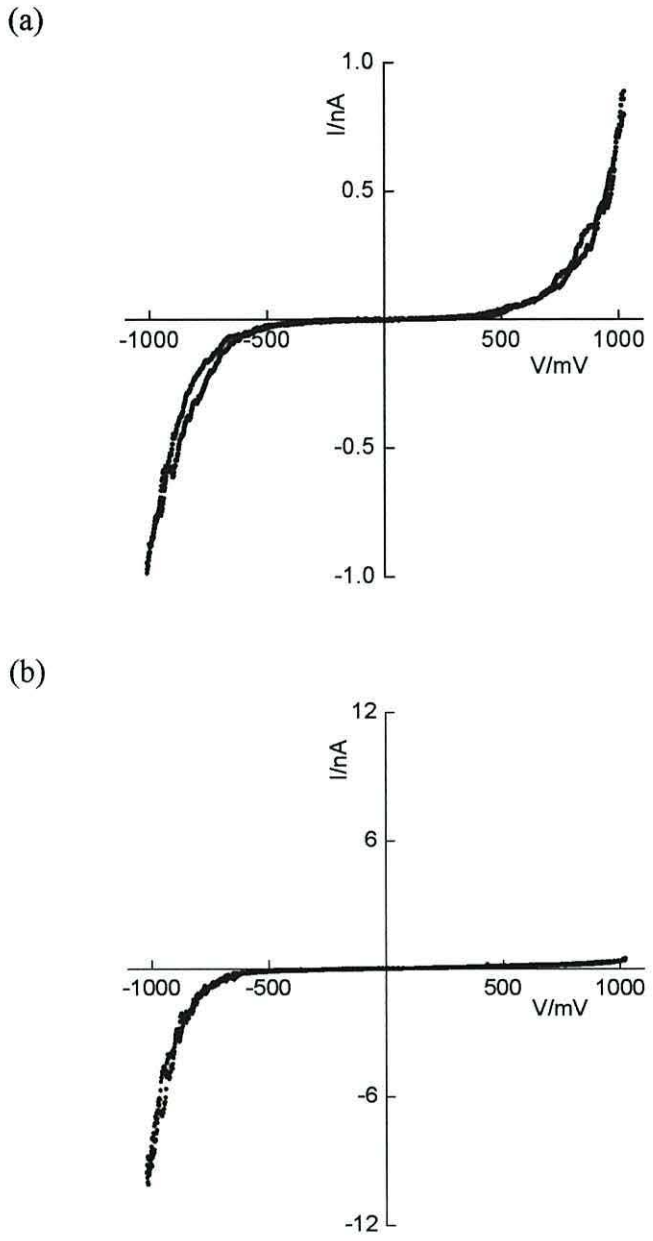

Figure 116 I-V characteristics of (a) protonated form of wire [Au–$7H_2^{2+}(Cl^-)_2$], and (b) bilayer assembly Au–$7H_2^{2+}[CuPc(SO_3^-)_4(Na^+)_n]_{2/(4-n)}$. SAMs contacted by a gold probe for set point current and sample bias of (a) 0.3 nA, 0.03 V, and (b) 0.8 nA, 0.035 V respectively.

An STM image of Au–$7H_2^{2+}[CuPc(SO_3^-)_4(Na^+)_n]_{2/(4-n)}$ bilayer structure on gold-coated HOPG was obtained using a gold tip at a set point current of 0.5 nA and sample bias of 0.05 V. The bilayer film is highly disordered with dimensions that probably correspond to an edge on arrangement of phthalocyanine anions (see Figure 117).

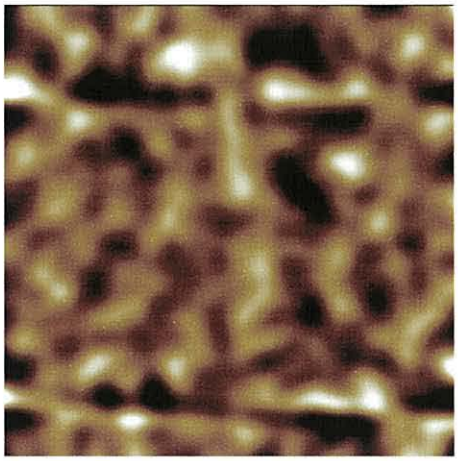

Figure 117 8.0 nm x 8.0 nm STM image of the disordered surface of the bilayer structure $Au-7H_2^{2+}[CuPc(SO_3^-)_4(Na^+)_n]_{2/(4-n)}$.

Another example of a rectifying junction was obtained by protonating the 10 nm long wire molecules and ionically coupling them with anionic donors (see Figure 118). In this case the two systems were studied to provide a donor-acceptor bilayer arrangement. The first system incorporated copper(II) phthalocyanine, and the second LiTCNQ.

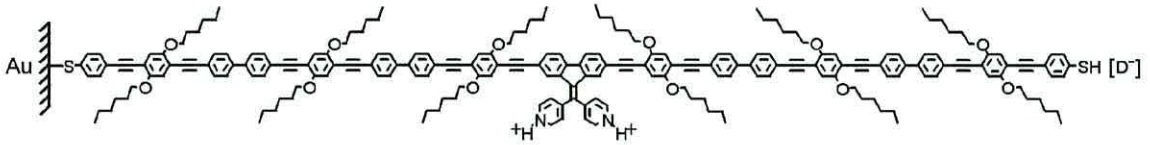

Figure 118 The assembled structure of the protonated wire **8** ionically coupled with anionic donor. In this case D^- means $CuPc(SO_3^-)_4(Na^+)_n$ or $TCNQ^-$.

UV/visible spectroscopy provided essential information about the presence of the chemisorbed cationic layer ionically coupled with copper(II) phthalocyanine on platinum-coated glass. Figure 119 shows an absorption band at 395 nm characteristic of the molecular wire **8,** it also shows the phthalocyanine Q band split into peaks at 616 nm and (less intensive) at 687 nm.

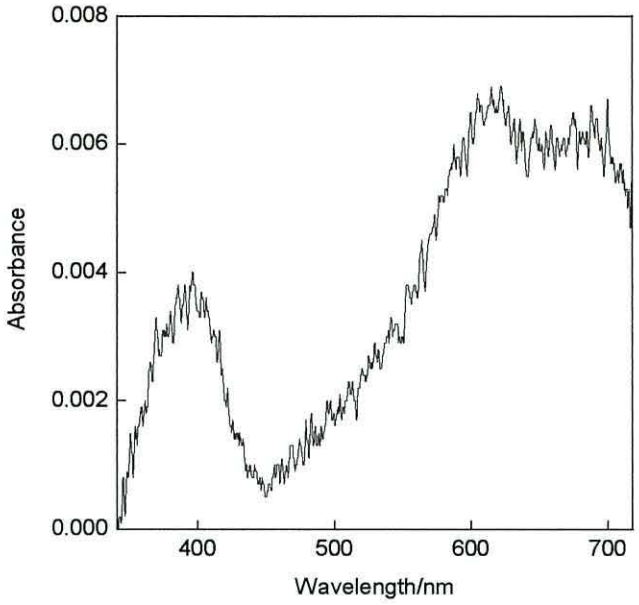

Figure 119 UV/visible absorption spectrum of the rectifying structure $\mathbf{8}H_2^{2+}[CuPc(SO_3^-)_4(Na^+)_n]_{2/(4-n)}$ on a platinum-coated glass substrate.

QCM analysis provided an average area of about 0.61 ± 0.03 nm^2 $molecule^{-1}$ for the negatively charged phthalocyanine, and 0.28 ± 0.02 nm^2 $molecule^{-1}$ for the $TCNQ^-$ (Figure 120). Both molecules were deposited on monolayers of cationic wire **8**. Complete monolayers were obtained after *ca.* 200 and 100 minutes for deposition of phthalocyanine and LiTCNQ respectively, both values of area are consistent with the molecules standing on edge.

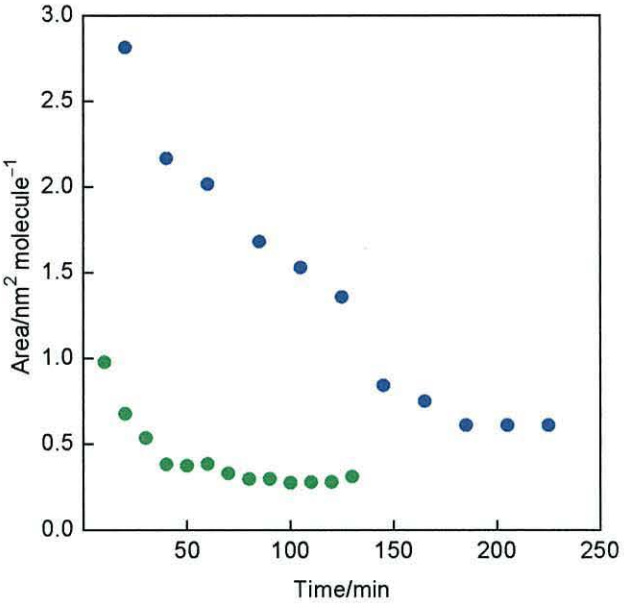

Figure 120 Variation of molecular area with the combined period of immersion time of quartz crystal in: an aqueous acetone solution of the self-assembling $CuPc(SO_3^-)_4(Na^+)_4$ (blue); the ethanol solution of the self-assembling Li^+TCNQ^- (green), onto the prior deposited and then protonated wire **8**. Both calculations were done considering elimination of NaCl and LiCl from bilayers for depositions of phthalocyanine and LiTCNQ respectively.

STM analysis confirmed the rectifying behaviour of both systems with the higher current observed at negative bias (see Figure 121a,b). This would suggest that electron flow was from the bottom electrode (Au-coated: quartz crystal or HOPG) through the cationic surface of the molecular wire to the anionic surface of phthalocyanine or $TCNQ^-$, and then to the tip. The direction of electron flow was the same as for similar systems incorporating electron-accepting molecular wires of different lengths. I-V characteristics exhibited stronger asymmetry with rectification ratios in the range 10-25 at ± 1 V for Au–$\mathbf{8}H_2^{2+}[CuPc(SO_3^-)_4(Na^+)_n]_{2/(4-n)}$ (Figure 121a), and weaker current ratios in the range 7-14 at ± 1 V for Au–$\mathbf{8}H_2^{2+}[TCNQ^-]$ (Figure 121b). However, electrical studies of the protonated wire **8** exhibited reproducible symmetrical behaviour (see Figure 121c) as for the other protonated wires studied.

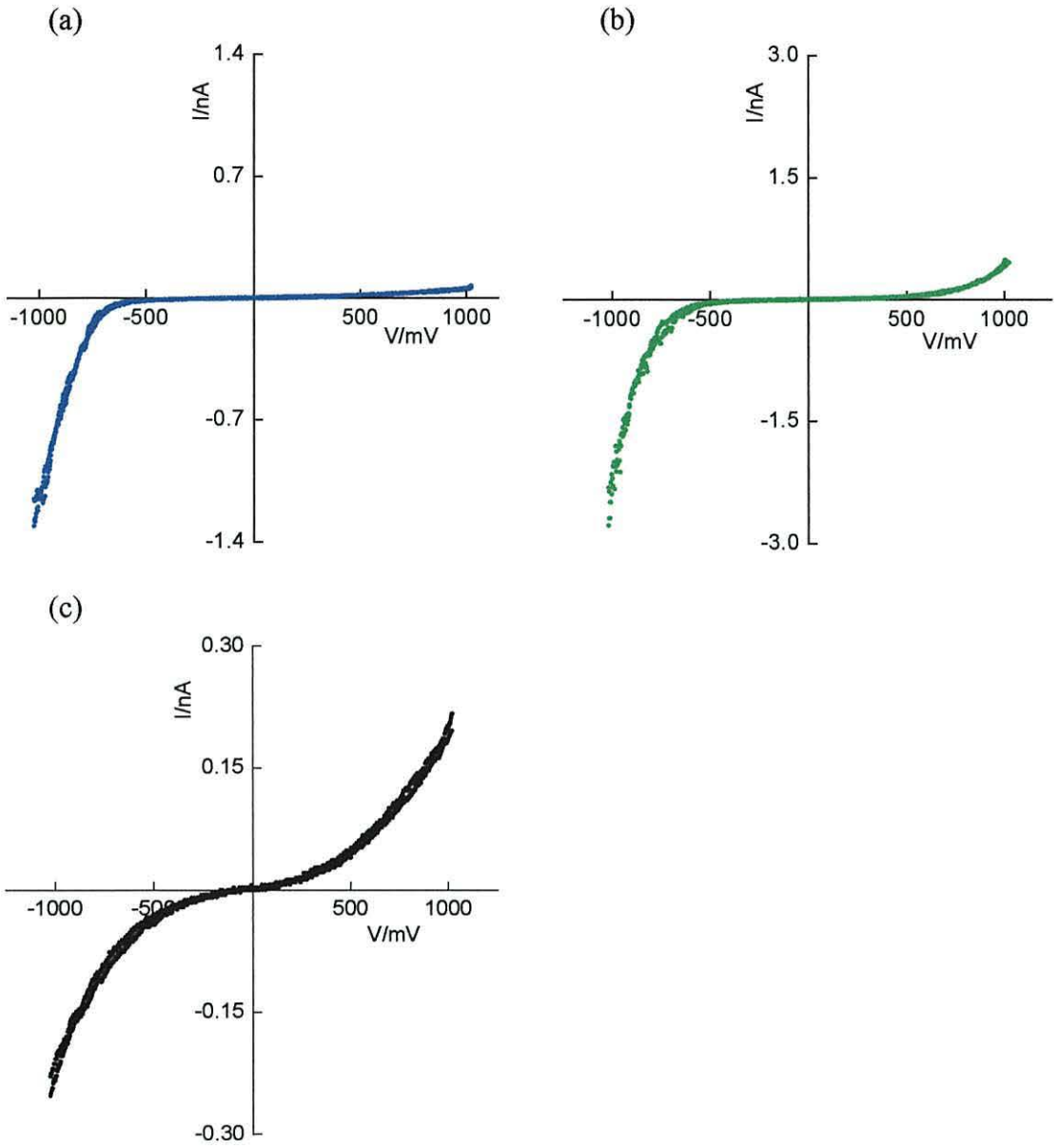

Figure 121 I-V characteristics: (a) bilayer assembly Au–$\mathbf{8}H_2^{2+}[CuPc(SO_3^-)_4(Na^+)_n]_{2/(4-n)}$ with typical rectification ratio of 10-25 at ± 1V; (b) bilayer assembly Au–$\mathbf{8}H_2^{2+}[TCNQ^-]$ with typical rectification ratio of 7-14 at ± 1V; (c) a protonated form of wire $[Au–\mathbf{8}H_2^{2+}(Cl^-)_2]$. SAMs contacted by a gold probe for set point current and sample bias of (a) 0.4 nA, 0.02 V; (b) 0.6 nA, 0.02 V; (c) 0.4 nA, 0.3 V, respectively.

9.2.3 Summary

In Chapter 9.2. a variety of techniques have shown that electron-accepting molecular wires **5**, **6**, **7** and **8**, both in their neutral form, and when protonated by HCl, invariably showed non-rectifying behaviour. The single-molecule current of molecular wires **5**, **6**, **7**

and **8** yielded varied results. The reason for this behaviour is certainly attributable to the different lengths of molecules, donor-acceptor character strength and even molecular structure packing. These revelations resulted in the publications I, III and IV listed in Chapter 12.

Although not discussed here, further theoretical studies (performed with the cooperation of Prof. C. Lambert from Lancaster University) using a combination of the DFT theory code SIESTA and Green's function scattering approach, were used to calculate the electron transport properties of the molecular wires **6** and **7**. To ease the computational system, methoxy groups were substituted for the hexyloxy side chains. Theoretical I-V characteristics were in agreement with the shape of the experimental curve, and with the magnitude of the experimental current (jump) at 0.3 V. Moreover, the sensitivity to the character of the side groups attached to the fluorene unit was reflected in the energy levels of the isolated molecular wires. For molecule **6** the HOMO-LUMO gap was much larger than that of molecule **7,** and also the three LUMO resonances were more varied. In molecule 7, the LUMO resonances consisted of two levels close together, with one further away. These results suggest that molecular wires **6** and **7** possess useful structural features, which allowed the conductance of the molecules to be altered by changing the properties of the side groups attached to the fluorene backbone units. This opens up the possibility of using these molecular wires as single-molecule sensors. These revelations resulted in the publications III and IV, see Chapter 12.

The SAMs of molecular wires with electron accepting character ($\mathbf{5}H_2^{2+}(Cl^-)_2$, $\mathbf{6}H^+Cl^-$, $\mathbf{7}H_2^{2+}(Cl^-)_2$, and $\mathbf{8}H_2^{2+}(Cl^-)_2$) and an electron donating upper layer of copper(II) phthalocyanine (or $TCNQ^-$) were specifically chosen to create rectifying devices. There are few examples of organic rectifying junctions [104],[171],[198],[199]. However they do involve layers of donors and acceptors. The junctions reported here possessed monolayers of each, and exhibited diode-like behaviour; the polarity for rectification was consistent with that suggested by Aviram-Ratner model. Asymmetric I-V curves obtained from these bilayer structures exhibited higher rectification ratios with the phthalocyanine upper layer, and this revelation resulted in publications I and IV (see Chapter 12). The striking difference in the I-V characteristics of the SAMs of the neutral

wires **5**, **6**, **7** and **8** and the ionic bilayers assemblies; $\mathbf{5}H_2^{2+}D^-$, $\mathbf{6}H^+D^-$ $\mathbf{7}H_2^{2+}D^-$ $\mathbf{8}H_2^{2+}D^-$ with symmetrical I-V characteristics, and rectifying behaviour, respectively, in STM experiments conclusively proved the presence of the wires in the junctions.

9.3 Electrical studies of the 2 nm long thiol terminated phenylene-ethynylene molecular wires

To reveal the nature of the 2 nm long phenylene-ethynylene rigid oligomers, further electrical investigations were performed. The I(t) method previously developed by Haiss *et al.*, using STM, was used for the measurements of single-molecule current of these wires. The starting point for these measurements was the adsorption of a low coverage of dithiol molecules on gold-coated surfaces. This condition resulted in flat-lying molecules and enabled the formation of single-molecule wires with high probability. The structures of molecular wires **9**, **10** and **11** are similar; the difference is only in the side-chains on the central ring and the terminal protecting group.

SAMs of molecular wire **9** (see Figure 122) were formed by immersion of gold-coated substrates in THF solution (0.05 mg ml^{-1}), and the process was monitored from the frequency changes following deposition onto quartz crystal and through rinsing with THF to remove the physisorbed material.

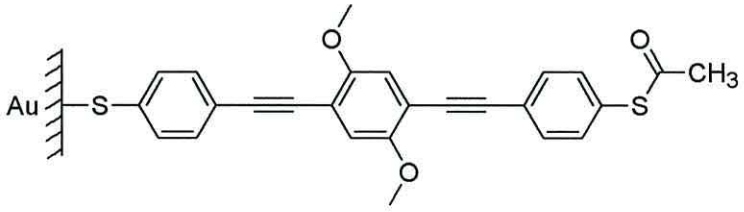

Figure 122 Molecular structure of wire **9** with the terminal sulphur showing the acetyl group intact when formed without the deprotecting agent.

The mean area occupied by the molecule was 0.60 ± 0.09 nm^2 $molecule^{-1}$ for deposition from THF solution of **9**, and 0.5 ± 0.1 nm^2 $molecule^{-1}$ for deposition from the same solution to which a few drops of ammonia were added to deprotect the thiolates (see Figure 123). The frequency stabilised after about 150 minutes in the presence of the deprotecting agent, whereas in its absence the time increased to about 400 minutes.

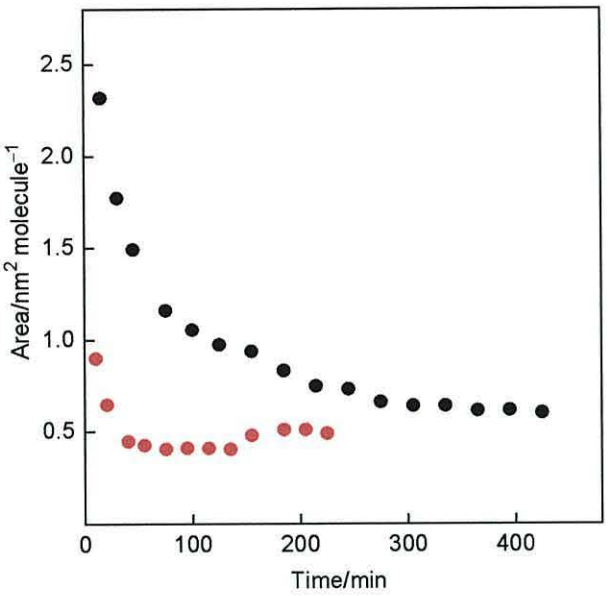

Figure 123 Variation of the molecular area with the period of immersion time for wire **9** in THF (black circles) and to the same solution to which deprotecting agent was added (red circles).

With regards to the concentration effects on the quality of the monolayer, STM studies were performed on quartz crystals as well as HOPG. Results of monolayer deposition on gold-coated quartz crystals showed a high level of noise, but only in some cases. Nevertheless, the obtained electrical results were exactly the same for both gold-coated substrates.

Examples of the I-V characteristics of wire **9** on gold are presented in Figure 124. All curves from six samples contacted by Au or PtIr tip were symmetrical. The only difference was in the current, depending on the sample and the initial current set point, which was within the range 0.5-1.5 nA. The deprotecting agent used during the deposition affected, and thus improved, the shape of the I-V characteristics (see Figure 124).

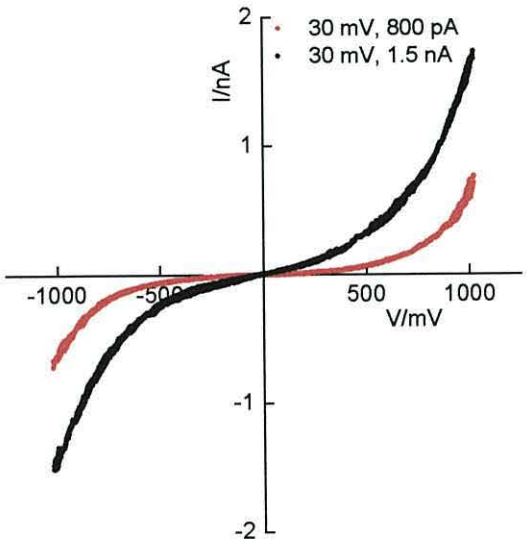

Figure 124 I-V characteristics of the Au-**9** structure contacted by an Au probe. Curves red and black are characteristic of deprotected and non-deprotected molecules, respectively.

The I(t) technique, which allowed the study of the dependence of a single molecule current on the contact spacing, was used to characterise the wire. A typical current trace recorded by this method during the formation and breaking of a molecular bridge between the gold STM tip and gold substrate is shown in Figure 125a. Observations of direct molecular contact allowed construction of a histogram showing a large number of current jumps recorded at different locations on the substrate. The histogram of 73 current jumps is shown in Figure 125b. About 50 % (36 events) of all current jumps were in the range 0.45-0.50 ± 0.05 nA, and each adsorption/desorption persisted from 10 to 450 ms. Nine of the seventy-three recorded events exhibited current jumps in the range 0.95-1.00 ± 0.05 nA, which was double the aforementioned value and probably corresponds to the probe contacting two molecules. There was also evidence of higher multiples, with two events centred at 1.5 and 2.0 nA (Figure 125b), which is indicative of three-molecule contacts. These events correspond to only 2 % of the total, and therefore the histogram reveals a current for a single-molecule of **9**.

Single-molecule current studies of the molecule **9** performed by Haiss *et al.* [202] also showed reproducible characteristic for single and multi contact events, resulting in a rise of current jump events. Moreover, it was revealed that changing the angle between the

planes of the central phenyl ring and the outer (co-planar) phenyl rings of the molecule (from 60° to 0°) was seen to result in an increase in the conductivity.

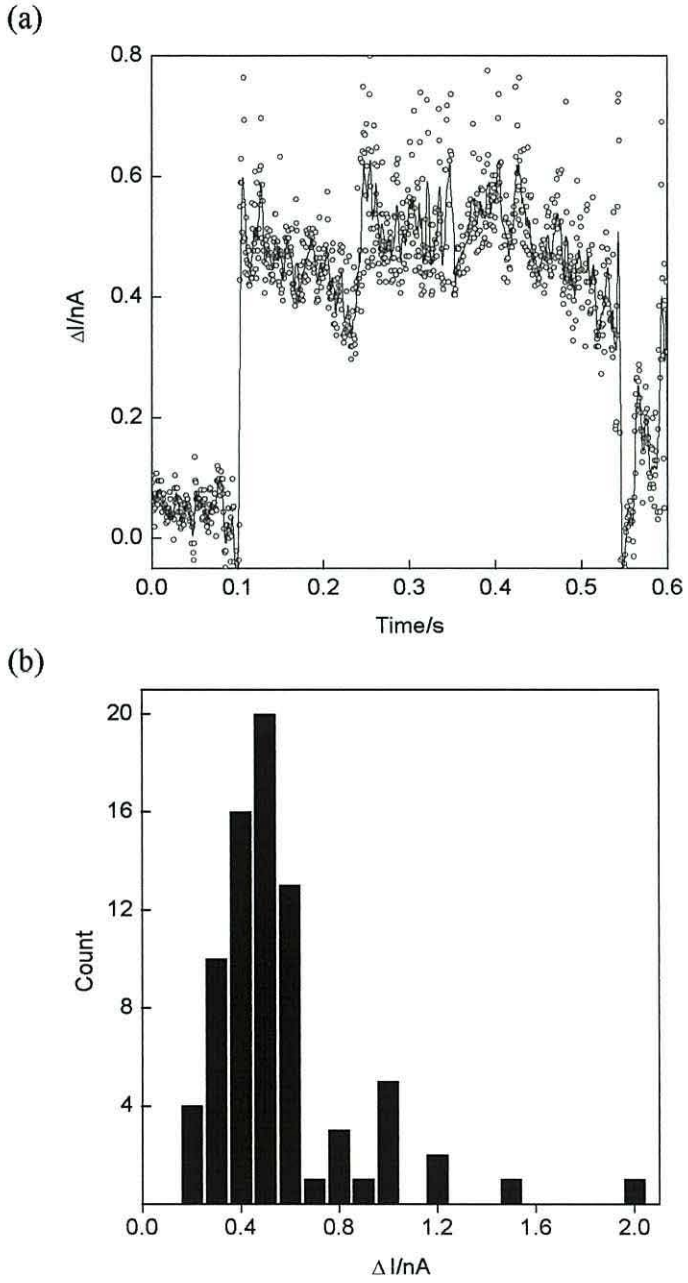

Figure 125 (a) Typical current jump with the gold STM probe located at a fixed height above the SAM with a sample bias of –0.3 V. The increased current, which was attributed to adsorption of the terminal thiol group to the gold probe persisted for ca. 450 ms in this case, and is the longest of the recorded events. (b) Histogram of 73 current jumps for **9**, recorded at a sample bias of –0.3 V, and a set point current of 1 nA.

Another conformationally rigid molecular wire (**10**, see Figure 126), an analogue of the molecular wire **9** was investigated to reveal the electrical behaviour.

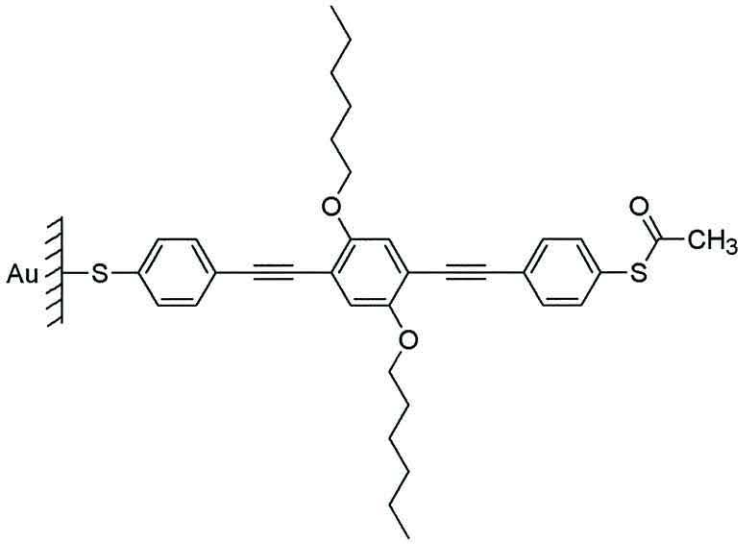

Figure 126 Molecular structure of the wire **10** with the terminal sulphur showing the acetyl group intact when formed without the deprotecting agent.

For wire **10**, the frequency stabilised after 650 minutes, Sauerbrey analysis provided an area of 0.65 ± 0.50 nm^2 $molecule^{-1}$ for deposition from solution without the presence of the deprotecting agent. In the presence of ammonia the time decreased to *ca.* 350 minutes, and the calculated area was 1.20 ± 0.04 nm^2 $molecule^{-1}$ (Figure 127).

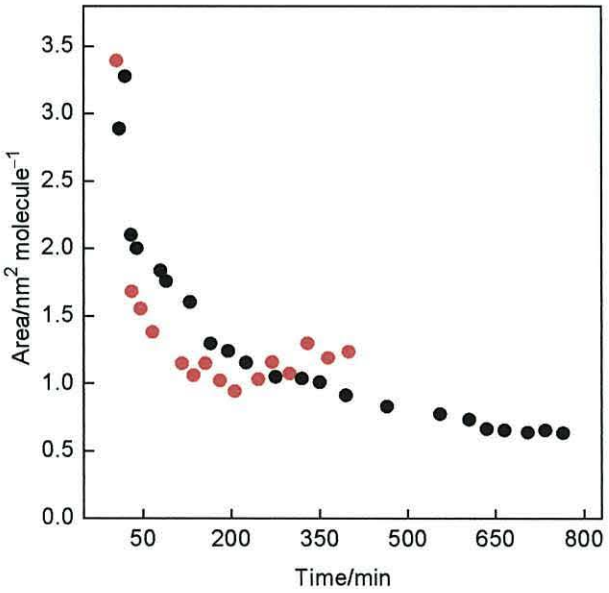

Figure 127 Variation of the molecular area with the period of immersion time for wire **10** in THF (black circles) and to the same solution to which deprotecting agent was added (red circles).

The deposition process in the presence of ammonia was less ordered, significantly yielded a higher value of molecular area than previously observed for the same molecule, which may indicate that the physisorption process dominated under blocks of chemisorbed wires.

SAMs of **10** on gold-coated HOPG were investigated using STM techniques, each time the film was investigated at several locations across the surface. The I–V characteristics were averaged from multiple scans and were symmetrical as expected; a representative scan is presented in Figure 128.

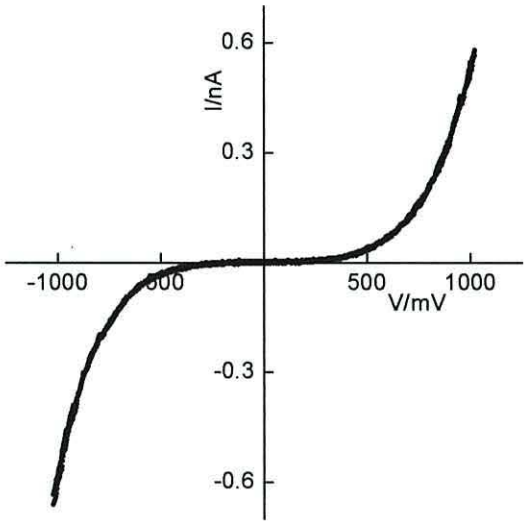

Figure 128 I-V characteristics of the Au-**10** structure contacted by an Au probe with a set point current of 0.4 nA and sample bias of 0.02 V.

The electrical conductivity of a single molecule of wire **10** that possessed chemical, and hence electrical, contacts to metal electrodes at both ends can be observed in Figure 129a. I(t) measurements on the surfaces showed large current fluctuations consistent with fast formation and breaking of thiol-gold contacts of molecular wires. A large number of current jumps, recorded at different locations on the substrate, were analysed to yield the histogram shown in Figure 129b. The single molecule current was calculated from a group of events demonstrating the highest column. It was attributed to the current jumps resulting from molecular bridging recorded at 0.2 ± 0.05 nA for a surface bias of -0.3 V. Also, periodic current jump features can be observed, so it could be assumed that for other current columns, the STM tip probes higher numbers of molecules.

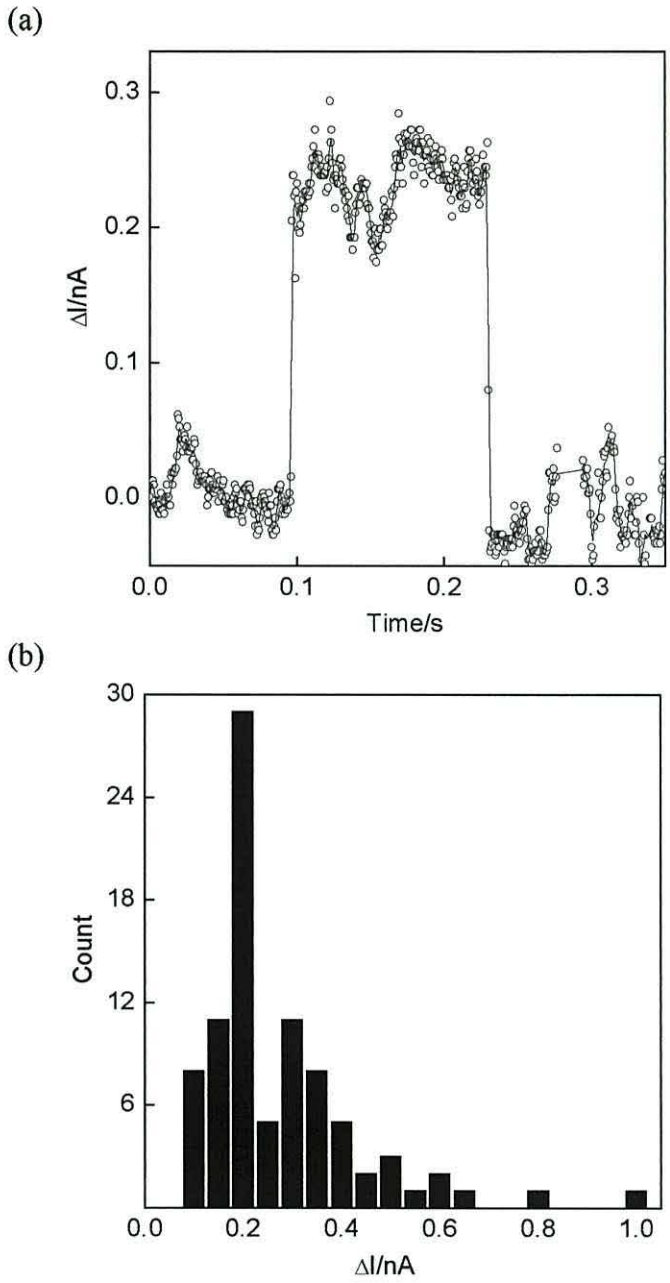

Figure 129 (a) Typical current jump with the gold STM probe located at a fixed height above the SAM with a sample bias of –0.3 V. (b) Histogram of 80 current jumps for **10**, recorded at a sample bias of –0.3 V, and a set point current of 0.4 nA.

The same molecule, but with cyanoethyl protection groups, was also investigated in order to confirm the electronic properties, and the SAM on gold is presented in Figure 130.

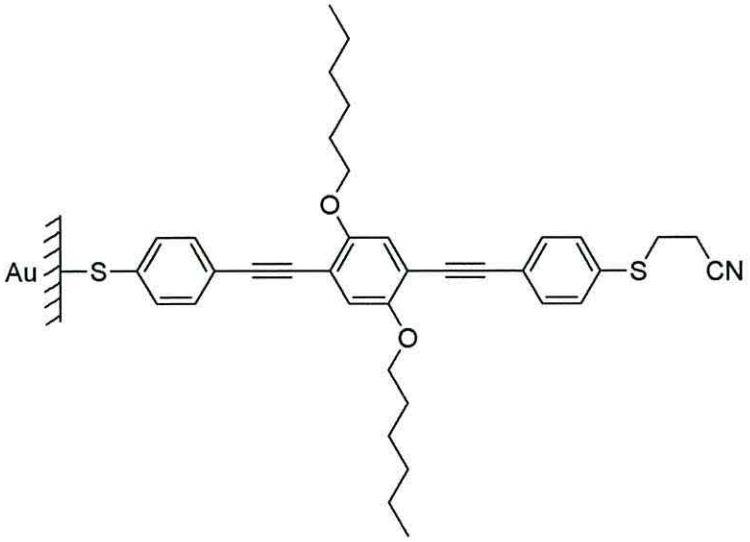

Figure 130 Molecular structure of wire **11** with the terminal sulphur showing the cyanoethyl group intact when formed without the deprotecting agent.

QCM studies were performed for four crystals and deposition, similar to wire **10** without deprotection, lasted about 10 hours with a mean area of 0.57 ± 0.23 nm^2 $molecule^{-1}$ (Figure 131). For deposition in the presence of sodium methoxide a similar the mean area was achieved with a value of 0.47 ± 0.12 nm^2 $molecule^{-1}$ (Figure 131).

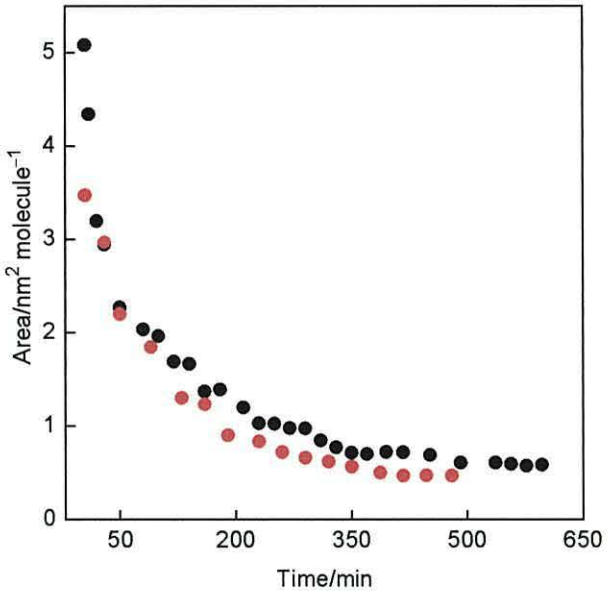

Figure 131 Variation of the molecular area with the period of immersion time for wire **11** in THF (black circles) and to the same solution to which deprotecting agent was added (red circles).

STM studies of molecule **11** were straightforward and the registered I-V plots were symmetrical (see Figure 130). The symmetry was unaffected as the conditions to land the probe were varied; for example the substrate bias was varied from 0.02 to 1 V, at a constant set point current of 0.4 nA and symmetrical or almost symmetrical I-V characteristics were obtained each time.

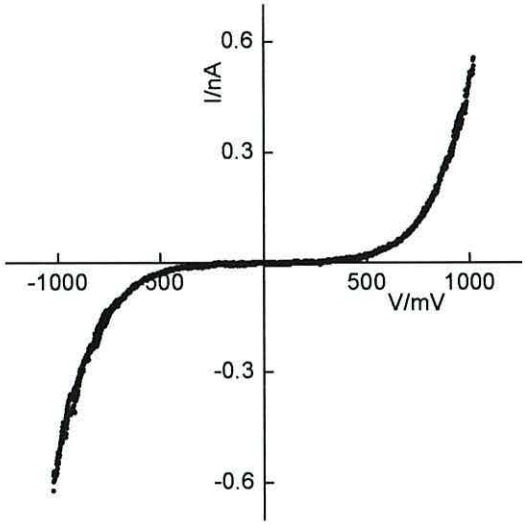

Figure 132 I-V characteristics of the Au-**11** structure contacted by an Au probe.

The current flowing through a single molecule of **11** was determined from histograms of current jumps, which were collected at different sample bias in the range of 0.02-1 V. The corresponding single molecule conductance did not depend on the applied potential significantly in the studied range, and all values were found to be 0.20 ± 0.05 nA. The histogram of I(t) jumps measured at -0.3 V, and a constant tunnelling current of 0.4 nA, predominantly exhibited the attachment of a single molecule, and is presented in Figure 133. Conductivity measurements of single molecules at different sample bias lead to the following conclusion; the adsorption of the terminal thiol group to the gold probe, which was attributed to the increased current, persisted for shorter time with increasing sample bias. The longest recorded event lasted for *ca.* 520 ms and was measured at 20 mV. Measurements of molecule conductance revealed another difference, namely, jumps that persisted for a longer time (recorded at a small sample bias) were smoother compared to the current jumps recorded at a large bias. The average times of adsorption persistence for a single molecule current at an individual sample bias were collected and are compared in Table 1.

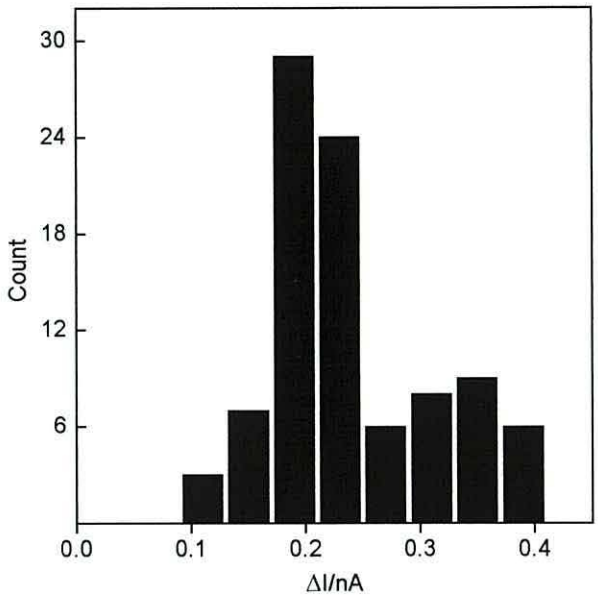

Figure 133 Histogram of 92 current jumps for **11**, recorded at a sample bias of –0.3 V, and a set point current of 0.4 nA.

Table 1. The average times of the adsorption persistence of molecule **11** to the gold probe at an individual sample bias.

Average time / ms	**Sample bias / mV**
210	20
100	50
100	100
100	300
90	400
90	500
70	700
30	1000

Even though the statistics of the formation of molecular bridges did not influence the different sample bias, the time of persisting current jumps decreased with increasing sample bias. This feature is in good agreement with theory, and it is considered that with this technique, it is possible to measure the electrical conductivity of single molecules [114],[115],[116],[118].

The SAMs of the next two compounds were prepared using a sequence of 5 or 10 minutes immersions from 0.08 mg ml^{-1} solutions of each wire in THF. The structures of molecular wires **12** and **13** are similar; the difference is in the central part, one of them contains thiophene, and the other a fluorene unit. Molecular wire **12** self-assembled to gold is presented in Figure 134.

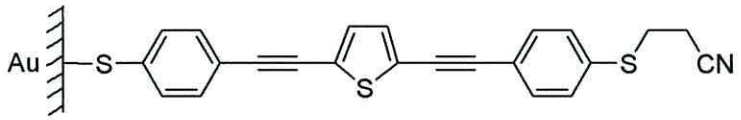

Figure 134 Molecular structure of wire **12** with the terminal sulphur showing the cyanoethyl group intact when formed without the deprotecting agent.

The optimum deposition for the non-deprotected molecular wire **12** was achieved after *ca.* 400 minutes and the resultant monolayer had an area per molecule of 0.46 ± 0.13 nm^2 $molecule^{-1}$ (see Figure 135). In the presence of sodium methoxide the time decreased to about 250 minutes yielded an area of 0.40 ± 0.06 nm^2 $molecule^{-1}$.

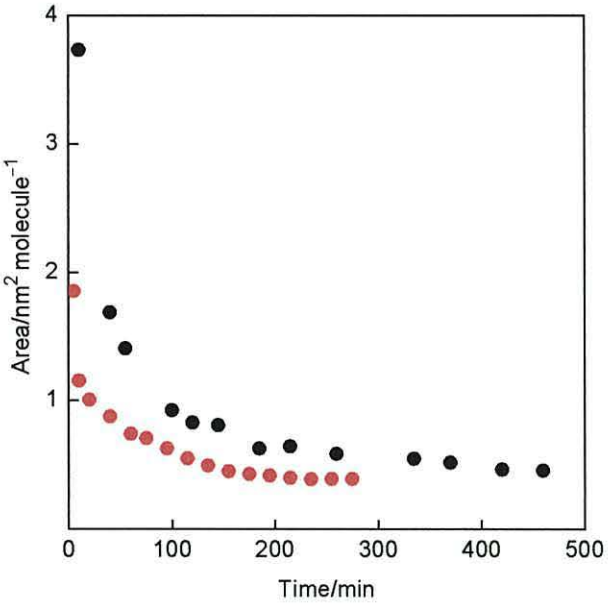

Figure 135 Variation of the molecular area with the period of immersion time for wire **12** in THF (black circles) and to the same solution to which deprotecting agent was added (red circles).

The I-V plots of molecule **12** obtained by STM using a gold tip were symmetrical (see Figure 136), showing no rectification at all. The set point current and voltage only did affect the magnitude of the tunnelling current by influencing the distance between the probe and the surface.

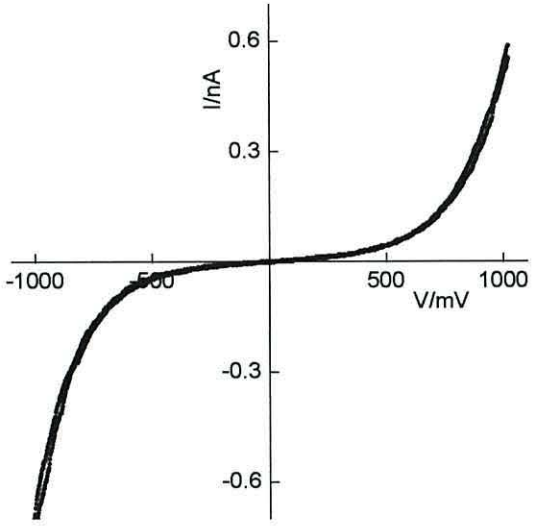

Figure 136 I-V characteristic of the Au-**12** structure contacted by an Au probe.

I(t) measurements on gold surfaces showed large current fluctuations consistent with fast formation and breaking of molecular wires, and a typical current trace is shown in Figure 137a. A large number of current jumps, recorded at different locations on the substrate, were analysed to yield the histogram shown in Figure 137b. This exhibits a pronounced maximum at 0.15 ± 0.01 nA, which may be attributed to the single molecule current and therefore adsorption via a single thiolate link to the gold probe. Attachment of two molecules to the gold probe (multiple molecular junctions) was also possible (Figure 137b).

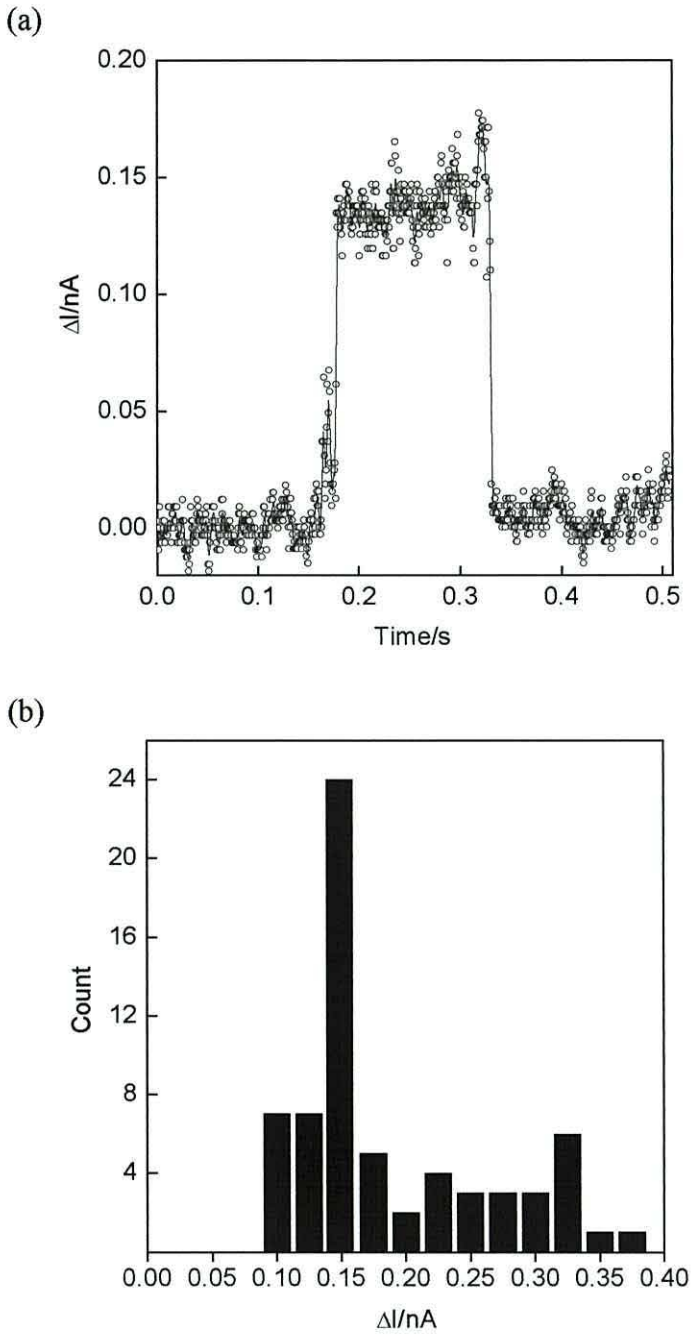

Figure 137 (a) Typical current jump with the gold STM probe located at a fixed height above the SAM with a sample bias of –0.3 V. (b) Histogram of 66 current jumps for **12**, recorded at a sample bias of –0.3 V, and a set point current of 0.4 nA. The fundamental peak in the histogram corresponds to the conductivity of the single molecular wire.

The next studies on self-assembly were performed using molecular wire **13**, which was an analogue of the wire **12**. The molecular structure of **13** self-assembled to gold is presented in Figure 138.

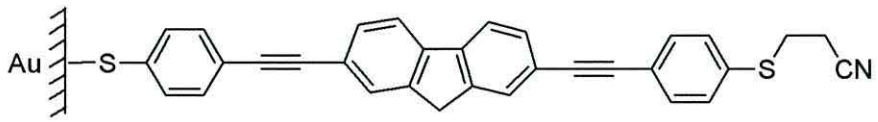

Figure 138 Molecular structure of wire **13** with the terminal sulphur showing the cyanoethyl group intact when formed without the deprotecting agent.

The result of the QCM analysis of wire **13** is presented in Figure 139. The mean molecular area amounted to 0.54 ± 0.07 nm^2 $molecule^{-1}$ for the chemisorbed wire without deprotecting agent. In the presence of sodium methoxide the time decreased resulting in an area per molecule of 0.64 ± 0.02 nm^2 $molecule^{-1}$.

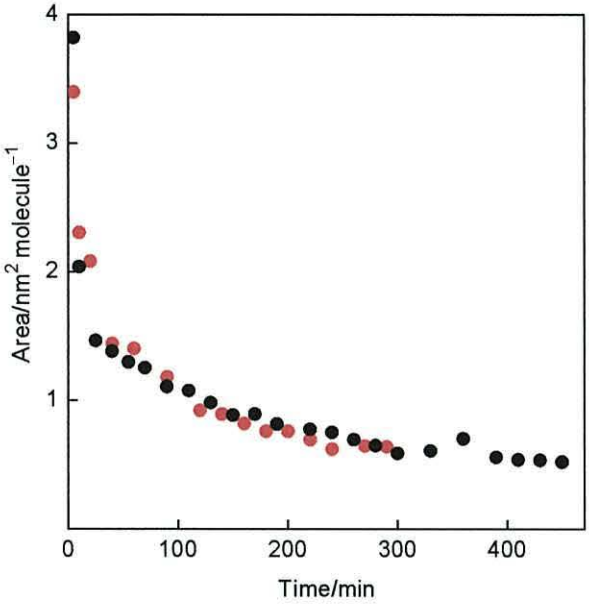

Figure 139 Variation of the molecular area with the period of immersion time for wire **13** in THF (black circles) and to the same solution to which deprotecting agent was added (red circles).

The I-V plots of molecule **13** obtained by STM using a gold tip were symmetrical. The set point current and voltage had very little effect on the profile of the I-V curves but they did affect the magnitude of the tunnelling current by influencing the distance between the probe and the surface (see Figure 140). This is a common feature from STM studies on wire-like molecules. This behaviour was reproducible for all films investigated as well as for different regions of each.

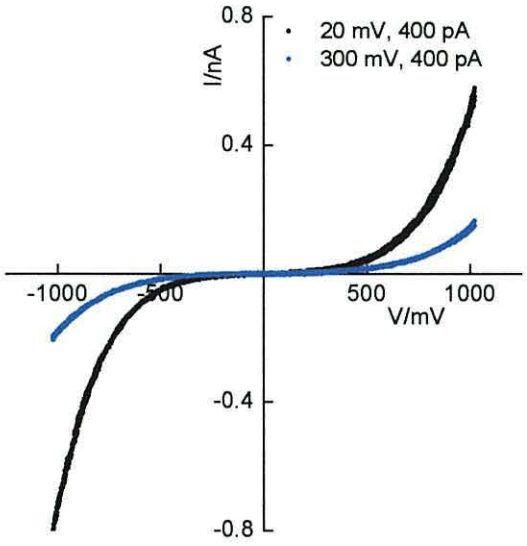

Figure 140 The extreme I-V characteristics of the Au–**13** structure contacted by an Au probe.

The STM "current jump" method seemed to work effectively for the Au–**13** structure, as the observed current jumps were reproducible for each point of the SAM that was probed by an Au tip. The most common current jump observed with time is presented in Figure 141a. Observations of direct molecular contact allowed construction of a histogram showing all recorded current jumps. Determination of the current flowing through a single molecule was from the histogram of 139 current jumps shown in Figure 141b. This data was collected at a sample bias of –0.3 V and set point current of 0.4 nA, and the most observable current jump was 0.10 ± 0.02 nA. The statistic describing the formation of multiple junctions leading to the formation of two, three and even higher multiples of molecular junctions was also observed (Figure 141b).

(a)

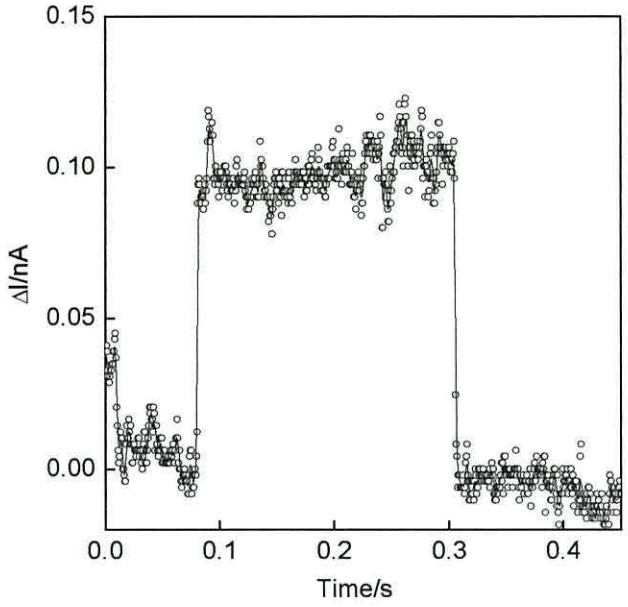

(b)

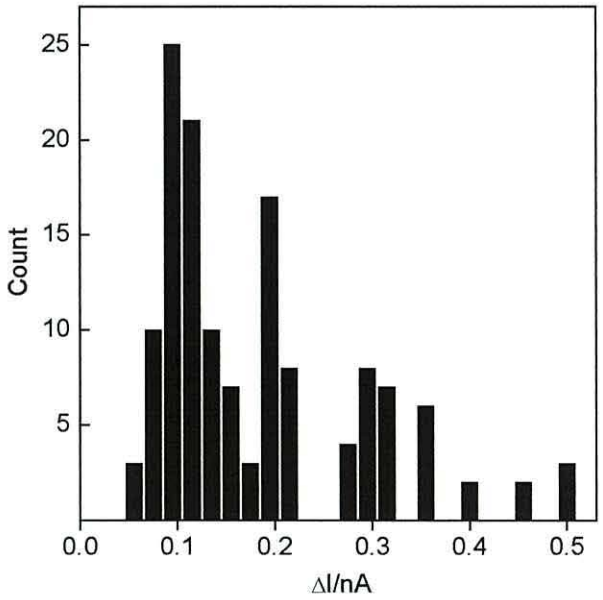

Figure 141 (a) Typical current jump with the gold STM probe located at a fixed height above the SAM with a sample bias of –0.3 V. (b) Histogram of 136 current jumps for **13**, recorded at a sample bias of –0.3 V, and a set point current of 0.4 nA.

9.3.1 Summary

Reproducible electrical behaviour from I-V characteristics was observed for all conformationally rigid molecular wires. Each film exhibited electrical symmetry in a similar range, and deprotection of the molecules did not significantly affect the shape of the I-V curves.

The STM I(t) method used for determination of the single-molecule current of individual wires seemed to work effectively. The electrical properties of molecular wires, registered, as current jumps were also reproducible. The single molecule current of the molecules **9-13** gave varied results. The reason for this behaviour was almost certainly attributable to the donor-acceptor character strength, and even molecular structure packing. The value of single molecule current of **9** obtained with the I(t) technique was higher compared to the results of the analogues **10** and **11**. The reason for this might be the close packing of the molecules of **9** on the gold surface, additionally facilitated by the short side-chains on the central phenyl ring. This could increase the possibility of the molecule adsorption via the single thiolate link to the gold probe. Furthermore, molecular wires **10** and **11** could deposit in different arrangements due to their bulky hexyloxy side-chains on the central phenyl ring of both molecules. In this case, the formation of the molecular bridges between the STM gold tip and substrate by thiol link was unlikely. Consequently, the consistent value of single-molecule current of **10** and **11** could be due to contacting different parts of the molecules by the STM tip. Single-molecule measurements of **10,** performed at different sample bias in the range 0.2-1.0 V, and at the constant set point current of 0.4 nA, did not change with increasing sample bias. However, it was also observed that for the smaller tip-sample separations the probability of the wire formations increased. Thus this is in good agreement with theory.

10. Conclusions

The study of the Au–S–C_nH_{2n}–A^+–π–D | D^- systems has been used to investigate ionically coupled cationic acceptors to anionic donor layers in the formation of rectifying junctions. The structures are akin to the Aviram and Ratner model. Thus it can be assumed that on one side of the device electrons flowed from the substrate to the LUMO of the acceptor, and from the HOMO of the donor to the tip on the other side. The results have varied with rectification ratios from 30 to 3000 at ± 1 V. The most significant rectification ratio emanated from the location of an anionic donor of copper(II) phthalocyanine to the electron donating end of an isoquinolinium hemicyanine dye (**3**), the latter being connected to and aligned by a gold substrate. The method of assembling the rectifying monolayer structures from an aqueous solution of the component cationic and anionic dyes seems to have great potential in developing assemblies for molecular electronic applications. The advantage of this in the form of the resulting I-V characteristics can be seen in Figure 142. Also, the system incorporating the quinolinium iodide (**4**) and copper(II) phthalocyanine (deposited in the same way) showed comparable results and is a significant enhancement compared with values for the iodide salt of this cationic moiety. These rectification ratios are substantially higher than intrinsic ratios reported from other organic films, and are on a par with characteristic ratios from structures where the behaviour arose from oxide-induced Schottky contacts.

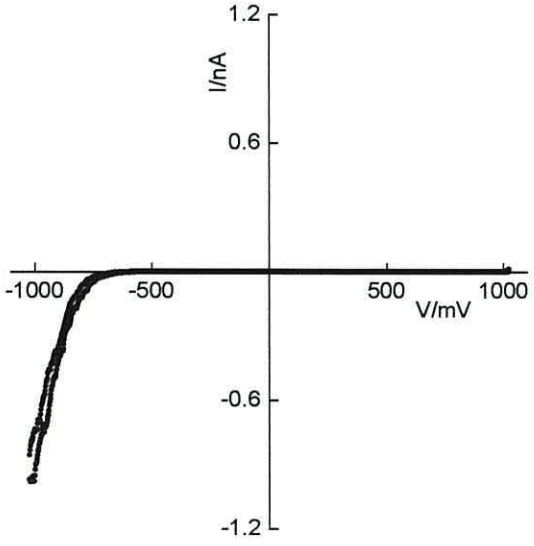

Figure 142 The I-V characteristics exhibited by Au–S–$C_{10}H_{20}$–A^+–π–D | D^- system.

The new molecular diodes presented in this thesis, incorporating cationic donor-(π-bridge)-acceptor dyes coupled with anionic donors yielded radically improved rectification behaviour. Significant rectification depends on a strong donor-acceptor combination, and the application of the phthalocyanine dye had a direct influence in improved electrical asymmetry from films of the ionically coupled structures. These results were published in a paper in *Physical Chemistry Chemical Physics*. It was the most-accessed paper in 2006, and the third most-accessed paper in 2007. Furthermore, the article was designated as a "Hot Article" by the Royal Society of Chemistry, reviewed in *Chemistry World* and *Chemical Science* and also highlighted in several other countries.

The pyridyl functionality of the conjugated molecular wires of different lengths served to obtain rectifying junctions. Therefore, a new effective method of assembling bilayer structures with electron accepting molecular wires of different lengths and an electron donating upper layer of copper(II) phthalocyanine or $TCNQ^-$ was found that resulted in high rectification ratios in the range 10-80 at ± 1 V. STM measurements showed the higher current at forward bias in the negative quadrant of the I-V curves. The direction of the current flow occurred in accordance with the Aviram-Ratner model, and an example I-V plot presenting diode-like behaviour along with the characteristics from a symmetrical neutral wire are shown in Figure 143.

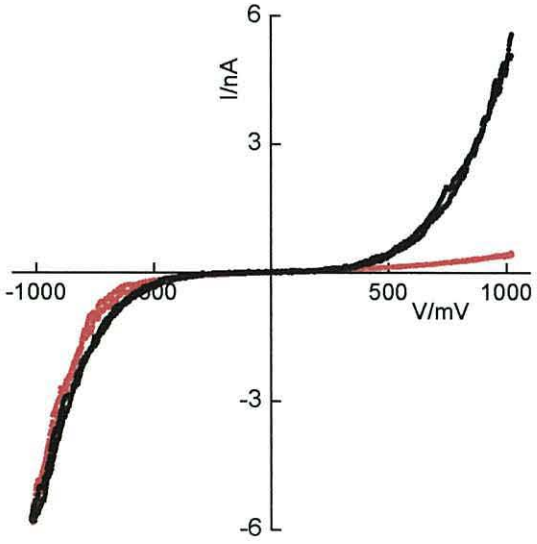

Figure 143 Rectifying I-V characteristics of the Au–$\mathbf{7}H_2^{2+}[CuPc(SO_3^-)_4(Na^+)_n]_{2/(4-n)}$ bilayer assembly (red). I-V characteristics of the molecular wire **7** deposited as a SAM on gold-coated HOPG (back).

The striking difference in the I-V characteristics of SAMs of the non-protonated wires and the ionic bilayer assemblies conclusively proves the presence of the wire molecules in junctions. This electrostatic interaction between the protonated molecular wires and electron-donating layer provide an easy and effective way of assessing molecules for their suitability for use in rectifying junction. Results of the 7 nm long molecular wires were published in *Chemical Communications*, and the article was designated as a "Hot Article" and as a "Top Ten Article" by the Royal Society of Chemistry, also it was reviewed in Utilise Gold bulletin.

The STM I(t) and I(s) methods were used for the first time to reveal single-molecule current of individual wires. It has been found that the current of single wires **6** and **7** exhibited the same value, whereas for the longest molecular wire **8** the value of single-molecule current was the smallest. The upper limiting current exhibited by I-V curves of all molecular wires studied, approached the corresponding single molecule values obtained from the current jump method as the set point conditions were altered to minimise the gap between the surface and the STM tip.

Further single-molecule studies of the 2 nm long phenylene-ethynylene molecular wires that have chemical, and hence electrical, contacts to metal electrodes at both ends, have been demonstrated, and it has been found that the current could be attributed to the single molecule was reproducible each time. The studies performed at different sample bias in the range 0.2-1.0 V, and at the constant set point current of 400 pA, are in good agreement with theory, and confirmed that the time of persisting current jumps decreased with increasing sample bias. Observations of single molecular current using both I(t) and I(s) methods should be a standard technique that could help with the calculations of conductance of single molecules.

11. Outlook

Molecules are obvious candidates for bottom-up assembly of electronic devices, and a single molecule represents the smallest unit of matter with well-defined connectivity. To make even the simplest electronic device such as molecules connected between two electrodes, several practical difficulties appear. Most importantly is the verification of the molecule in the junction, connected and oriented to the electrodes in the intended way. Fabrication of the new organic electronic devices is a challenge because of the difference in scale between a molecule, the electrodes and the small gap between them. An important issue in technological progress for the near future is to find efficient techniques of placing molecules in circuits, providing good electrical contacts and mechanically stable junctions. Many interesting methods have been employed to create metal-molecule-metal junctions, and some of them were presented in this thesis such as: MCBJ, crossed wires, mercury junctions, nanopores and STM junctions. The presented results of the single-molecule current and the current asymmetry measurements have also made a significant contribution in this matter and can be used for further studies in the molecular electronics area.

Understanding charge transport at the molecular level is the crucial factor for developing molecular assemblies with uncommon properties for novel applications. Taking full advantage of the latest achievements of nano-scale microscopy and spectroscopy, it is possible to study the properties of single molecules. Synthetic chemistry has also made enormous progress and more organic components, which can be used for building molecular electronic systems, have become commercially available. The variety of the demonstrated structures has led to original ideas for the architecture of future molecular electronic circuits. However, the present strategy is based on the adaptation of molecular functional elements into the architectural concept of current inorganic devices. Building hybrid silicon – organic field-effect transistors (FETs), compatible with existing technology, would be more beneficial than a complete replacement of the manufacturing processes in order to apply unconventional solutions.

12. Publications

I. G.J. Ashwell, W.D. Tyrrell, B. Urasinska, C. Wang, M.R. Bryce, "Organic rectifying junctions from an electron-accepting molecular wire and an electron-donating phthalocyanine", *Chemical Communications*, **15**, 1640-1642, 2006.

II. G.J. Ashwell, B. Urasinska, W.D. Tyrrell, "Molecules that mimic Schottky diodes", *Physical Chemistry Chemical Physics*, **8**, 3314-3319, 2006.
Designated by the Royal Society of Chemistry as a "Hot Article", the most accessed paper in 2006 and the third most accessed paper in 2007. Also, reviewed by C. Boothby in Chemical Science (3, C58, 2006) and Chemistry World, K. Langer in PAP-Poland (2006/07/10 and 2006/07/14) and in Global Trends Briefing-Korea (2006/07/15). Paper featured on the journal's cover.

III. G.J. Ashwell, B. Urasinska, C. Wang, M.R. Bryce, I. Grace, C.J. Lambert, "Single-molecule electrical studies of a 7 nm long molecular wire", *Chemical Communications*, **45**, 4706-4708, 2006.
Designated as a "Hot Article" and as a "Top Ten Article" by the Royal Society of Chemistry and also reviewed in Utilise Gold bulletin.

IV. C. Wang, A.S. Batsanov, M.R. Bryce, G.J. Ashwell, B. Urasinska, I. Grace, C.J. Lambert, "Electrical characterisation of 7 nm long conjugated molecular wires: experimental and theoretical studies", *Nanotechnology*, **18**, no 044005, 2007.

V. K. Palewska, M. Sujka, B. Urasińska-Wójcik, J. Sworakowski, J. Lipiński, S. Nešpůrek, J. Rakušan, M. Karásková, "Light-induced effects in sulfonated aluminum phthalocyanines-potential photosensitizers in the photodynamic therapy. Spectroscopic and kinetic study", *Journal of Photochemistry and Photobiology A: Chemistry*, **197**, 1-12, 2008.

13. References

[1] Feynman, R. P., There's plenty of room at the bottom, [Web Page], 1960. Available at: http://www.zyvex.com/nanotech/feynman.

[2] Aviram, A. and Ratner, M. A., Molecular Rectifiers, *Chem. Phys. Lett.*, vol. 29, pp. 277-283, 1974.

[3] Aviram, A., Molecular Electronics-Science and Technology, *Angew. Chem., Int. Ed.*, vol. 28, pp. 520-521, 1989.

[4] Mantooth, B. A. and Weiss, P. S., Fabrication, Assembly, and Characterisation of Molecular Electronic Components, *Proc. IEEE*, vol. 11, pp. 1785-1802, 2003.

[5] Moore, G. E., Cramming more components onto integrated circuits, *Electron.*, vol. 38, pp. 114-117, 1965.

[6] Jones, R. A. L., Soft Machines Nanotechnology and Life, *Oxford University Press*, United Kingdom, 2004.

[7] Goldhaber-Gordon, D., Montemerlo, M. S., Love, C. J., Opiteck, G. J., and Ellenbogen, J. C., Overview of Nanoelectronic Devices, *Proc. IEEE*, vol. 85, pp. 521-540, 1997.

[8] Hutchby, J. A., Bourianoff, G. I., Zhirnov, V. V., and Brewer, J. E., Extending the Road Beyond CMOS, *IEEE Circuits & Devices Mag.*, vol. 18, pp. 28-41, 2002.

[9] Intel Corporation, Moore's law, [Web page]. Avaiable at: http://www.intel.com/technology/mooreslaw/.

[10] Metzger, R. M., Unimolecular Electrical Rectifiers, *Chem. Rev.*, vol. 103, pp. 3803-3834, 2003.

[11] Metzger, R. M., Unimolecular Rectifiers and Prospects for Other Unimolecular Electronic Devices, *The Chem. Rec.*, vol. 4, pp. 291-304, 2004.

[12] Carroll, R. L. and Gorman, C. B., The Genesis of Molecular Electronics, *Angew. Chem., Int. Ed.*, vol. 41, pp. 4378-4400, 2002.

[13] Richter, C. A. and Stewart, D. R., Metrology for Molecular Electronics, *Conference paper - GOMACTech*, vol. 28, pp. 281-284, 2003.

[14] Metzger, R. M., Baldwin, J. W., Shumate, W. J., Peterson, I. R., Mani, P., Mankey, G. J., Morris, T., Szulczewski, G., Bosi, S., Prato, M., Comito, A., and Rubin, Y., Electrical Rectification in a Langmuir-Blodgett Monolayer of Dimethyanilinoazafullerene Sandwiched between Gold Electrodes, *J. Phys. Chem. B*, vol. 107, pp. 1021-1027, 2003.

[15] Metzger, R. M., Unimolecular rectifiers and what lies ahead, *Colloids Surf., A*, vol. 284-285, pp. 2-10, 2006.

[16] Metzger, R. M., Unimolecular rectifiers: Methods and challenges, *Anal. Chim. Acta*, vol. 568, pp. 146-155, 2006.

[17] Metzger, R. M., Unimolecular rectifiers: Prestent status, *Chem. Phys.*, vol. 326, pp. 176-187, 2006.

[18] Dijk, E. H. , Myles, D. J. T., Veen, M. H., and Hummelen, J. C., Synthesis and Properties of an Anthraquinone-Based Redox Switch for Molecular Electronics, *Org. Lett.*, vol. 8, pp. 2333-2336, 2006.

[19] Pease, A. R., Jeppesen, J. O., Stoddart, J. F. L. Y., and Collier, C. P. H. J. R., Switching Devices Based on Interlocked Molecules, *Acc. Chem. Res.*, vol. 34, pp. 433-444, 2001.

[20] Reed, M. A. , Zhou, C. J., Burgin, T. P., and Tour, J. M., Conductance of a Molecular Junctions, *Science*, vol. 278, pp. 252-254, 1997.

[21] Reed, M. A. , Molecular-Scale Electronics, *Proc. IEEE*, vol. 87, pp. 652-658, 1999.

[22] Shaw, J. M. and Sheidler, P. F., Organic electronics: Introduction, *IBM J. Res. & Dev.*, vol. 45, pp. 3-9, 2001.

[23] Maruccio, G., Cingolani, R., and Rinaldi, R., Projecting the nanoworld: Concepts, results and perspectives of molecular electronics, *J. Mater. Chem.*, vol. 14, pp. 542-554, 2004.

[24] Dodabalapur, A., Organic light emitting diodes, *Solid State Commun.*, vol. 102, pp. 259-267, 1997.

[25] Petty, M. C., Bryce, M. R., and Bloor, D., An introduction to molecular electronics, *Edward Arnold*, United Kingdom, 1995.

[26] Tour, J. M. , Kozaki, M., and Seminario, J. M., Molecular Scale Electronics: A Synthetic/Computational Approach to Digital Computing, *J. Am. Chem. Soc.*, vol. 120, pp. 8486-8493, 1998.

[27] Parviz, B. A., Ryan, D., and Whitesides, G. M., Using Self-Assembly for the Fabrication of Nano-Scale Electronic and Photonic Devices, *IEEE Trans. Adv. Pack.*, vol. 26, pp. 233-241, 2003.

[28] Schreiber, F., Self-assembled monolayers: from 'simple' model systems to biofunctionalized interfaces, *J. Phys.: Condens. Matter.*, vol. 16, pp. R881-R900, 2004.

[29] Schreiber, F., Structure and growth of self-assembling monolayers, *Prog. Surf. Sci.*, vol. 65, pp. 151-256, 2000.

[30] Bigelow W.C., Pickett D.L., and Zisman W.A., Oleophobic monolayers, *J. Colloid Science*, vol. 1, pp. 513-538, 1946.

[31] Barnes, G. T. and Gentle, I. R. Interfacial Science. An Introduction, *Oxford University Press*, United Kingdom, 2005.

[32] Forrest, S. R., Ultrathin Organic Films Grown by Organic Molecular Beam Deposition and Related Techniques, *Chem. Rev.*, vol. 97, pp. 1793-1896, 1997.

[33] Nuzzo, R. G. and Allara, D. L., Adsorption of bifunctional organic disulfides on gold surface, *J. Am. Chem. Soc.*, vol. 105, pp. 4481-4483, 1983.

[34] Allara, D. L., Parikh, A. N., and Rondelez, F., Evidence for a Unique Chain Organization in Long Chain Silane Monolayers Deposited on Two Widely Different Solid Substrates, *Langmuir*, vol. 11, pp. 2357-2360, 1995.

[35] Ulman, A., Formation and Structure of Self-Assembled Monolayers, *Chem. Rev.*, vol. 96, pp. 1533-1554, 1996.

[36] Slowinski, K., Slowinska, K. U., and Majda, M., Electron Tunneling Across Hexadecanethiolate Monolayers on Mercury Electrodes: Reorganisation Enegry, Structure and Permeability of the Alkane/Water Interface, *J. Phys. Chem. B*, vol. 103, pp. 8544-8551, 1999.

[37] Slowinski, K., Chamberlain II, R. V., Bilewicz, R., and Majda, M., Evidence for Inefficient Chain-to-Chain Coupling in Electron Tunneling through Liquid Alkanethiol Monolayer Films on Mercury, *J. Am. Chem. Soc.*, vol. 118, pp. 4709-4710, 1996.

[38] Kemula, W. and Kublik, Z., Application de La Goutte Pendante de Mercure a La Determination De Minimes Quantites De Differents Ions, *Anal. Chim. Acta*, vol. 18, pp. 104-111, 1958.

[39] Tran, E., Rampi, M. A., and Whitesides, G. M., Electron Transfer in a Hg-SAM//SAM-Hg Junction Mediated by Redox Centres, *Angew. Chem. Int. Ed.*, vol. 43, pp. 3835-3839, 2004.

[40] Love, J. C. , Estroff, L. A., Kriebel, J. K., Nuzzo, R. G. , and Whitesides, G. M., Self-Assembled Monolayers of Thiolates on Metals as a Form of Nanotechnology, *Chem. Rev.*, vol. 105, pp. 1103-1169, 2005.

[41] Vargas, M. C., Glannozzi, P., Selloni, A., and Scoles, G., Coverage-Dependent Adsorption of CH_3S and $(CH_3S)_2$ on Au(111): a Density Functional Theory Study, *J. Phys. Chem. B*, vol. 105, pp. 9509-9513, 2001.

[42] Roper, M. G., Skegg, M. P., Fisher, C. J., Lee, J. J. , Dhanak, V. R., Woodruff, D. P., and Jones, R. G., Atop adsorption site of sulphur head groups in gold-thiolate self-assembled monolayers, *Chem. Phys. Lett.*, vol. 389 , pp. 87-91, 2004.

[43] Grönbeck, H., Curioni, A., and Andreoni W., Thiols and Disulfides on the Au (111) Surface: The Headgroup-Gold Interaction, *J. Am. Chem. Soc.*, vol. 122, pp. 3839-3842, 2000.

[44] Standard, J. M., Gregory, B. W., and Clark, B. K., Computational studies of copper, silver, and gold alkanethiolates and alkaneselenates, *J. Mol. Struct.:THEOCHEM*, vol. 803, pp. 103-113, 2007.

[45] Fenter, P., Eberhardt, A., Liang, K. S., and Eisenberger, P., Epitaxy and chainlength dependent strain in self-assembled monolayers, *J. Chem. Phys.*, vol. 106, pp. 1600-1608, 1997.

[46] Dubois, L. H., Zegarski, B. R., and Nuzzo, R. G., Molecular ordering of organosulfur compounds on Au(111) and Au(100): Adsorption from solution and in ultrahigh vacuum, *J. Chem. Phys.*, vol. 98, pp. 678-688, 1993.

[47] Somorjai, G. A., Introduction to Surface Chemistry and Catalysis, *Wiley*, New York, 1994.

[48] Stapleton, J. J., Harder, P., Daniel, T. A., Reinard, M. D., Yao, Y., Price, D. W., Tpor, J. M., and Allara, D. L., Self-Assembled Oligo(phenylene-ethylene) Molecular Electronic Switch Monolayers on Gold: Structures and Chemical Stability, *Langmuir*, vol. 19, pp. 8245-8255, 2003.

[49] Lee, K. A. B., Electron Transfer into Self-Assembling Monolayers on Gold Electrodes, *Langmuir*, vol. 6, pp. 709-712, 1990.

[50] Strong, L. and Whitesides, G. M., Structures of Self-Assembled Monolayer Films of Organosulfur Compounds Adsorbed on Gold Single Crystals:Electron Diffraction Studies, *Langmuir*, vol. 4, pp. 546-558, 1988.

[51] Barclay, D. J. and Caja, J., Structural Factors Involved in Ionic Adsorption, *Croat. Chem. Acta*, vol. 43, pp. 221-227, 1971.

[52] Yamada, R., Wano, H., and Uosaki, K., Effect of Temperature on Structure of the Self-Assembled Monolayer of Decanethiol on Au (111) Surface, *Langmuir*, vol. 16, pp. 5523-5525, 2000.

[53] McDermott, C. A., McDermott, M. T., Green, J. B., and Porter, M. D., Structural Origins of the Surface Depressions at Alkanethiolate Monolayers on Au (111): A Scanning Tunneling and Atomic Force Microscopic Investigation, *J. Phys. Chem.*, vol. 99, pp. 13257-13267, 1995.

[54] Schönenberger, C., Sondag-Huethorst, J. A. M., Jorritsma, J., and Fokkink, L. G. J., What Are the "Holes" in Self-Assembled Monolayers of Alkanethiols on Gold?, *Langmuir*, vol. 10, pp. 611-614, 1994.

[55] Poirier, G. E., Characterisation of Organosulfur Molecular Monolayers on Au (111) using Scanning Tunneling Microscopy, *Chem. Rev.*, vol. 97, pp. 1117-1127, 1997.

[56] Iler, R. K. , Multilayers of colloidal particles, *J. Colloid Interface Sci.*, vol. 21, pp. 569-594, 1966.

[57] Decher, G., Fuzzy Nanoassemblies: Toward Layered Polymeric Multicomposites, *Science*, vol. 277, pp. 1232-1237, 1997.

[58] Decher, G., Lvov, Y., and Schmitt, J., Proof of multilayer structural organization in self-assembled polycation-polyanion molecular films, *Thin Solid Films*, vol. 244, pp. 772-777, 1994.

[59] Lvov, Y., Essier, F., and Decher, G., Combination of Polycation/Polyanion Self-Assebmly and Langmuir-Blodgett Transfer for the Construction of Superlattice Films, *J. Phys. Chem.*, vol. 97, pp. 13773-13777, 1993.

[60] Mukherjee, B. and Pal, A. J., Rectification in molecular assemblies of donor-acceptor monolayers, *Chem. Phys. Lett.*, vol. 416, pp. 289-292, 2005.

[61] Bertrand, P., Jonas, A., Laschewsky, A., and Legras, R., Ultrathin polymer coatings by complexation of polyelectrolytes at interfaces: suitable materials, structure and properties, *Macromol. Rapid Commun.*, vol. 21, pp. 319-348, 2000.

[62] Pigoń, K. and Ruziewicz, Z., Chemia fizyczna, *PWN*, Warszawa, 1986.

[63] Jung, T. A. , Schlitter, R. R., Gimzewski, J. K., Tang, H. , and Joachim, C., Controlled Room-Temperature Positioning of Individual Molecules: Molecular Flexure and Motion, *Science*, vol. 271, pp. 181-184, 1996.

[64] Gimzewski, J. K. and Joachim, C., Nanoscale Science of Single Molecules Using Local Probes, *Science*, vol. 283, pp. 1683-1688, 1999.

[65] Lidzey, D., Bradley, D. D. C., Alvaradado, S. F., and Seidler, P. F., Electroluminescence in polymer films, *Nature*, vol. 386, pp. 135-136, 1997.

[66] Marx, K. A., Quartz Crystal Microbalance: A Useful Tool for Studying Thin Polymer Films and Complex Biomolecular Systems at the Solution-Surface Interface, *Biomacromolecules*, vol. 4, pp. 1099-1120, 2003.

[67] Martin, S. J., Granstaff, V. E., and Frye, G. C., Characterization of a Quartz Crystal Microbalance with Simultaneous Mass and Liquid Loading, *Anal. Chem.*, vol. 63, pp. 2272-2281, 1991.

[68] Whelan, C. M., Smyth, M. R., Barnes, C. J., Brown, N. M. D., and Anderson, C. A., An XPS study of heterocyclic thiol self-assembly on Au(111), *Appl. Surf. Sci.*, vol. 134, pp. 144-158, 1998.

[69] Cooke, S. J. and Roberts, G. G., Monolayer and multilayer film characterisation using surface plasmon resonance, *Thin Solid Films*, vol. 210-211, pp. 685-688, 1992.

[70] Eberhardt, A., Fenter, P., and Eisenberger, P., Growth kinetics in self-assembling monolayers: a unique adsorption mechanism, *Surf. Sci.*, vol. 397, pp. L285-L290, 1998.

[71] Baba, A., Kaneko, F., and Advincula, R. C., Adsorption properties of polyelectrolytes in ultrathin multilayer assemblies: investigations using the quartz crystal microbalance (QCM) technique, *Polym. Prepr. (Am. Chem. Soc., Div. Polym. Chem.)*, vol. 40, pp. 488-489, 1999.

[72] Chah, S., Yi, J., Pettit, C. M., Roy, D., and Fendler, J. H., Ionisation and Reprotonation of Self-Assembled Mercaptopropionic Acid Monolayers Investigated by Surface Plasmon Resonance Measurements, *Langmuir*, vol. 18, pp. 314-318, 2002.

[73] Lu, F., Lee, H. P., Lu, P., and Lim, S. P., Finite element analysis of interference for the laterally coupled quartz crystal microbalances, *Sens. Actuators, A*, vol. 119, pp. 90-99, 2005.

[74] O'Sullivan, C. K. and Guilbault, G. G., Commercial quartz crystal microbalances - theory and applications, *Biosens. Bioelectr.*, vol. 14, pp. 663-670, 1999.

[75] Bruckenstein, S. and Shay, M., Experimental Aspects of Use of The Quartz Crystal Microbalance in Solution, *Electrochim. Acta*, vol. 30, pp. 1295-1300, 1985.

[76] Buttry, D. A. and Ward, M. D., Measurements of Interfacial Processes at Electrode Surfaces with the Electrochemical Quartz Crystal Microbalance, *Chem. Rev.*, vol. 92, pp. 1355-1379, 1992.

[77] Sauerbrey, G., Verwendung von schwingquarzen zur wagung dunner schechten and zur mikrowagung, *Z. Phys.*, vol. 155, pp. 206-222, 1959.

[78] Hayakawa, T., Yoshinari, M., and Nemoto, K., Quartz-Crystal Microbalance-Dissipation Technique for the Study of Initial Adsorption of Fibronectin Onto Tresyl Chloride-Activated Titanium, *J. Biomed. Mater. Res., Part B*, vol. 73B, pp. 271-276, 2005.

[79] The Nobel Prize in Physics 1986, [Web page]. Avaiable at: http://nobelprize.org/nobel_prizes/physics/laureates/1986/index.html.

[80] Samori, P., Scanning probe microscopes beyond imaging, *J. Mater. Chem.*, vol. 14, pp. 1353-1366, 2004.

[81] Samori, P. and Rabe, J. P., Scanning probe microscopy explorations on conjugated (macro)molecular architectures for molecular electronics, *J. Phys.: Condens. Matter.*, vol. 14, pp. 9955-9973, 2002.

[82] Dekker, C., Tans, S. J., Oberndorff, B., Meyer, R., and Venema, L. C., STM imaging and spectroscopy of single copperphthalocyanine molecules, *Synth. Met.*, vol. 84, pp. 853-854, 1997.

[83] McCreery, R. L., Molecular Electronic Junctions, *Chem. Mater.*, vol. 16, pp. 4477-4496, 2004.

[84] Klein, H., Battaglini, N., Bellini, B., and Dumas, P., STM of mixed alkylthiol self-assembled monolayers on Au(111), *Mater. Sci. Eng., C*, vol. 19, pp. 279-283, 2002.

[85] Wakamatsu, S., Akiba, U., and Fujihira, M., Electronic tunnelling through a single molecule embedded in self-assembled monolayer matrices, *Colloids Surf., A*, vol. 198-200, pp. 785-790, 2002.

[86] Gaudioso, J. and Ho, W., Single-Molecule Vibrations, Conformational Changes, and Electronic Conductivity of Five-Membered Heterocycles, *J. Am. Chem. Soc.*, vol. 123, pp. 10095-10098, 2001.

[87] Zou, J., Wang, X., Bullen, D., Ryu, K., Liu, C., and Mirkin, C. A., A modul - and - transfer technology for fabricating scanning probe microscopy probes, *J. Micromech. Microeng.*, vol. 14, pp. 204-211, 2004.

[88] Li, B., Wang, H., Yang, J., and Hou, J. G., High-resolution scanning tunnelling microscopy for molecules, *Ultramicroscopy*, vol. 98, pp. 317-334, 2004.

[89] Moresco, F. , Meyer, G., Tang, H., Joachim, C., and Reider, K. H., Investigation of mechanical and electronic properties of large molecules by low temperature STM, *J. Elec. Spec. Rel. Phen.*, vol. 129, pp. 149-155, 2003.

[90] Pomerantz, M., Aviram, A., McCorkle, R. A., Li, L., and Schrott, A. G., Rectification of STM Current to Graphite Covered with Phthalocyanine Molecules, *Science*, vol. 255, pp. 1115-1118, 1992.

[91] Joachim, C. , Gimzewski, J. K., and Aviram, A., Eelctronics using hybrid-molecular and mono-molecular devices, *Nature*, vol. 408, pp. 541-548, 2000.

[92] Nitzan, A. and Ratner, M. A., Electron Transport in Molecular Wire Junctions, *Science*, vol. 300, pp. 1384-1389, 2003.

[93] Simmons, J. G., Generalized Formula for the Electric Tunnel Effect between Similar Electrodes Separated by a Thin Insulating Film, *J. Appl. Phys.*, vol. 34, pp. 1793-1804, 1963.

[94] Holmlin, R. E., Haag, R., Chabinyc, M. L., Ismagilov, R. F., Cohen, A. E., Terfort, A., Rampi, M. A. , and Whitesides, G. M., Electron Transport through Thin Organic Films in Metal-Insulator-Metal Junctions Based on Self-Assembled Monolayers, *J. Am. Chem. Soc.*, vol. 123, pp. 5075-5085, 2001.

[95] Segal, D., Nitzan, A., Davis, W. B., Wasieleski, M. R., and Ratner, M. A., Electron Transfer Rates in Bridged Molecular Systems 2. A Steady-State Analysis of Coherent Tunnelling and Thermal Transitions, *J. Phys. Chem. B*, vol. 104, pp. 3817-3829, 2000.

[96] Joachim, C. and Ratner, M. A., Molecular electronics: Some views on transport junctions and beyond, *PNAS*, vol. 102, pp. 8801-8808, 2005.

[97] Reed, M. A. and Tour, J. M., Computing with Molecules, *Sci. Am.*, pp. 86-93, 2000.

[98] Chen, J., Reed, M. A., Rawlett, A. M., and Tour, J. M., Large On-Off Ratios and Negative Differential Resistance in a Molecular Electronic Device, *Science*, vol. 286, pp. 1550-1552, 1999.

[99] Zhou, C., Deshpande, M. R., Reed, M. A., Jones II, L., and Tour, J. M., Nanoscale metal/self-assembled monolayer/metal heterostructures, *Appl. Phys. Lett.*, vol. 71, pp. 611-613, 1997.

[100] Chang, S. C., Li, Z., Lau, C. N., Larade, B., and Williams, R. S., Investigation of a model molecular-electronic rectifier with an evaporated Ti-metal top contact, *Appl. Phys. Lett.*, vol. 83, pp. 3198-3200, 2003.

[101] Lenfant, S., Krzeminski, C., Delerue, C., Allan, G., and Vuillaume, D., Molecular Rectifying Diodes from Self-Assembly on Silicon, *Nano Lett.*, vol. 3, pp. 741-746, 2003.

[102] Meinhard, J. E., Organic Rectifying Junction, *J. Appl. Phys.*, vol. 35, pp. 3059-3060, 1964.

[103] Guliants, E. A., Ji, C., Song, Y. J., and Anderson, W. A., A 0.5-μm-thick polycrystalline silicon Schottky diode with rectification ratio 10^6, *Appl. Phys. Lett.*, vol. 80, pp. 1474-1476, 2002.

[104] Anderson, T. L., Komplin, G. C., and Pietro, W. J., Rectifying Junctions in Peripherally-Substituted Metallophthalocyanine Bilayer Films, *J. Phys. Chem.*, vol. 97, pp. 6577-6578, 1993.

[105] Fan, F. R. and Faulkner, L. R., Photovoltaic effects of metalfree and zinc phthalocyanines.I. Dark electrical properties of rectifying cells, *J. Chem. Phys.*, vol. 69, pp. 3334-3340, 1978.

[106] Chabinyc, M. L., Chen, X., Holmlin, R. E., Jacobs, H., Skulason, H., Frisbie, C. D., Mujica, V., Ratner, M. A., Rampi, M. A., and Whitesides, G. M., Molecular Rectification in a Metal-Insulator-Metal Junction Based on Self-Assembled Monolayers, *J. Am. Chem. Soc.*, vol. 124, pp. 11730-11736, 2002.

[107] Ashwell, G. J., Mohib, A., and Miller, J. R., Induced rectification from self-assembled monolayers of sterically hindered π-bridged chromophores, *J. Mater. Chem.*, vol. 15, pp. 1160-1166, 2005.

[108] Kushmerick, J. G., Holt, D. B., Pollack, S. K., Ratner, M. A., Yang, J. C., Schull, T. L., Naciri, J., Moore, M. H., and Shashidhar, R., Effect of Bond-Length Alternation in Molecular Wires, *J. Am. Chem. Soc.*, vol. 124, pp. 10654-10655, 2002.

[109] Kushmerick, J. G., Holt, D. B., Yang, J. C., Naciri, J., Moore, M. H., and Shashidhar, R., Metal-Molecule Contacts and Charge Transport across Monomolecular Layers: Measurement and Theory, *Phys. Rev. Lett.*, vol. 89, pp. 086802-1–086802-4, 2002.

[110] Kushmerick, J. G., Naciri, J., Yang, J. C., and Shashidhar, R., Conductance Scaling of Molecular Wires in Parallel, *Nano Lett.*, vol. 3, pp. 897-900, 2003.

[111] Blum, A. S., Kushmerick, J. G., Long, D. P., Patterson, C. H., Yang, J. C., Henderson, J. C., Yao, Y., Tour, J. M., Shashidhar, R., and Ratna, B. R., Molecularly inherent voltage-controlled conductance switching, *Nat. Mater.*, vol. 4, pp. 167-172, 2005.

[112] Blum, A. S., Kushmerick, J. G., Pollack, S. K., Yang, J. C., Moore, M., Naciri, J., Shashidhar, R., and Ratna, B. R., Charge Transport and Scaling in Molecular Wires, *J. Phys. Chem. B*, vol. 108, pp. 18124-18128, 2004.

[113] Xu, B. and Tao, N. J., Measurements of Single-Molecule Resistance by Repeated Formation of Molecular Junctions, *Science*, vol. 301, pp. 1221-1223, 2003.

[114] Haiss, W., Nichols, R. J., Zalinge, H., Higgins, S. J., Bethell, D., and Schiffrin, D. J., Measurement of single molecule conductivity using the spontaneous formation of molecular wires, *Phys. Chem. Chem. Phys.*, vol. 6, pp. 4330-4337, 2004.

[115] Haiss, W., Zalinge, H., Higgins, S. J., Bethell, D., Hobenreich, H., Schiffrin, D. J., and Nichols, R. J., Redox State Dependence of Single Molecule Conductivity, *J. Am. Chem. Soc.*, vol. 125, pp. 15294-15295, 2003.

[116] Haiss, W., Nichols, R. J., Higgins, S. J., Bethell, D., Höbenreich, H., and Schiffrin, D. J., Wiring nanoparticles with redox molecules, *Faraday Discuss.*, vol. 125, pp. 179-194, 2004.

[117] Haiss, W., Albrecht, T., Zalinge, H., Higgins, S. J., Bethell, D., Höbenreich, H., Schiffrin, D. J. , Nichols, R. J., Kuznetsov, A. M., Zhang, J., Chi, Q., and Ulstrup, J., Single-Molecule Conductance of Redox Molecules in Electrochemical Scanning Tunneling Microscopy, *J. Phys. Chem. B*, vol. 111, pp. 6703-6712, 2007.

[118] Haiss, W., Zalinge, H., Bethell, D., Ulstrup J., Schiffrin D.J., and Nichols, R. J., Thermal gating of the single molecule conductance of alkanedithiols *Faraday Discuss.*, vol. 131, pp. 253-264, 2006.(Abstract)

[119] Cui, X. D. , Primak, A., Zarate, X., Tomfohr, J., Sankey, O. F., Moore, A. L., Moore, T. A., Gust, D., Harris, G., and Lindsay, S. M., Reproducible Measurements of Single-Molecule Conductivity, *Science*, vol. 294, pp. 571-574, 2001.

[120] Patel, N., Davies, M. C., Lomas, M., Roberts, C. J., Tendler, S. J. B., and Williams, P. M., STM of Insulators with Probe in Contact with an Aqueous Layer, *J. Phys. Chem. B*, vol. 101 , pp. 5138-5142, 1997.

[121] Reed, M. A., Zhou, C., Muller, C. J., Burgin, T. P., and Tour, J. M., Conductance of a Molecular Junction, *Science*, vol. 278, pp. 252-254, 1997.

[122] Reichert, J., Ochs, R., Beckmann, D., Weber, H. B., Mayor, M., and Löhneysen, H., Driving Current through Single Organic Molecules, *Phys. Rev. Lett.*, vol. 88, pp. 176804-176807, 2002.

[123] Mayor, M., Weber, H. B., Reichert, J., Elbing, M., Hänisch, C., Beckmann, D., and Fischer, M., Electric Current through a Molecular Rod-Relevance of the Position of the Anchor Groups, *Angew. Chem. Int. Ed.*, vol. 42, pp. 5834-5838, 2003.

[124] Grill, L., Rieder, K. H., Moresco, F., Stojakovic, S., Gourdon, A., and Joachim, C., Controlling the Electronic Interaction between a Molecular Wire and Its Atomic Scale Contacting Pad, *Nano Lett.*, vol. 5, pp. 859-863, 2005.

[125] Bumm, L. A., Arnold, J. J., Cygan, M. T., Dunbar, T. D., Burgin, T. P., Jones II, L., Allara, D. L., Tour, J. M., and Weiss, P. S., Are Single Molecular Wires Conducting?, *Science*, vol. 271, pp. 1705-1707, 1996.

[126] Reinerth, W. A., Jones II, L., Burgin, T. P., Zhou, C. W., Muller, C. J., Deshpande, M. R., Reed, M. A., and Tour, J. M., Molecular scale electronics: syntheses and testing, *Nanotech.*, vol. 9, pp. 246-250, 1998.

[127] Tour, J. M., Molecular Electronics. Synthesis and Testing of Components, *Acc. Chem. Res.*, vol. 33, pp. 791-804, 2000.

[128] Joachim, C., Molecular and intramolecular electronics, *Superlatt. Microstruct.*, vol. 28, pp. 305-315, 2000.

[129] Carter, F. L., Molecular Level Fabrication Techniques and Molecular Electronic Devices, *Microel. Eng.*, vol. 2, pp. 11-24, 1984.

[130] Heeger, A. J., Kivelson, S., Schrieffer, J. R., and Su, W. P., Solitons in conducting polymers, *Rev. Mod. Phys.*, vol. 60, pp. 781-850, 1988.

[131] Cygan, M. T., Dunbar, T. D., Arnold, J. J., Bumm, L. A., Shedlock, N. F., Burgin, T. P., Jones II, L., Allara, D. L., Tour, J. M., and Weiss, P. S., Insertion, Conductivity, and Structures of Conjugated Organic Oligomers in Self-Assembled Alkanethiol Monolayers on Au {111}, *J. Am. Chem. Soc.*, vol. 120, pp. 2721-2732, 1998.

[132] Chen, J., Reed, M. A., Asplund, C. L., Cassell, A. M., Myrick, M. L., Rawlett, A. M., Tour, J. M., and Van Patten, P. G., Placement of conjugated oligomers in an alkanethiol matrix by scanned probe microscope lithography, *Appl. Phys. Lett.*, vol. 75, pp. 624-626, 1999.

[133] Xu, B., Xiao, X., and Tao, N. J., Measurements of Single-Molecule Electromechanical Properties, *J. Am. Chem. Soc.*, vol. 125, pp. 16164-16165, 2003.

[134] Selzer, Y. and Allara, D. L., Single-Molecule Electrical Junctions, *Annu. Rev. Phys. Chem.*, vol. 57, pp. 593-623, 2006.

[135] Gittins, D. I., Bethell, D., Schiffrin, D. J., and Nichols, R. J., A nanometre-scale electronic switch consisting of a metal cluster and redox-addressable groups, *Nature*, vol. 408, pp. 67-69, 2000.

[136] Metzger, R. M., Demonstration of Unimolecular Electrical Rectification in Hexadecylquinolinium Tricyanoquinodimethanide, *Adv. Mater. Opt. Electron.*, vol. 8, pp. 229-245, 1998.

[137] Metzger, R. M., Chen, B., Hopfner, U., Lakshmikantham, M. V., Vuillaume, D., Kawai, T., Wu, X., Tachibana, H., Hughes, T. V., Sakurai, H., Baldwin, J. W., Hosch, C., Cava, M. P., Brehmer, L., and Ashwell, G. J., Unimolecular Electrical Rectification in Hexadecylquinolinium Tricyanoquinodimethanide, *J. Am. Chem. Soc.*, vol. 119, pp. 10455-10466, 1997.

[138] Mujica, V. , Retner, M. A., and Nitzan, A., Molecular rectification: why is it so rare?, *Chem. Phys.*, vol. 281, pp. 147-150, 2002.

[139] Waldeck, D. H. and Beratan, D. N., Molecular Electronics: Observation of Molecular Rectification, *Science*, vol. 261, pp. 576-577, 1993.

[140] Aswal, D. K., Lenfant, S., Guerin, D., Yakhmi, J. V., and Vuillaume, D., Self assembled monolayers on silicon for molecular electronics, *Anal. Chim. Acta*, vol. 568, pp. 84-108, 2006.

[141] Wang, Q., Ward, S., Duda, A., Hu, J., Stradins, P., Crandall, R. S., and Branz, H. M., High-current-density thin-film silicon diodes grown at low temperature, *Appl. Phys. Lett.* , vol. 85, pp. 2122-2124, 2004.

[142] Armstrong, N., Hoft, R. C., McDonagh, A., Cortie, M. B., and Ford, M. J., Exploring the Performance of Molecular Rectifiers: Limitations and Factors Affecting Molecular Rectification, *Nano Lett.*, vol. 7, pp. 3018-3022, 2007.

[143] Fleming, J. A., Improvements in instruments for detecting and measuring alternating electric currents, *United Kingdom Patent*, 24 850, 1904.

[144] Shockley, W., The theory of p-n junctions in semiconductors and p-n junction transistors, *Bell Syst. Tech. J.*, vol. 28, pp. 435-489, 1949.

[145] Ellenbogen, J. C. and Love, J. C., Architectures for Molecular Electronic Computers: 1. Logic Structures and an Adder Designed from Molecular Elctronic Diodes, *Proc. IEEE*, vol. 88, pp. 386-426, 2000.

[146] Majumder, C., Mizuseki, H., and Kawazoe, Y., Molecuar Scale Rectifier: Theoretical Study, *J. Phys. Chem. A*, vol. 105, pp. 9454-9459, 2001.

[147] Kornilovitch, P. E., Bratkovsky, A. M., and Williams, R. S., Current Rectification by Molecules with Asymmetric Tunneling Barriers, *Phys. Rev. B*, vol. 66, pp. 165436.1-165436.11, 2002.

[148] Stokbro, K., Taylor, J., and Brandbyge, M., Do Aviram-Ratner Diodes Rectify?, *J. Am. Chem. Soc.*, vol. 125, pp. 3674-3675, 2003.

[149] Ashwell, G. J., Sambles, J. R., Martin, A. S., Parker, W. G., and Szablewski, M., Rectifying Characteristics of Mg |($C_{16}H_{33}$-Q3CNQ LB Film)| Pt Structures, *J. Chem. Soc. Chem. Commun.*, vol. 19, pp. 1374-1376, 1990.

[150] Martin, A. S., Sambles, J. R., and Ashwell, G. J., Molecular Rectifier, *Phys. Rev. Lett.*, vol. 70, pp. 218-221, 1993.

[151] Martin, A. S., Sambles, J. R., and Ashwell, G. J., Identification of the process producing observed rectifying characteristics of metal/Langmuir-Blodgett film/metal structures, *Thin Solid Films*, vol. 210-211, pp. 313-316, 1992.

[152] Martin, A. S. and Sambles, J. R., Molecular rectification, photodiodes and symmetry, *Nanotech.*, vol. 7, pp. 401-405, 1996.

[153] Metzger, R. M., Xu, T., and Peterson, I. R., Electrical Rectification by a Monolayer of Hexadecylquinolinium Tricyanoquinodimethanide Measured between Macroscopic Gold Electrodes, *J. Phys. Chem. B*, vol. 105, pp. 7280-7290, 2001.

[154] Xu, T., Peterson, I. R., Lakshmikantham, M. V., and Metzger, R. M., Rectification by a Monolayer of Hexadecylquinolinium Tricyanoquinodimethanide between Gold Electrodes, *Angew. Chem. Int. Ed.*, vol. 40, pp. 1749-1752, 2001.

[155] Xu, T., Morris, T. A., Szulczewski, G. J., Ameresh, R. R., Gao, Y., Street, S. C., Kispert, L. D., and Metzger, R. M., A Spectroscopic Study of Hexadecylquinolinium Tricyanoquinodimethanide as a Monolayer and in Bulk, *J. Phys. Chem. B*, vol. 106, pp. 10374-10381, 2002.

[156] Ashwell, G. J. and Gandolfo, D. S., Molecular rectification using a gold/(LB film)/gold structure, *J. Mater. Chem.*, vol. 11, pp. 246-248, 2001.

[157] Ashwell, G. J. and Gandolfo, D. S., Molecular rectification:dipole reversal in a cationic donor-(π-bridge)-acceptor dye, *J. Mater. Chem.*, vol. 12, pp. 411-415, 2002.

[158] Ashwell, J. A., Tyrrell, W. D., and Whittam, A. J., Molecular rectification:self - assembled monolayers of a donor-(π-bridge)-acceptor chromophore connected *via* a truncated Au-S-$(CH_2)_3$ bridge, *J. Mater. Chem.*, vol. 13, pp. 2855-2857, 2003.

[159] Ashwell, G. J., Tyrrell, W. D., and Whittam, A. J., Molecular Rectification:Self-Assembled Monolayers in Which Donor-(π-Bridge)-Acceptor Moieties Are Centrally Located and Symmetrically Coupled to Both Gold Electrodes, *J. Am. Chem. Soc.*, vol. 126, pp. 7102-7110, 2004.

[160] Tyrrell, W. D., PhD thesis, Cranfield University, 2005.

[161] Ashwell, G. J., Chwialkowska, A., and High, L. R. H., Rectifying Au-S-C_nH_{2n}-P3CNQ derivatives, *J. Mater. Chem.*, vol. 14, pp. 2848-2851, 2004.

[162] Ashwell, G. J., Chwialkowska, A., and High, L. R. H., Au-S-C_nH_{2n}-Q3CNQ: self-assembled monolayers for molecular rectification, *J. Mater. Chem.*, vol. 14, pp. 2389-2394, 2004.

[163] Krzeminski, C., Delerue, C., Allan, G., Vuillaume, D., and Metzger, R. M., Theory of electrical rectification in a molecular monolayer, *Phys. Rev. B*, vol. 64, pp. art. no. 0854052001.

[164] Vuillaume, D., Chen, B., and Metzger, R. M., Electron Transfer through a Monolayer of Hexadecylquinolinium Tricyanoquinodimethanide, *Langmuir*, vol. 15, pp. 4011-4017, 1999.

[165] Ashwell, G. J. and Mohib, A., Improved Molecular Rectification from Self-Assembled Monolayers of a Sterically Hindered Dye, *J. Am. Chem. Soc.*, vol. 127, pp. 16238-16244, 2005.

[166] Mohib, A., PhD thesis, Cranfield University, 2006.

[167] Ashwell, G. J. and Chwialkowska, A., Controlled alignment of molecular diodes via ionic assembly of cationic donor-(π-bridge)-acceptor molecules on anionic surfaces, *Chem. Commun.*, vol. 13, pp. 1404-1406, 2006.

[168] Chwialkowska, A., PhD thesis, Cranfield University, 2007.

[169] Mukherjee, B., Mohanta, K., and Pal, A. J., Tuning of Molecular Rectification in Donor/Acceptor Assemblies via Supramolecular Structures, *Chem. Mater.*, vol. 18, pp. 3302-3307, 2006.

[170] Ho, G., Heath, J. R., Kondratenko, M., Perepichka, D. F. , Arseneault, K., Pézolet, M., and Bryce, M. R., The First Studies of a Tetrathisfulvalene–σ–Acceptor Molecular Rectifier, *Chem. Eur. J.*, vol. 11, pp. 2914-2922, 2005.

[171] Ashwell, G. J., Ewington, J., and Robinson, B. J., Organic rectifying junction fabricated by ionic coupling, *Chem. Commun.*, vol. 6, pp. 618-620, 2006.

[172] Ashwell, G. J., Moczko, K., Sujka, M., Chwialkowska, A. , High, L. R. H., and Sandman, D. J., Molecular diodes and ultra-thin organic rectifying junctions: Au-S–C_nH_{2n}–Q3CNQ and TCNQ derivatives, *Phys. Chem. Chem. Phys.*, vol. 9, pp. 996-1002, 2007.

[173] Sanyasi, S. and Bhanuprakash, K., Role of the aromatic π–bridge on electron transport property in a donor-bridge-acceptor system: A computational study on frontier molecular orbitals, *J. Molec. Struct.: THEOCHEM*, vol. 761, pp. 31-38, 2006.

[174] Sirringhaus, H., Tessler, N., and Friend, R. H., Integrated Optoelectronic Devices Based on Conjugated Polymers, *Science*, vol. 280, pp. 1741-1744, 1998.

[175] Reed, M. A., Zhou, C., Deshpande, M. R., Muller, C. J., Burgin, T. P., Jones II/L., and Tour, J. M., The Electrical Measurement of Molecular Junctions, *Ann. N. Y. Acad. Sci.*, vol. 852, pp. 133-144, 1998.

[176] Kushmerick, J. G., Whitaker, C. M., Pollack, S. K., Schull, T. L., and Shashidhar, R., Tuning current rectification across molecular junctions, *Nanotech.*, vol. 15, pp. S489-S493, 2004.

[177] Kushmerick, J. G., Pollack, S. K., Yang, J. C., Naciri, J., Holt, D. B., Ratner, M. A., and Shashidhar, R., Understanding Charge Transport in Molecular Electronics, *Ann. N. Y. Acad. Sci.*, vol. 1006, pp. 277-290, 2003.

[178] Pollack, S. K., Naciri, J., Mastrangelo, J., Patterson, C. H., Torres, J., Moore, M., Shashidhar, R., and Kushmerick, J. G., Sequential Deprotection for Control of Orientation in the Self-Assembly of Asymmetric Molecules for Molecular Electronic Devices, *Langmuir*, vol. 20, pp. 1838-1842, 2004.

[179] Dhirani, A., Lin, P. H., Guyot-Sionnest, P., Zehner, R. W., and Sita, L. R., Self-assembled molecular rectifiers, *J. Chem. Phys.*, vol. 106, pp. 5249-5253, 1997.

[180] Morales, G. M., Jiang, P., Yuan, S., Lee, Y., Sanchez, A., You, W., and Yu, L., Inversion of the Rectifying Effect in Diblock Molecular Diodes by Protonation, *J. Am. Chem. Soc.*, vol. 127, pp. 10456-10457, 2005.

[181] Elbing, M. , Ochs, R., Koentopp, M., Fischer, M., Hänisch, C., Weigend, F., Evers, F., Weber, H. B., and Mayor, M., A single-molecule diode, *Proc. Natl. Acad. Sci. USA*, vol. 102, pp. 8815-8820, 2005.

[182] Darwent, J. R., Douglas, P., Harriman, A., Porter, G., and Richoux, M. C., Metal phthalocyanines and porphyrins as photosensitizers for reduction of water to hydrogen, *Coord. Chem. Rev.*, vol. 44, pp. 83-126, 1982.

[183] Deisbach, H. and Weid, E., Quelques sels complexes des o-dinitriles avec le cuivre et la pyridine, *Helvet. Chim. Act.*, vol. 10, pp. 886-888, 1927.

[184] Osugi, M. E., Carneiro, P. A., and Zanoni, M. V. B., Determination of the Phthalocyanine Textile Dye, Reactive Turquoise Blue, by Electrochemical Techniques, *J. Braz. Chem. Soc.*, vol. 14, pp. 660-665, 2003.

[185] Sagar, S., Saravanan, S., Kumar, S. S., Venkatachalam, S., and Anantharaman, M. R., Evidence for the existence of multiple equilibrium states in cobalt phthalocyanine tetramer: a study by dielectric spectroscopy, *J. Phys. D: Appl. Phys.*, vol. 39, pp. 1678-1683, 2006.

[186] Ambroz, M. , MacRobert, A. J., Morgan, J., Rumbles, G., Foley, M. S. C., and Phillips, D., Time-resolved fluorescence spectroscopy and intracellular imaging of disulphonated aluminium phthalocyanine, *J. Photochem. Photobiol. B: Biol.*, vol. 22, pp. 105-117, 1994.

[187] Urasińska, B., Electron spectra and luminescence properties of water solution sulfonated aluminium phthalocyanines, M. A. thesis, Politechnika Wrocławska, 2004.

[188] Sun, C., Sun, Y., Zhang, X., Xu, H., and Shen, J., Selective potentiometric determination of copper(II) ions by use of a molecular deposition film electrode based on water-soluble cooper phthalocyanine, *Anal. Chim. Acta*, vol. 312, pp. 207-212, 1995.

[189] Somashekarappa, M. P., Keshavayya, J., and Sampath, S., Self-assembled molecular films of tetraamino metal (Co, Cu, Fe) phthalocyanines on gold and silver. Electrochemical and spectroscopic characterisation, *Pure Appl. Chem.*, vol. 74, pp. 1609-1620, 2002.

[190] Zhang, X., Gao, M., Kong, X., Sun, Y., and Shen, J., Build-up a New Type of Ultrathin Film of Porphyrin and Phthalocyanine based on Cationic and Anionic Electrostatic Attraction, *J. Chem. Soc., Chem. Commun.*, pp. 1055-1056, 1994.

[191] Zhang, Y. J., Li, Y., Liu, Q., Jin, J., Ding, B., Song, Y., Jiang, L., Du, X., Zhao, Y., and Li, T. J., Molecular rectifying behaviors of a planar binuclear phthalocyanine studied by scanning tunneling microscopy, *Synth. Met.*, vol. 128, pp. 43-46, 2002.

[192] Hersam, M. C., Guisinger, N. P., and Lyding, J. W., Silicon-based molecular nanotechnology, *Nanotech.*, vol. 11, pp. 70-76, 2000.

[193] Schemtic of an experimental STM set-up, [Web Page]. Avaiable at: http://www.iap.tuwien.ac.at/www/surface/STM_Gallery/stm_schematic.html.

[194] Porter, M. D., Bright, T. B., Allara, D. L., and Chidsey, C. E. D., Spontaneously organized molecular assemblies. 4. Structural characterisation of *n*-alkyl thiol monolayers on gold by optical ellipsometry, infrared spectroscopy, and electrochemistry, *J. Am. Chem. Soc.*, vol. 109, pp. 3559-3568, 1987.

[195] McCreery, R. L., Dieringer, J., Solak, A. O., Synder, B. , Nowak, A. M., McGovern, W. R., and DuVall, S., Molecular rectification and conductance switching in carbon-based molecular junctions by structural rearrangement accompanying electron injection, *J. Am. Chem. Soc.*, vol. 126, pp. 6200-6200, 2004.

[196] Wildöer, J. W. G., Harmans, C. J. P. M., and Kempen, H., Observation of Landau levels at the InAs(110) surface by scanning tunneling spectroscopy, *Phys. Rev. B*, vol. 55, pp. 16013-16016, 1997.

[197] Boer, B., Hadipour, A., Mandoc, M. M., Woudenbergh, T., and Blom, P. W. M., Tuning of Metal Work Functions with Self-Assembled Monolayers, *Adv. Mater.*, vol. 17, pp. 621-625, 2005.

[198] Reda, T., Collings, A. F., Barton, C., and Lukins, P., Functionalised Nanoparticle Films with Rectifying Conduction Properties, *J. Phys. Chem. B*, vol. 107, pp. 13774-13781, 2003.

[199] Fischer, C. M., Burghard, M., Roth, S., and Klitzing, K., Organic Quantum Wells: Molecular Rectification and Single-Electron Tunnelling, *Europhys. Lett.*, vol. 28, pp. 129-134, 1994.

[200] Kohn, W., Becke A. D., Parr, R. G., Density Functional Theory of Electronic Structure, *J. Phys. Chem.*, vol. 100, pp. 12974-12980, 1996.

[201] Brandbyge, M., Mozos J. L., Ordejon, P., Taylor, J., Stokbro, K., Density-functional method for nonequilibrium electron transport, *Phys. Rev. B.*, vol. 65, pp. 165401-165417, 2002.

[202] Haiss, W., Wang C., Grace, I., Batsanov, A. S., Schiffrin, D. J., Higgins, S. J., Bryce, M. R., Lambert, C. J., and Nichols, R. J., Precision control of single-molecule electrical junctions, *Nat. Mater.*, vol. 5, pp. 995-1002, 2007.